A New Approach to Molecular Hydrodesulfurization Catalysts: Allyl-capped Trialkylphosphoranimide-bridged Late First-row Transition Metal Clusters

by

Fiona M. Nkala

A thesis submitted in partial fulfillment of the requirements for the degree of

Master of Science

Department of Chemistry
University of Alberta

Abstract

A series of new trialkylphosphoranimide allyl-capped clusters [M(η^3-allyl)$(NPR_3)]_2$, (M = Fe, Co or Ni, R = Et, ^{t}Bu or Ph) were synthesized. The nickel dimers [Ni(η^3-allyl)$(NPR_3)]_2$, R = Et, Ph are diamagnetic and have been fully characterized using NMR spectroscopy, X-ray crystallography, elemental analysis and IR spectroscopy. The paramagnetic clusters [Ni(η^3-allyl)$(NP^tBu_3)]_2$, [Co(η^3-allyl)$(NP^tBu_3)]_2$, and [Fe(η^3-allyl)$(NP^tBu)_3]_2$ have only been characterized by elemental analysis and IR spectroscopy. Addition of alane•dimethylethylamine to [Ni(η^3-allyl)$(NPEt_3)]_2$ affords the paramagnetic heterotrimetallic alane adduct [Ni(η^3-allyl)$(NPEt_3)]_2$•AlH_3.

The catalytic hydrogenation activity of [Ni(η^3-allyl)$(NPR_3)]_2$, R = Et, Ph and [M(η^3-allyl)$(NP^tBu)_3]_2$, M = Fe, Co was investigated under mild conditions (1 atm H_2, RT-80 °C, 16h). Hydrogenation studies suggest that these clusters react with hydrogen and decompose to heterogeneous material(s) at elevated temperatures. The nickel precatalyst [Ni(η^3-allyl)$(NPEt_3)]_2$ was the most active in diphenylacetylene partial hydrogenation, although the reactions proceed primarily to either *cis* or *trans*-stilbene, depending on conditions. [Ni(η^3-allyl)$(NPPh_3)]_2$ exhibited much lower reaction rates, attributed to slower precatalyst activation. The iron and cobalt clusters,

in contrast, activate under hydrogen at room temperature, although hydrogenation proceeds much more slowly than that of the nickel dimers.

The activity of $[Ni(\eta^3\text{-allyl})(NPEt_3)]_2$ in DBT hydrodesulfurization was investigated in the presence of various basic reagents (MTMP, MO^{t}Bu. M= Na or K) in stoichiometric amounts and under variable reaction conditions (1-34 atm H_2, 110-150 °C, 16 h). Hydrodesulfurization of DBT in the presence of the nickel precatalyst is highly dependent on the pKa of the base and the alkali metal. The highest conversion was obtained in the presence of highly basic potassium 2,2,6,6-tetramethylpiperidide whereas reactions using KO^{t}Bu as promoter are slower. Lower conversions were obtained with the corresponding sodium analogues. The slow reactions rates are attributed to varying rates of catalyst activation and decomposition. Supporting the allyl dimer on γ-Al_2O_3 dramatically improves HDS activity in the presence of KO^{t}Bu, suggesting improved catalyst stability and dispersion.

Acknowledgements

I would like to thank Professor Jeffrey M. Stryker for offering me an opportunity to pursue my graduate research studies in his lab and for his support and advice throughout the whole process.

I would also like to thank the Stryker group members for their assistance, guidance and support, in particular, Dr. R. J. Hamilton, Dr. K. Revunova, Orain Brown, Dr. T. Zhou, Asama Vorapattanapong, Aukse Braziunate, Jose Rodriguez and Mark Aloisio. Special mention to my friends for always being there for me in one way or the other especially, Dorothea Mung, Dan Dallyn, Shanyeak Thomas, Rene Tshulu, Huntley Hunter, Nickolet Ncube, Kayann Ferguson and Jasmine Roach.

I would also like to acknowledge the chemistry analytical and spectral staff for helping with characterization especially, Wayne Moffat, Jennifer Jones, Ema Sretenovic, Jeffery Kwasny, Mark Miskolzie, Dr. Mike Ferguson, and Dr. Bob McDonald.

Lastly, I would also like to express my heartfelt gratitude to my family for their prayers and forever believing in me.

Table of contents

List of tables

Chapter 1

Chapter 2

Chapter 3

List of Figures

Chapter 1

Chapter 2

Chapter 3

List of abbreviations

Å	angstroms
atm	atmosphere
COD	cyclooctadiene
cm^{-1}	wavenumber
Cp^-	cyclopentadienyl (anion)
DBT	dibenzothiophene
DMDBT	4,6-dimethyldibenzothiophene
EDTA	ethylenediaminetetraacetic acid
equiv	equivalents
Et	ethyl
ETH	Extended Hückel Theory
EXAFS	extended x-ray absorption fine structure
FT-IR	Fourier Transform- Infrared Spectroscopy
GC	gas chromatography
HDS	hydrodesulfurization
h	hours
^{i}Pr	*iso*-propyl
KH	potassium hydride
KO^{t}Bu	potassium *tert*-butoxide

NTA	nitrilotriacetic acid
M	metal
Me	methyl
MDBT	4-methyldibenzothiophene
MO	molecular orbitals
NMR	Nuclear Magnetic Resonance (Spectroscopy)
Ph	phenyl
ppm	parts per million
R	generic alkyl/aryl group
RT	room temperature
^{t}Bu	*tert*-butyl
wt%	weight percent
TMP	tetramethylpiperidine

Chapter 1. Allyl-capped Trialkylphosphoranimide-bridged Late First-row Transition Metal Clusters

1.1 Introduction

Sulfur content in crude oil varies between 0.05 to 5 wt%, depending on the feedstock.[1] Sulfur in fuels is one of the key causes of air pollution. When sulfur is combusted, toxic sulfur oxides are emitted.[2] In addition, traces of sulfur in fuel also inhibit and poison precious metal catalysts used in catalytic converters.[3] Catalytic converters convert toxic, incomplete combustion by-products in exhaust systems, like carbon monoxide and nitrogen oxides, into less hazardous carbon dioxide and nitrogen gas.[4] Residual sulfur, however, poisons precious metal catalysts, increasing the emission of hazardous pollutants.[5] For these reasons, North America and EU introduced stringent environmental regulations to significantly reduce sulfur levels in crude oil and refined fuels. The regulations mandate sulfur levels in gasoline be reduced to less than 14 ppm by 2019.[6]

Hydrodesulfurization (HDS) is a catalytic industrial process used to achieve ppm levels of sulfur in refined fuels. Before HDS, heavy petroleum feedstocks undergo delayed coking, a thermal process used to transform asphaltene-rich petroleum residues into solid coke.[7] Delayed coking purportedly breaks-down asphaltene fractions of bitumen into lighter hydrocarbons.[8] However, asphaltene conversion into coke, which

must be discarded, is a major reaction pathway for desulfurization.[9] During catalytic HDS, polycyclic aromatic organosulfur compounds react with hydrogen at high pressure (~130 atm) and temperature (>300 °C) over heterogeneous cobalt- (or nickel-) promoted molybdenum (or tungsten) sulfide catalysts supported on alumina.[10] The reaction proceeds with the co-production of H_2S (Eq. **1.1**).[11] The resulting H_2S, a catalyst inhibitor, is removed from the reactor as it is produced, separated from the recycled hydrogen, and converted into elemental sulfur and/or sulfuric acid.[12]

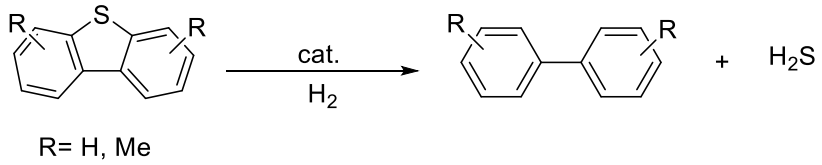

Equation 1.1

The industrial catalysts efficiently remove sulfur from thiols, thioethers, and thiophenes. However, the removal of refractory, often sterically-hindered polyaromatic sulfur compounds such as dibenzothiophene (DBT), 4-methyldibenzothiophene (4-MDBT) and 4,6-dimethyldibenzothiophene (4,6-DMDBT) (Figure **1.1**) is challenging.[13,14] As a result, designing cheaper, earth-abundant, and less toxic transition metal catalysts capable of HDS under milder reaction conditions, is mandatory.[15,16,17]

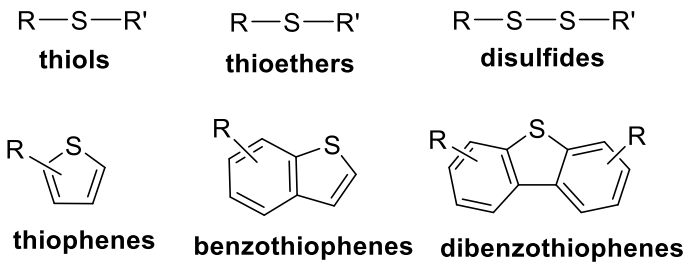

Figure 1.1: Typical organosulfur compounds found in crude oil

Thus, our group has developed new first-row transition metal (Fe, Co, Ni) trialkylphosphoranimide clusters as potential HDS catalysts. Chapter 1 highlights the main reasons for this ligand choice and of the allyl ligand for precatalyst stabilization. This chapter also details the syntheses and characterization of $[M(\eta^3\text{-}C_3H_5)(NPR_3)]_2$, M = Fe, Co and Ni clusters. The catalytic activity of these clusters in alkene and alkyne hydrogenation is reported in Chapter 2. Chapter 3 highlights the recent advancements in developing HDS catalysts, along with preliminary results using the allyl Ni cluster for DBT hydrodesulfurization.

1.1.1 Trialkylphosphoranimide ligands: structure and bonding

Staudinger and Meyer first reported the monoanionic trialkylphosphoranimide ligand, NPR_3^-, as triphenylphosphine phenylimide, in 1919.[18] While a discrete anion is still unknown, the alkali metal salts exist as tetramers or hexamers, depending on the steric size of the substituents on phosphorous.[19,20]

The anionic phosphoranimide ligand is often compared to the cyclopentadienyl anion (Cp^-). Both ligands bear one formal negative charge and show similar bonding and structural features when coordinated to transition metals. According to Extended Hückel Theory (EHT) calculations, the phosphoranimide ligand, like cyclopentadienyl, can donate up to 6-electrons to a metal centre *via* both σ- and π-bonding (Figure **1.2**).[21] Resonance **A**, best describes the bonding in the anion; the nitrogen-phosphorous bond is a double bond. Upon coordination to a metal centre, the negative charge on the nitrogen increases with a corresponding decrease in the nitrogen-phosphorus bond order. For this reason, resonance **B** best describes the nitrogen-phosphorous bond in metal-bound phosphoranimide ligands.

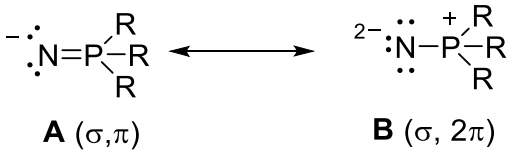

Figure 1.2: Resonance structures of the phosphoranimide anion

EHT calculations also suggest that the highest occupied molecular orbitals of the free ligand are one *sp*-hybridized orbital and a set of two degenerate *p*-orbitals, similar in symmetry to those of Cp^- (Figure **1.3**).[22] Thus the phosphoranimide and cyclopentadienyl ligands are isolobal.

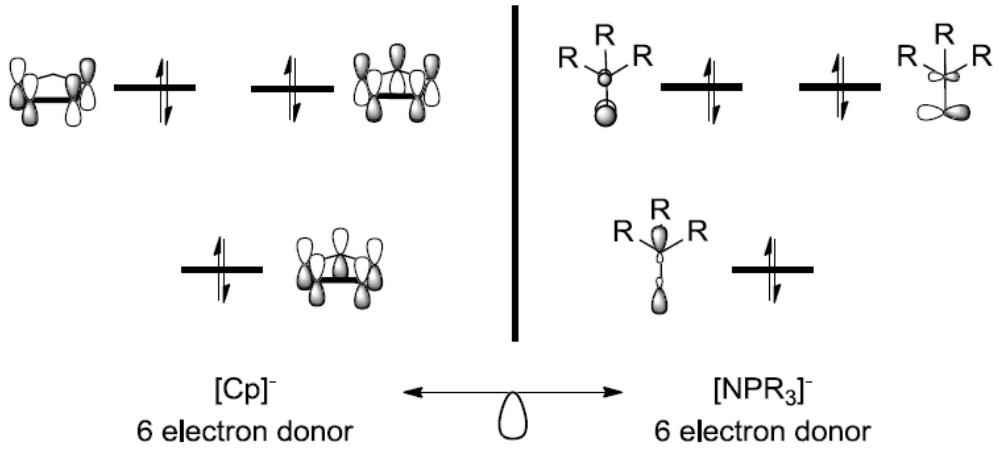

Figure 1.3: The isolobal relationship between the cyclopentadienyl and phosphoranimide ligands.

Stephan *et al*., highlighted the isolobal relationship between the two ligands when they studied $[CpTiCl(NP^tBu_3)]_2$ **1** and $[CpTiCl(NP^iPr_3)]_2$ **2** for ethylene polymerization, as alternatives to metallocene clusters.[23] The group observed that the total buried volume of tri-*tert*-butylphosphoranimide and cyclopentadienyl in **1** are similar, 87° and 83°, respectively (Figure **1.4**). While the total buried volume do not differ, the distances between the metal centre and the ligand's steric bulk are markedly different. The Ti-P distance is 3 Å while the Ti-Cp centroid distance is just 2.2 Å.[24] The nitrogen acts as a spacer atom and displaces the bulk of the phosphoranimide ligand away from the metal centre. This leaves ample room for the metal to participate in other chemistry. Half-sandwich titanium and zirconium phosphoranimide complexes, upon activation with a co-catalyst, show high olefin polymerization activity, partly due to metal's availability to the incoming substrate.[25,26,27,28,29,30,31]

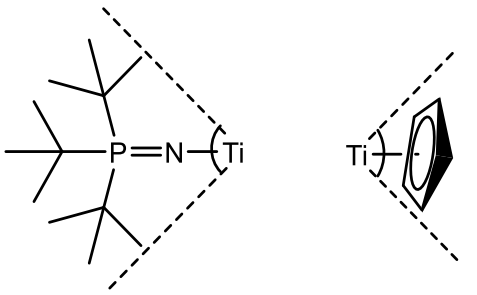

Figure 1.4: Cone angles for cyclopentadienyl and tri-*tert*-butyl phosphoranimide titanium complexes.[24]

When coordinated to transition metals, the phosphoranimide ligand shows versatile coordination chemistry. The bonding mode adopted depends on the oxidation state and d-orbital occupancy of the metal(s). High oxidation state transition metals show bonding modes **C** and/or **D** while low oxidation state metals prefer μ^2- or μ^3-bridging modes **F** and **G** (Figure **1.5**). In mode **C**, the ligand's set of frontier orbitals (σ, 2π) are involved in a metal-nitrogen triple bond. Manners and colleagues observed these features in $[WCl_5(NPCl_3)]$ **3**[32] which has an almost linear W–N–P bond angle of 176.2°. Similarly, both $[ReO_3(NPPh_3)]$ **4**[33] and $[Mo(NPPh_3)_4]^{2+}$ **5**[34] also adopt bonding mode **C**.

In bonding mode **D**, the complexes have bent M-N-P bond angles and the phosphoranimide ligand is at most a 4-electron donor, as in $[WCl_4(NPCl_2Ph)_2]$ **6**[32] and $[VoF_2(NPPh_3)]$ **7**.[35] The W-N-P bond angles for **6** average 160°, while the V-N-P bond angle in complex **7** is 137.4°.

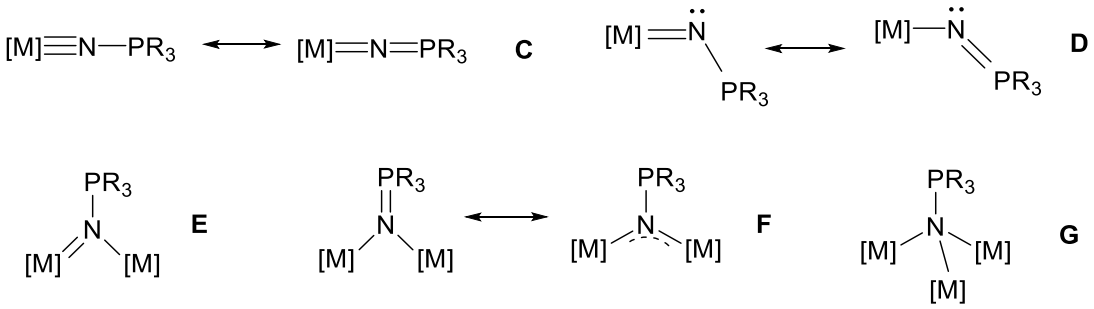

Figure 1.5: Various coordination modes of the phosphoranimide ligand to metals

In bimetallic bonding modes **E** and **F**, the phosphoranimide ligand acts as a μ^2-bridging ligand. Bonding in mode **E** is unsymmetrical, and the two M-N bond lengths are different. For example, the Ti-N bond lengths in $[TiCl_3(NPEt_3)]_2$ **8**[36] are 184.7 and 210.3 pm. Meanwhile in mode **F**, the bonding is symmetric and the two metal-nitrogen bond lengths are equivalent, as in $[FeCl_2(NP^tBu_3)]_2$ **9**, 191.0 and 191.7 pm.[37]

In general, phosphoranimide ligands coordinate to electron-rich or high spin metals *via* bonding mode **G**. Here the phosphoranimide nitrogen triply-bridges three metal centres as in the heterocubane clusters **10**, $[MCl(NPR_3)]$, M = Fe or Co (Figure **1.6**).[38] Interestingly, the Stephan group showed that the dimensionality and nuclearity of iron phosphoranimide clusters depends on the steric bulk of the phosphoranimide ligands. The group successfully synthesized and characterized a mixed valance Fe(II)/Fe(III) tri-*tert*-butylphosphoranimide dimer, $[Fe_2Cl_3(NP^tBu_3)_2]$ **11** (Figure **1.6**).[37] In **11**, the phosphoranimide ligand is limited sterically to doubly bridging the two iron

centres. J. Bunquin in our group later synthesized and characterized dimeric $[CoCl(NP^tBu_3)]_2$ **12**.[39]

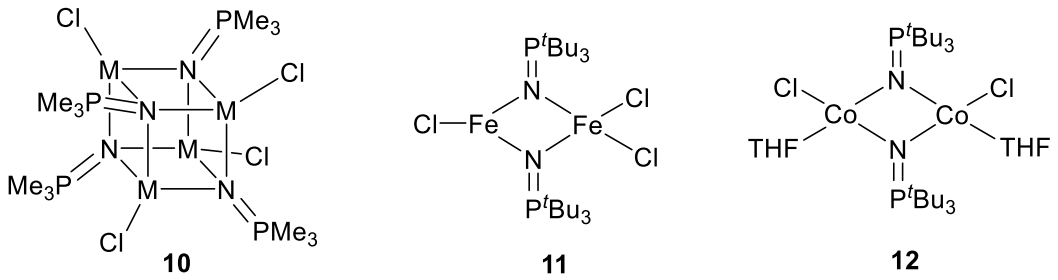

Figure 1.6: Molecular structures of $[MCl(NPEt_3)]_4$ **10** (M = Fe or Co)**,** **[**$Fe_2Cl_3(NP^tBu_3)_2$] **11** and $[CoCl(NP^tBu_3)]_2$ **12**, as determined in the solid state by X-ray crystallography.

The Stryker group further developed phosphoranimide-based late first-row transition metal cluster synthesis to investigate reactivity toward heteroaromatic C-S and C-N bond cleavage. First-row transition metal sulfides, as bulk or nanostructured materials, are inactive for HDS when compared to conventional Co- or Ni-promoted molybdenum sulfide systems.[40,41] By incorporating the phosphoranimide ligand, we hoped to mimic the high energy surface of the conventional HDS catalysts in several ways: (1) The ligand nitrogen atom readily bridges two or three transition metal centres. This "single-atom" bridging character is proposed to result in coordinatively unsaturated clusters, as determined for conventional catalysts. (2) Cluster formation also results in the presentation of adjacent metal centres, promoting metal-metal cooperativity, as proposed for the heterogeneous catalysts. (3) Meanwhile, the distal steric bulk is anticipated to maintain some degree of coordinative unsaturation at the metal(s),

essential for substrate coordination and hydrogen activation. Dr. H. Brown in this group synthesized the first cobalt tetraalkyl heterocubane cluster **13** with these features (Figure **1.7**).[22] Brown also proposed that Co-C hydrogenolysis occurs upon treating the cluster with hydrogen, with concomitant hydride cluster formation, thought to be the active HDS catalyst.

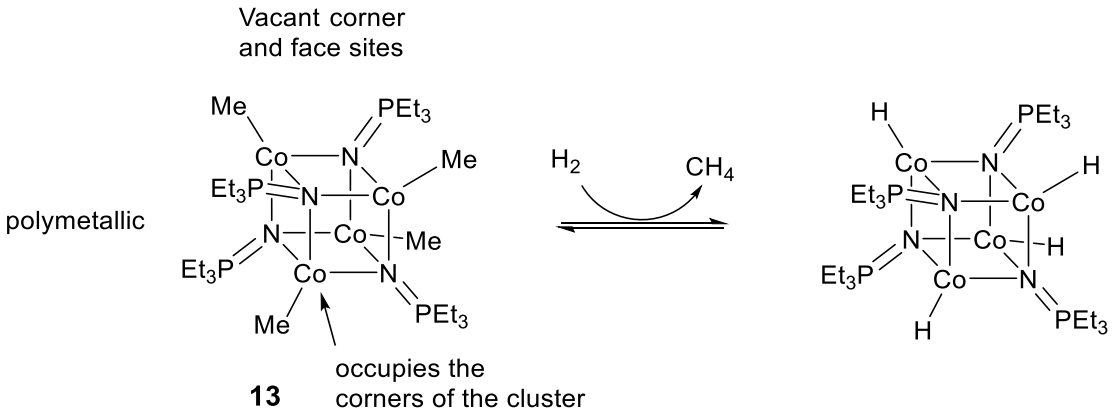

Figure 1.7: $[MeCo(NPEt_3)]_4$ design principals

By altering the electron-donating capabilities of the ligand, we can also investigate electronic effects on catalytic activity. For example, we expect strongly electron-donating ligands to promote the oxidative addition of the substrate to the metal or metals. Increasing the electron density on the metal(s) should also weaken the resulting M-S bond, encouraging M-S bond cleavage upon hydrogenation.[42] These properties should result in thermally robust and active catalysts.

1.1.2 Trialkylphosphoranimide ligand syntheses

The synthesis and installment of phosphoranimide ligands onto transition metals is achieved using various methods. Dehnicke, *et al.,* reported the first method, in which they added anhydrous metal halides to molten trimethylsilyl-trialkylphosphoranimides in the presence of excess sodium or potassium fluoride.[43] However, selectivity, reproducibility and scalability remain significant challenges. Trimethylsilyltrialkylphosphoranimide precursors are synthesized from silylazide reagents and the phosphine. When used on a large scale, trimethylsilyl azide is potentially explosive and acutely toxic.[44] This procedure also limits the ligand scope to a few low-melting solids (R = Me, Et).

To solve these problems, Dr. R. Hamilton in our group adapted an older, azide-free procedure used to synthesize N-alkyltriphenylphosphoranimides. In the original procedure, Zimmer *et al*., treat triphenylphosphine dibromide with sodium amide in liquid ammonia.[45] In our modified procedure (Scheme **1.1**), we treat trialkylphosphine dibromide with potassium amide prepared *in situ*. The excess base then deprotonates the resulting phosphoranium salt to give the corresponding potassium trialkylphosphoranimide.

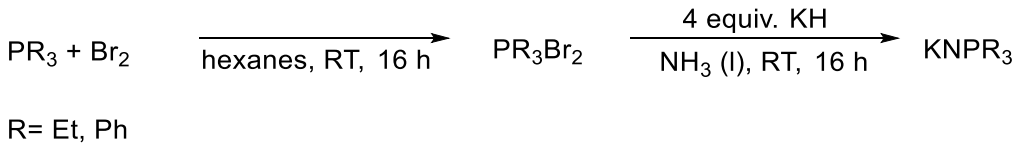

Scheme 1.1

Although effective for synthesizing a wide range of trialkylphosphoranimide salts, this procedure cannot be used to prepare the tri-*tert*-butylphosphoranimide analogue. Instead, Staudinger's reaction is used to synthesize (*N*-trimethylsilyl)tri-*tert*-butylphosphoranimide (TMSNP^{t}Bu^3) **14**.[18] Hamilton modified the procedure to include desilylation of **14** using anhydrous potassium hydrogen difluoride. This step affords phosphoranium fluoride **15**.[46] Deprotonation of **15** by methyllithium gives tri-*tert*-butylphosphoranimine **16**. Potassium hydride deprotonates **16** to give potassium tri-*tert*-butylphosphoranimide **17** (Scheme **1.2**) as the final product.

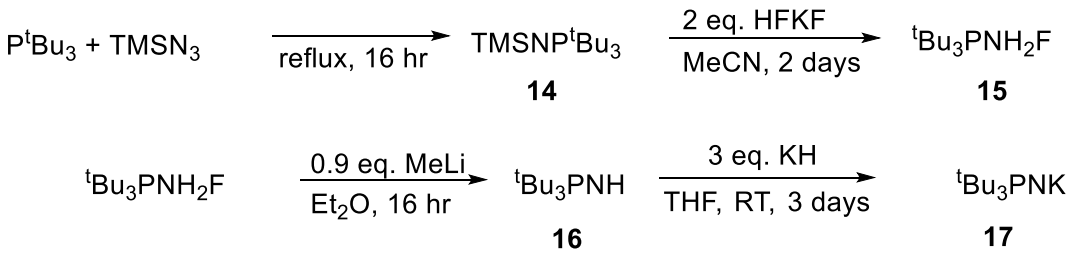

Scheme 1.2

1.1.3 Dimeric bis(phosphoranimide) clusters [M(NP^{t}Bu$_3$)$_2$]$_2$

By optimizing trialkylphosphoranimide synthesis, we expanded our ligand scope and prepared a series of dimetallic, trimetallic and tetrametallic late first-row transition metal trialkylphosphoranimide clusters. This section reports previous group research relevant to this thesis: dimeric bis(phosphoranimide) precatalyst complexes. These

clusters contain the same number of metal sites as the systems targeted, prepared, and discussed in this thesis.

D. Hebert pioneered homoleptic bimetallic clusters syntheses, $[M(NP^tBu_3)_2]_2$, using a salt metathesis reaction between a metal halide and 1.9 equivalents of $LiNP^tBu_3$.[47] Hebert synthesized, isolated, and characterized $[Fe(NP^tBu_3)_2]_2$ **18** (yellow-green powder) and $[Co(NP^tBu_3)_2]_2$ **19** (dark green powder). Orain Brown later synthesized and characterized $[Ni(NP^tBu_3)_2]_2$ **20**.[48] In these clusters, tri-*tert*-butylphosphoranimide is both a bridging and a terminal ligand (Figure **1.8**).

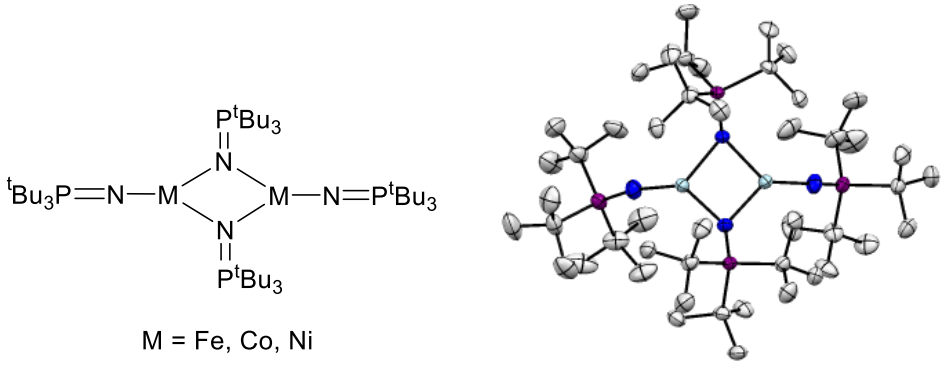

Figure 1.8: Homoleptic bimetallic clusters $[M(NP^tBu_3)_2]_2$, M= Fe, Co or Ni. ORTEP diagram of $[Ni(NP^tBu_3)_2]_2$ **20**. The atoms are shown by Gaussian ellipsoids at 30% probability level and the hydrogens were omitted for clarity.

Hebert and Brown conducted preliminary catalysis studies using $[M(NP^tBu_3)_2]_2$, M = Co, Ni, under initially homogeneous conditions. Hydrogenation of model alkenes (e.g. allylbenzene) and alkynes (e.g. diphenylacetylene) using cobalt precatalyst **19** and

hydrogen at one atmosphere affords irreproducible results, with substrate conversions varying between 30% and 90%, depending on temperature.[47]

Orain Brown investigated HDS of a typical model compound, DBT, using nickel cluster **20**, a basic scavenger/promoter, stoichiometric potassium *tert*-butoxide, and 34 atm H_2. After 16 hours, 17% and 6% of biphenyl and 2-thiolbiphenyl were obtained, suggesting **20** itself is not an ideal deep HDS precatalyst.[48]

Contrary to expectations, $[M(NP^tBu_3)_2]_2$ M = Co, Ni show poor catalytic activity. The low activities are likely due to catalyst inhibition by tri-*tert*-butylphosphoranimine, the basic byproduct of M–N bond hydogenolysis. Irreproducibility calls into question catalyst homogeneity. Heterogeneous catalysts have multiple active sites which vary with catalyst preparation, particle size, and/or catalytic conditions, resulting in different rates of reactivity.[49] Our results suggest that at elevated temperatures, the precatalyst decomposes to give heterogeneous metal particles. However, in this system homogeneity tests have not been conducted to determine the phase of the actual catalysts. Also, the precatalyst clusters are paramagnetic, and hence NMR spectroscopy cannot be used to assess catalyst activation and reaction intermediates. A lack of detailed mechanistic studies makes catalyst development inherently challenging.

Thus, it became essential to refine the functionality of the dimeric clusters. We considered developing heteroleptic phosphoranimide clusters with a much more

"hydrogenolysis-ready" terminal ligand. Under standard reaction conditions, the ligand should undergo hydrogenolysis and hydrogenation, producing a non-coordinating adduct, incapable of catalyst poisoning. The ligand also needs to be multidentate, to provide stabilization of the precataylsts prior to activation.

During our literature search, we encountered aziridide dimer [Ni(η^3-C_3H_5)(N_2H_4)]$_2$ **21** (Eq. **1.2**),[50] prepared by the reaction of **22** and 1-lithioaziridine($LiNC_2H_4$). The facile displacement of the halides without destroying the coordination of the allyls motivated us to design a set of dimeric μ^2-bridged trialkylphosphoranimide first-row transition metal clusters capped with ancillary η^3-allyl groups.

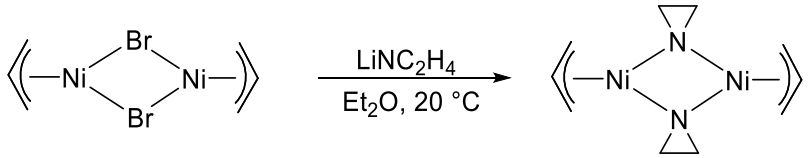

22 **21**

Equation 1.2

1.1.4 Allyl ligand: selection criteria and properties

The η^3-allyl ligand is an ideal ancillary ligand for several reasons. First, the η^3-allyl ligand is a 4-electron donor which occupies two coordination sites (Figure **1.9**), promoting lower-nuclearity precatalysts. Second, the allyl ligand also has a low-lying π*-orbital, promoting metal backbonding when coordinated to electron-rich metal

centres (Figure **1.10**). If a square planar nickel complex is formed, we anticipate a diamagnetic state, facilitating multinuclear NMR spectroscopy. These studies enable mechanistic determinations necessary for efficient catalyst development. Last, when treated with hydrogen, the allyl ligand can undergo hydrogenolysis and hydrogenation to give active metal hydrides and much more stable propane.[51] Combining these properties with those of the phosphoranimide ligand, we anticipate the formation of thermally robust clusters active in HDS.

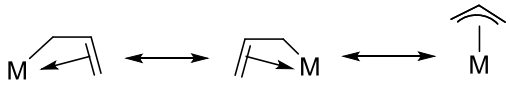

Figure 1.9: η^3-allyl ligand-metal resonance coordination forms

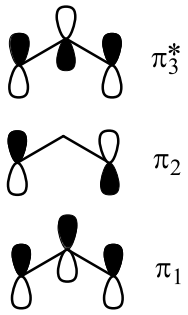

Figure 1.10: π-System molecular orbitals for the anionic allyl ligand

Transition metal η^3-allyl syntheses, characterization and reaction chemistry dates to the late 1950's. Smidt and Hafner (1959) and Moiseev *et al.* (1959) prepared and reported the first η^3-allyl-capped complex, $[PdCl(\eta^3\text{-}C_3H_5]_2$ **23**. The group obtained

dimer **23** by treating allyl alcohol with $PdCl_2$.[52] Numerous transition metal η^3-allyl complexes have since been reported.[53,54,55]

Fischer and Burger reported the first dimeric allylnickel halides $[NiX(\eta^3\text{-}C_3H_5)]_2$ **22**, from treating nickel carbonyl $[Ni(CO)_4]$ with an allyl halide.[56] $Ni(CO)_4$ is acutely toxic and the reaction affords low yields, 10%. For these reasons, bis(cycloocta-1,5-diene)nickel $[Ni(COD)_2]$ is the preferred nickel(0) source for allyl synthesis. $Ni(COD)_2$ shows superior activity and improved stability, and when treated with allyl bromide, results in a 90% yield of complex **22**.[53]

1.2 Results and discussion

1.2.1 Synthesis and characterization of $[Ni(\eta^3\text{-}C_3H_5)(NPEt_3)]_2$ 24

Dimeric nickel allyl trialkylphosphoranimide complexes were prepared using a two-step process, beginning with bis(allyl)di-μ-bromonickel **22** synthesis (Eq. **1.3**). The red crystalline compound was synthesized in 90% yield according to the literature procedure, by treating commercial bis(1,5-cyclooctadiene)nickel(0) with allyl bromide.[53] The synthesis is not trivial; ^{1}H NMR spectroscopy and elemental analysis reveal that trace amounts of cyclooctadiene contaminate the product. The product decomposes slowly at room temperature, requiring storage at -35 °C in the drybox refrigerator.

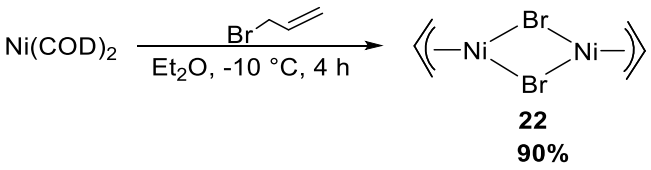

22
90%

Equation 1.3

T. Zhou in this group initially synthesized [Ni(η^3-C_3H_5)($NPEt_3$)]$_2$ **24** (Eq. **1.4**) by treating [NiBr(η^3-allyl)]$_2$ **22** with $KNPEt_3$ at room temperature. The reaction affords an 80% yield of a golden-brown sticky solid, soluble in pentane. The product is unstable at room temperature and requires low temperature storage to prevent decomposition to colloidal Ni(0), suggested by the presence of a black precipitate insoluble in common organic solvents. Upon purification, the complex was characterized using elemental analysis, ^{1}H NMR and ^{31}P NMR spectroscopy, and X-ray crystallography.[57]

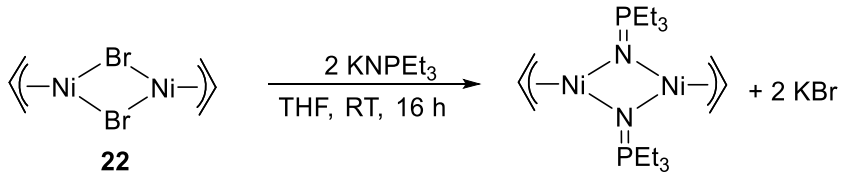

22

24
80%

Equation 1.4

The ^{31}P NMR spectrum of dimeric **24** shows two singlet peaks with close to a 1 : 1 ratio, at 34.165 and 34.626 ppm, representing inequivalent triethylphosphoranimides. The ^{1}H NMR spectrum shows two sets of allyl signals, suggesting **24** is a mixture of

stereochemical isomers. The central allyl protons appear as triplet of triplets at 5.293 and 5.229 ppm. The *syn*-protons show as two sets of doublets at 2.190 and 2.153 ppm, while the *anti*-protons, shielded by the metal, appear further upfield, as two doublets at 1.479 and 1.450 ppm. The *syn* and *anti*-proton signals in each case, are split because of coupling to the central proton. The *syn* and *anti*-protons are also inequivalent; however, geminal coupling at sp^2-centres is small and generally not observed. This might explain the first order, A_2M_2X spin system observed for the allyl ligands, as opposed to a second order, AA′BB′X pattern. Chien *et al*., first described the ^1H NMR spectrum of the η^3-allyl group in palladium allyl complex **23** as arising from an A_2M_2X pattern.[58] Using higher resolution NMR spectroscopy however, Shaw, *et al*., later showed that the coupling in complex **23** is actually second order.[59] Cotton and McClellen respectively, reported similar second order spectra for $[Mn(\eta^3\text{-}C_3H_5)(CO)_4]$[60] and $[Co(\eta^3\text{-}C_3H_5)(CO)_3]$.[61]

Zhou obtained single crystals of allyl dimer **24** from a saturated solution in pentane at -35 °C in the drybox. X-ray crystallography confirmed in the solid state what was observed in the solution ^1H NMR spectrum – the allyl group coordinates in an η^3-fashion, occupying two coordination sites. Each of the triethylphosphoranimides act as μ^2-bridging ligands through the nitrogen centre. The overall geometry about each nickel is square planar; thus, complex **24** is diamagnetic.[57] The allyl ligands are highly disordered in the solid state, confirming that more than one allyl ligand orientation exists, suggesting that the ^1H NMR results indeed define geometrical isomers.

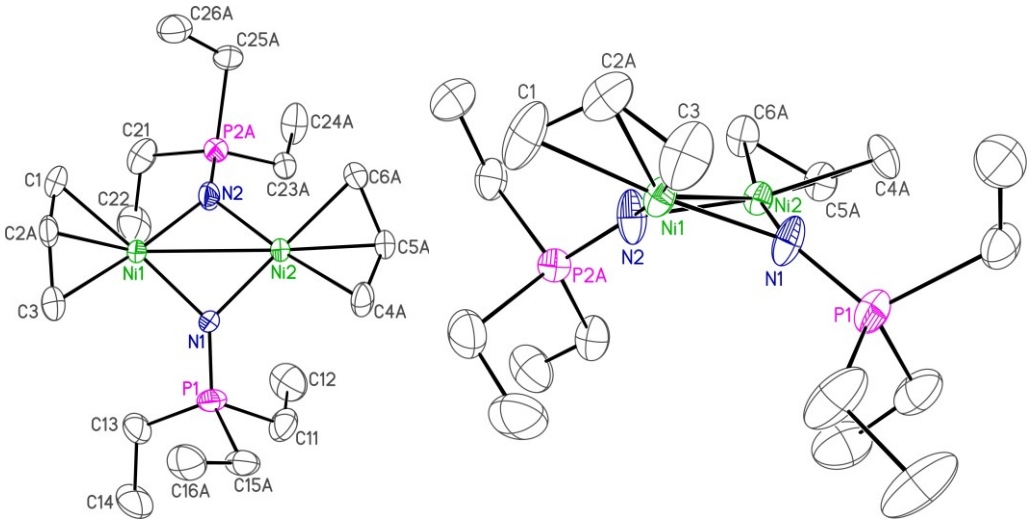

Figure 1.11: ORTEP diagram of $[Ni(\eta^3\text{-}C_3H_5)(NPEt_3)]_2$ **24**. The atoms are shown by Gaussian ellipsoids at 30% probability level and the hydrogens are omitted for clarity. This image represents one of the possible orientations of the disordered allyl group.

Combining the NMR spectroscopy and single crystal X-ray structure, we propose that the allyl dimer **24** exists as a set of *syn* and *anti* allyl isomers (Figure **1.12**). In the product, the isomers occur in a 1 : 1 ratio. This fact, however, does not define the relative orientation of the allyl and phosphoranimide ligands in each isomer.

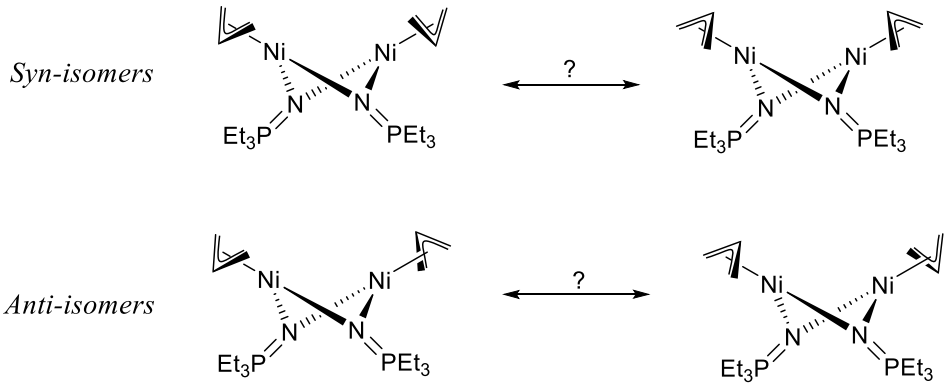

Figure 1.12: $[Ni(\eta^3\text{-}C_3H_5)(NPEt_3)]_2$ **24** *syn* and *anti*-isomers.

Most η^3-allyl metal complexes show dynamic behavior in solution, which can usually be monitored by ^{1}H NMR spectroscopy.[62,63] Hence we performed variable temperature (20 °C–100 °C, in 20 °C increments) ^{1}H and ^{31}P NMR spectroscopy and compared the spectra. The ^{31}P NMR spectrum at all temperatures resembles that of the starting material, suggesting a strong and static Ni-N bond. In the ^{1}H NMR spectrum, the two sets of the allyl peaks broaden at 80 °C and coalesce at 100 °C (Figure **1.13**). Broadening and coalescing of the allyl peaks suggests a rapid exchange between the *syn* and *anti*-isomers.

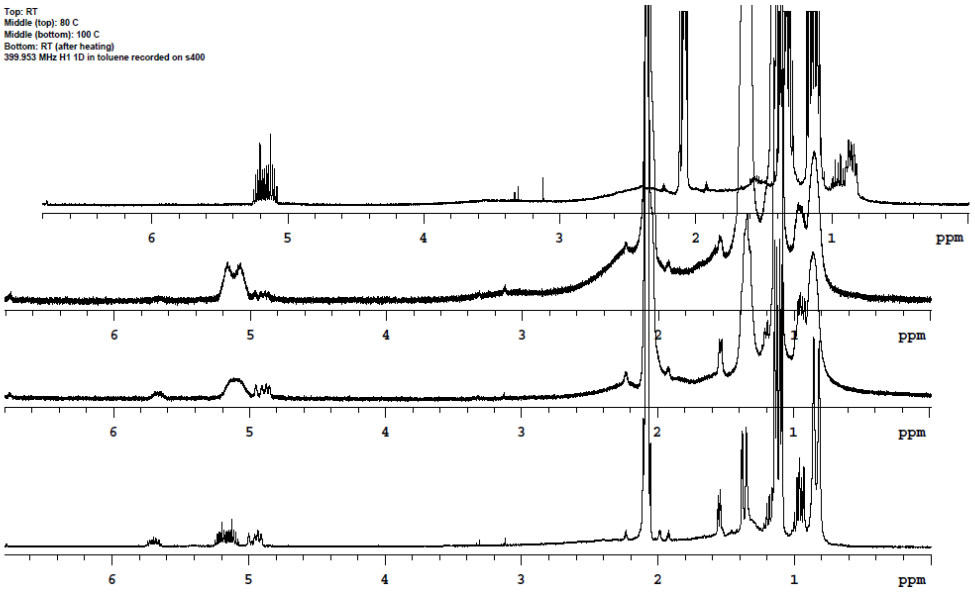

Figure 1.13: Variable temperature ^{1}H NMR spectra of **24**. Top: RT, middle (top): 80 °C, middle (bottom): 100 °C and bottom: RT (after heating). Phosphoranimide ethyl groups are shown off-scale.

The exchange most probably involves an η^3-η^1-η^3 interconversion of the allyl ligands (Scheme **1.3**).[64] Although we have not yet identified an η^1-intermediate, the

complex decomposes slowly at higher temperature. A second possible isomerization mechanism is in-plane rotation of the allyl group (Scheme **1.3**).[65] This mechanism prominent in transition metal complexes with weak metal-allyl backbonding, which may well be the case (*vide infra*).[66]

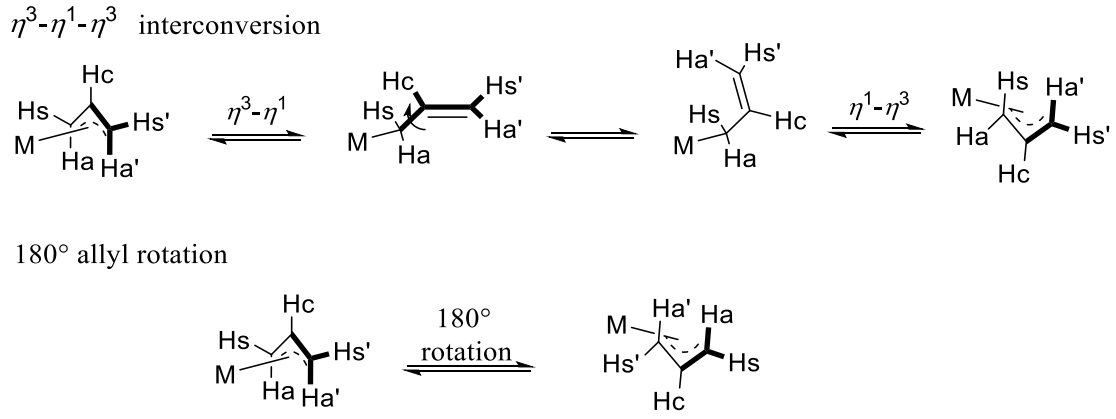

Scheme 1.3

At 80 °C, a new set of downfield peaks emerges at 4.954 ppm, again suggesting decomposition. The resonances become pronounced at 100 °C, and another downfield signal appears at 5.673 ppm. Upon cooling to room temperature, the starting allyl complex resonances reappear, but the byproduct resonances persist. By comparison to an authentic sample, the byproduct is 1,5-hexadiene, suggesting reversible formation of the elusive η^1-intermediate. The weakly-bound η^1-allyl undergoes homolytic bond cleavage, generating the allyl radical, which then dimerizes. The dimerization could proceed *via* a solvent-caged radical pair or *via* the addition of the allyl radical released to the other (still coordinated) allyl ligand at the terminal allyl position. For the latter, the

dimerization rate will be concentration dependent, therefore the effect of **24** concentration on the rate of 1,5-hexadiene formation must be investigated.

1.2.2 Synthesis and characterization of [Ni(η^3-C_3H_5)($NPEt_3$)]$_2$•AlH_3 25

We modified [Ni(η^3-C_3H_5)($NPEt_3$)]$_2$ **24** by adding a neutral Lewis acid, aluminium hydride, in anticipation of forming a particularly active catalyst after allyl hydrogenolysis. Dropwise addition of commercial alane-dimethylethylamine to **24** at room temperature yields a black-brown powder, soluble in pentanes. [Ni(η^3-C_3H_5)($NPEt_3$)]$_2$•AlH_3 **25** was characterized as an adduct by elemental analysis. Analysis by ^{1}H NMR spectroscopy reveals only peaks corresponding to **24**. Aluminium hydride resonances generally cannot be detected directly by ^{1}H NMR spectroscopy because of quadrupolar broadening. Attempts to obtain a crystal structure are still ongoing.

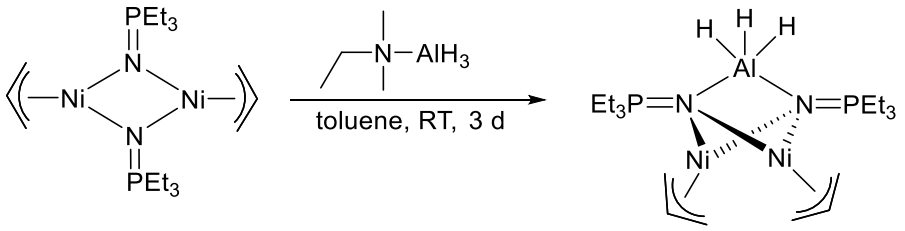

24 **25** **50%**

Equation 1.5

1.2.3 Synthesis and characterization of $[Ni(\eta^3\text{-}C_3H_5)(NPPh_3)]_2$ 26

To assess the electronic and steric tunability of allyl-capped phosphoranimide clusters, we extended the synthesis to include the triphenyl and tri-*tert*-butyl analogues. $[Ni(\eta^3\text{-}C_3H_5)(NPPh_3)]_2$ **26** was obtained as an orange powder by treating **22** with $KNPPh_3$ (Eq. **1.6**). The product is soluble in toluene and in contrast to dimer **24**, stable at room temperature. Electron donating or withdrawing groups, as well as temperature, influence the stability and behaviour of allyl complexes.[53] For instance, Birkenstock, *et. al*. reported that dimeric η^3-allylnickel alkoxide complexes $[Ni(\eta^3\text{-}C_3H_5)(OR)]_2$, R = Et or Ph, decompose in the solid state. The decomposition of these complexes depends on the R group; the ethoxide adduct decomposes at 25 °C, while the phenoxide adduct is unstable at 65 °C.[50]

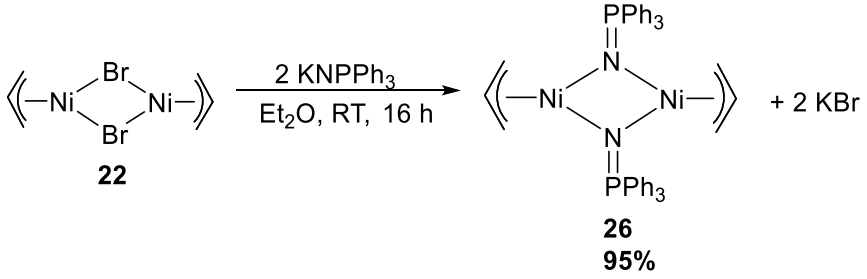

Equation 1.6

For our clusters, we expect that electron withdrawing substituents on the phosphorous will increase nitrogen-to-phosphorous electron donation and reduce the electron density donated to nickel. This promotes an η^3-allyl coordination mode. In this mode, the allyl group donates four electrons. Greater electron donating substituents on

the phosphorous reduce nitrogen-to-phosphorous electron donation, increasing electron donation from nitrogen to the nickels. Increased electron density on nickel promotes a dynamic allyl system, reducing the stability of the dimer.

Single crystal X-ray crystallography confirmed the predicted structure of **26** (Figure **1.14**). Surprisingly, substituting a relatively electron rich and less bulky ethyl group with the electron withdrawing and more bulky phenyl group has very little effect on the structural features. The average Ni-N bond lengths are 1.901 (2) Å for **24** and 1.915 (3) Å for **26** while N-P bond lengths are 1.559 (11) Å and 1.550 (4) Å respectively.

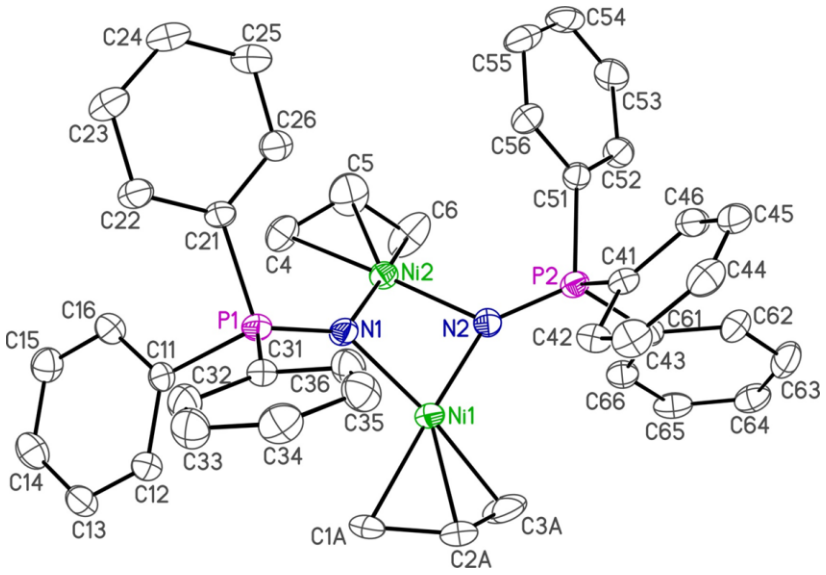

Figure 1.14: ORTEP diagram showing the major orientation (80%) of the allyl group in $[Ni(\eta^3\text{-}C_3H_5)(NPPh_3)]_2$ **26**. The atoms are shown by Gaussian ellipsoids at 30% probability level and the hydrogens have been omitted for clarity.

The complex shares similar ^{1}H and ^{31}P NMR spectra as observed for **24**; dimer **26** also exists as an equilibrating set of *syn* and *anti*-isomers. Two singlets in the ^{31}P NMR spectrum appear at 24.025 and 24.796 ppm, in a ratio close to 1 : 1. The corresponding ^{1}H NMR spectrum shows two sets of triplet of triplets for the central allyl protons, at 5.106 and 4.844 ppm. Two doublets for the *syn*-protons appear downfield at 1.770 and 1.728 ppm and the *anti*-protons resonate as doublets at 1.625 and 1.174 ppm.

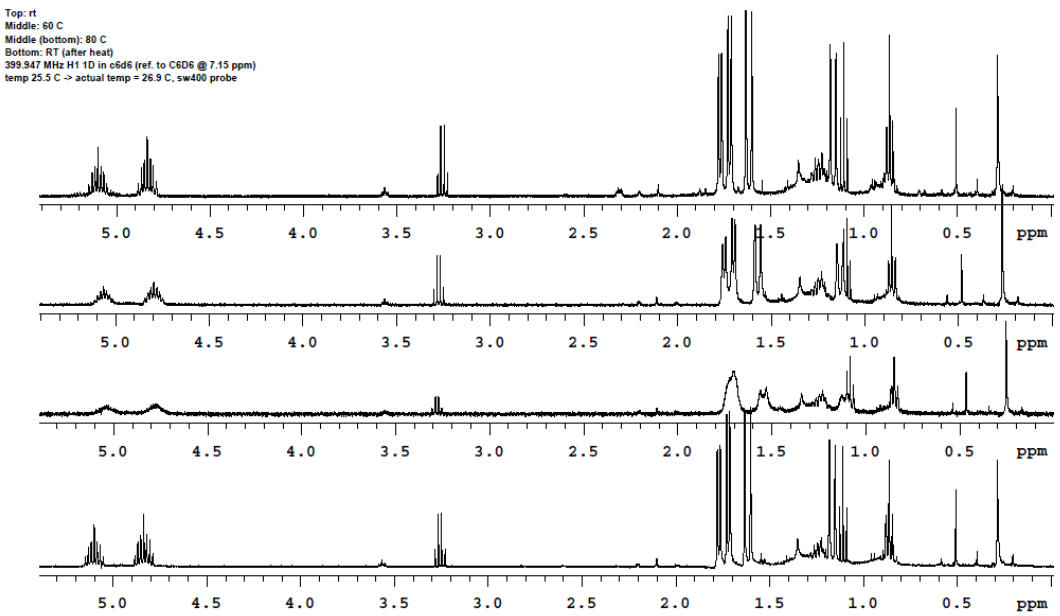

Figure 1.15: Variable temperature ^{1}H NMR spectra of **26**. Top: RT, middle (top): 60 °C, middle (bottom): 80 °C and (bottom): RT (after heating).

Variable temperature ^{1}H and ^{31}P NMR spectroscopy was also performed, at room temperature and in 20 °C increments up to 80 °C. Broadening of the ^{1}H NMR resonances is observed at 80 °C while ^{31}P NMR spectra, at all temperatures, regenerate

the starting material resonances, also suggesting a static Ni-N bond. Upon cooling to room temperature, the allyl peaks of the starting material reappear (Figure **1.15**). No decomposition product is formed at 80 °C, but rapid interchange between the *syn* and *anti*-isomers occurs here, similar to dimer **24**.

1.2.4 Synthesis and partial characterization of $[Ni(\eta^3\text{-}C_3H_5)(NP^tBu_3)]_2$ 27

The tert-butylphosphoranimide complex $[Ni(\eta^3\text{-}C_3H_5)(NP^tBu_3)]_2$ **27** was synthesized according to Equation **1.7**. The pentane-soluble adduct **27** is a green powder, pure by elemental analysis. However, recrystallization of the powder on numerous occasions gave crystals of $[Ni(NP^tBu_3)_2]_2$ **20** and $(^tBu_3PNH)_2NiBr_2$ **28**. These results suggest that dimer **27** is thermally unstable and uniquely proton-sensitive in solution.

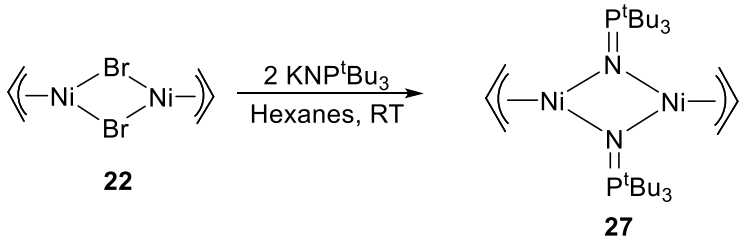

22 **27**

Equation 1.7

Nickel(II) complexes show various magnetic behaviours, depending on the ligand and the coordination environment.[67] Complex **27**, unlike the two analogues, is paramagnetic in solution. Most d^8-complexes of the square planar geometry are diamagnetic.[68] The metal $dx^2\text{-}y^2$ orbital strongly σ-bonds to the ligand, leaving the σ^*

orbital unoccupied.[69] In contrast, in tetrahedral d^8 complexes, degenerate or nearly degenerate orbitals prefer single occupation; therefore, bonding is driven by lower pairing energy and reduced steric interactions. Thus, the sterically bulky *tert*-butyl groups in **27** might be distorted toward the tetrahedral geometry.

1.2.5 Synthesis and characterization of $[Co(\eta^3\text{-}C_3H_5)(NPEt_3)]_2$ 30

The allylcobalt analogues have also been prepared, in collaboration with Dr. K. Revunova in this group. Allylcobalt dimer **29**, a pentane-soluble green solid, was synthesized by slow addition of allyl magnesium bromide to a suspension of $CoCl_2$ in Et_2O. The reaction results in a product pure by elemental analysis, but isolated in low yields, ca. 40%. Repeated attempts to grow single crystals were unsuccessful. Crude **29**, as a THF-soluble adduct, was further used to synthesize a series of allylcobalt trialkylphosphoranimide dimers.

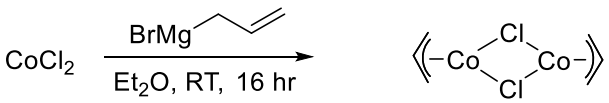

29
40%

Equation 1.8

The reaction of $KNPEt_3$ with **29** provided impure $[Co(\eta^3\text{-}C_3H_5)(NPEt_3)]_2$ **30** (Eq. **1.9**), as determined by elemental analysis. The crude product(s) varied from purple to

green to yellow for different batches, suggesting that the expected product is thermally unstable. Synthesis of **30** at a lower temperature, -78 °C, however, also did not yield clean product. Recrystallization was unsuccessful, suggesting the presence of multiple products, potential redox disproportion, and high disorder. The crude product(s) were paramagnetic, limiting characterization.

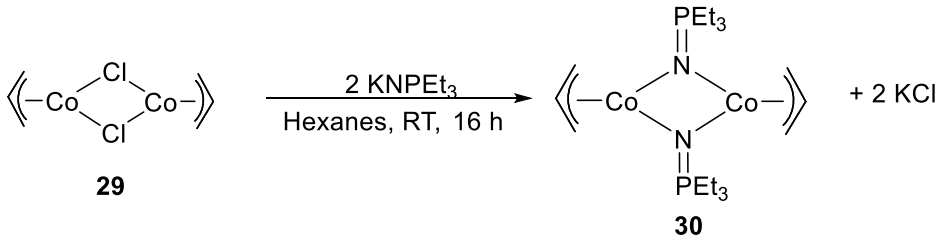

29 **30**

Equation 1.9

1.2.6 Synthesis and partial characterization of [Co(η^3-C_3H_5)(NP^{t}Bu$_3$)]$_2$ 31

The synthesis of [Co(η^3-C_3H_5)(NP^{t}Bu$_3$)]$_2$ **31**, on the other hand (Eq. **1.10**), yields a pentane soluble, orange-brown powder, albeit in low isolated yields (ca. 20%). The

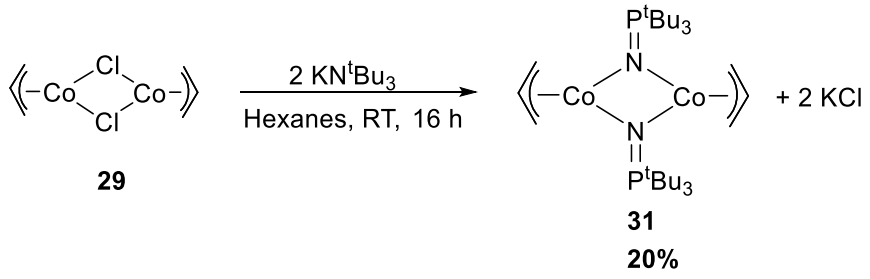

29 **31** **20%**

Equation 1.10

isolated cluster is pure by elemental analysis and was further analyzed using FT-IR spectroscopy (Table **1.1**). This discussion is deferred until the end of this chapter. Analysis of the product by NMR spectroscopy proved impossible as the product is paramagnetic, as expected for Co(II), which is formally d^7. No single crystals have been obtained to date.

1.2.7 Synthesis and partial characterization of $[Fe(\eta^3\text{-}C_3H_5)(NP^tBu_3)]_2$ 33

Due to the abundance, non-toxicity and affordability of iron, designing a catalytically active iron-based precatalyst would be ground-breaking. Thus we synthesized $[Fe(\eta^3\text{-}C_3H_5)(NP^tBu_3)]_2$ **33** using the same two-step method. A suspension of $FeCl_2$ was treated with allyl magnesium bromide overnight, as $FeCl_2$ has low solubility in Et_2O. The reaction yields a pale green powder (50% yield), consistent with the anticipated combustion analysis. We attribute the yields to the poor solubility of $FeCl_2$ and/or product decomposition during the reaction, which can presumably be addressed by further optimization. The product, which may be oligomeric, is partially soluble in THF and insoluble in other organic solvents.

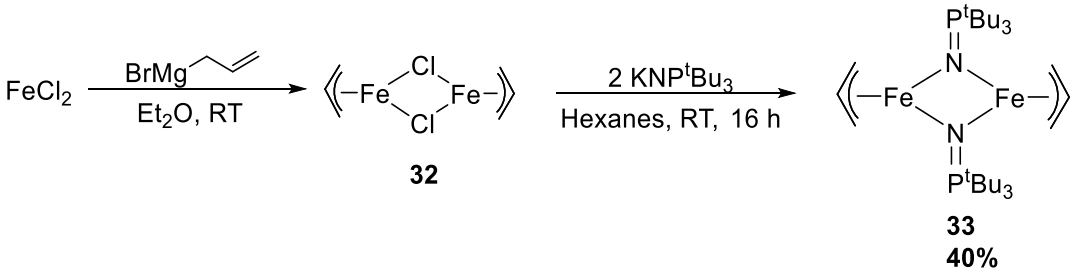

Equation 1.11

Treatment of this material with KNP^tBu_3 afforded a golden yellow powder in 40% yield, which passed elemental analysis for the empirical formula of **33**. To optimize this reaction, we investigated several solvents: THF, toluene and hexanes. A pure batch of **33**, completely soluble in pentanes, was obtained only from the reaction in hexanes. The reactants themselves are soluble in more polar solvents, making purification challenging. Attempts to obtain single crystals have been unsuccessful. The paramagnetic product could not be analyzed by NMR spectroscopy.

1.2.8 FT-IR characterization of complexes, 24, 31 and 33

FT-IR was used to further assess the purity and identities of allylmetal complexes **31** and **33** (Table **1.1**). Nickel dimer **24**, which is fully characterized, was also analyzed and used as a reference standard. We also used the measured IR absorptions for palladium complex **23** as a primary reference for assigning the η^3-allyl absorption peaks.

Assignment of the η^3-allyl and phosphoranimide (N-P) IR absorptions is challenging as the peaks occur in the fingerprint region, from 900–1500 cm^{-1} and near 1000 cm^{-1}, respectively.[70] The M-N absorption is in the far-infrared region, ~500 cm^{-1}, and was not identified.[70] For all three allyl phosphoranimide compounds, however, strong alkyl group C-H absorptions appear from 2800–2990 cm^{-1}, suggesting trialkylphosphoranimide is present in the three clusters.

For the η^3-allyl absorptions of the allylpalladium complex **23**, Nakamato *et al*., assigned the band at 1491 cm^{-1} to the antisymmetric C-C-C stretch, while the bands at 1461 and 1383 cm^{-1} correspond to the CH_2 asymmetric and antisymmetric scissoring modes.[71] The two bands at 1193 and 913 cm^{-1}, are the out-of-plane and in-plane C-H bending modes.[71] Analysis of the IR spectra data for **24**, **31** and **33** (Table **1.1**), reveals similar absorptions in all cases, albeit with slight shifts. The electronic and steric properties of the four complexes differ significantly hence the shift in bond strengths. The absence of a C=C stretch at 1650 cm-^{1} and of an alkene C-H stretch at 3050 cm^{-1}, as observed in η^1-allyl complexes, is also evidence for η^3-allyl coordination to the metal centres.

Table 1.1: Infrared spectra of $[M(\eta^3\text{-}C_3H_5)R]_2$ in the high frequency region[a]

$[Pd(C_3H_5)Cl]_2$ **23**	$[Ni(C_3H_5)(NPEt_3)]_2$ **24**	$[Co(C_3H_5)(NP^tBu_3)]_2$ **31**	$[Fe(C_3H_5)(NP^tBu_3)]_2$ **33**
1491 (w)	1490 (w)	1484 (s)	1484 (s)
1461 (s)	1454 (m)	1473 (s)	1471 (s)
1383 (s)	1411 (m)	1387 (s)	1388 (s)
1193 (w)	1192 (w)	1191 (w)	1189 (w)
913 (w)	908 (w)	930 (w)	929 (w)

Frequency reported in cm^{-1}. [a] Samples were dissolved in pentane in the drybox and submitted as a cast film on KBR plates designed for air sensitive samples. w= weak, m= medium, s= strong

Although IR spectroscopy is not definitive, the observed bands show that η^3-allyl and phosphoranimide ligands exist in complexes **31** and **33**. These crude products thus correspond to the proposed structures. However, X-ray crystallography is imperative to confirm the proposed structures.

1.3 Conclusion

In summary, clusters of the form $[M(\eta^3\text{-}C_3H_5)(NPR_3)]_2$, M = Fe, Co and Ni; R = Et, Ph and ^{t}Bu, have been successfully synthesized and at least partially characterized. Attempts to fully characterize the solid state structures of the three $[M(\eta^3\text{-}C_3H_5)(NP^tBu_3)]_2$ clusters, M = Fe, Co and Ni, using X-ray crystallography remain under pursuit. The structures of $[Ni(\eta^3\text{-}C_3H_5)(NPEt_3)]_2$ **24** and $[Ni(\eta^3\text{-}C_3H_5)(NPPh_3)]_2$ **26** were completely characterized. Variable temperature NMR spectroscopy of nickel complexes **24** and **26** suggest a dynamic allyl system. At reaction conditions, this is expected to encourage allyl hydrogenolysis and hydrogenation, forming the active hydride clusters essential for catalysis.

The series of complexes show distinct electronic and steric properties; hence, we anticipate different catalytic activities. Catalysis of simple hydrogenation reactions will in turn help us optimize our hydrotreatment catalyst design. Additionally, with ready

access to diamagnetic clusters **24** and **26,** mechanistic NMR studies can be done. These studies will in turn be used for further catalyst development.

Chapter 2. Hydrogenation of alkenes and alkynes using dimeric allyl-capped trialkylphosphoranimide clusters

2.1 Introduction

Transition metal-catalyzed hydrogenation of unsaturated organic compounds is extensively studied in organometallic chemistry because of its diverse applications in general organic synthesis as well as in industry (e.g. petrochemicals and food industries).[72,73,74,75] In the food industry, hydrogenation is predominantly used for processing vegetable oils (polyunsaturated fatty acids). During hydrogenation, fatty-acids are partially hydrogenated into solid or semi-solid fats.[76,77] Partially hydrogenated fats are stable towards oxidation and available in various consistencies.[78] In petrochemical processes, hydrogenation is used to saturate alkenes and aromatic compounds into stable and less toxic alkanes and cycloalkanes.[79,80] High aromatic content in fuels results in carcinogenic exhaust particle formation along with poor fuel quality.[81] Hence it is essential to reduce aromatic content in fuels.

Industrial processes predominantly involve heterogeneous catalysts. A heterogeneous catalyst exists in a different phase from the reaction medium. As a result, catalyst separation from products and/or reactants is facile.[82] This often results in lower operational costs and isolation of pure products. Heterogeneous catalysts are also thermally more stable, which increases their lifetime in industrial reactors. However,

such catalysts generally show low activity under mild reaction conditions, since the reaction only occurs on the exposed surface. When the active surface is saturated with reactants, the reaction cannot proceed until some products leave the surface, creating adsorption sites for new reactants. Hence many processes require harsh reaction conditions. Because these catalysts are insoluble and lack well-defined active sites,[83] catalyst development can be very challenging. Furthermore, synthetic procedures and catalytic reaction conditions influence active site formation and evolution.[84] These active sites show different reaction rates and pathways leading to unpredictable and/or reduced catalyst selectivity.

A conceptual alternative to heterogeneous catalysis is homogeneous catalysis. Homogeneous catalysts are soluble and have well-defined active sites, which facilitate spectroscopic and mechanistic studies.[83] For this reason, homogeneous catalysis' reaction mechanisms are better understood and can be used to "fine-tune" catalyst design. Unlike heterogeneous catalysts, homogeneous catalysts can show high activity under milder reaction conditions.[84] In the latter, the catalyst exists in the same phase as the reactants; hence, all active sites are accessible for reaction. These active sites also have identical steric and electronic environments, promoting "single site" catalysis and increased selectivity. However, recovery of the often-expensive homogeneous catalysts is challenging. Catalyst recovery often involves product distillation at high temperatures, which can lead to catalyst decomposition.[85] As a result, only a few homogeneous catalysts are used in industry.

The distinction between homogeneous and heterogeneous catalysis for any specific process is not, however, trivial because soluble transition metal complexes can decompose into soluble nanoclusters.[86] A common method to assess homogeneity *versus* heterogeneity is catalyst-poisoning using mercury. Excess Hg(0) in catalytic reactions generally poisons heterogeneous metal(0) catalysts by physi-adsorption or amalgamation, suppressing the catalyst's activity.[49] However, false-negative and false-positive results can occur. First, mercury does not form stable amalgam with all metals, in particular with iron.[87,88,89] For this reason, the absence of suppressed activity is not absolute proof of homogeneity. Second, mercury can react with some complexes in solution, deactivating homogeneous catalysts, resulting in false-positive results.[90] Thus, Finke *et al*., summarized a four-category general approach that must be used to conclusively distinguish between homogeneous and heterogeneous catalysts (Figure **2.1**).[91]

Recent advances in catalytic hydrogenation target selective partial alkyne hydrogenation.[92] This process has diverse applications in the pharmaceutical and petrochemical industries.[93,94,95] Hydrogen sources other than H_2 have also been investigated, including ammonia borane (NH_3BH_3), methanol (MeOH), formic acid (HCOOH), triethyl silane (Et_3SiH), and several basic amines because of their ease of transportation and handling.[96]

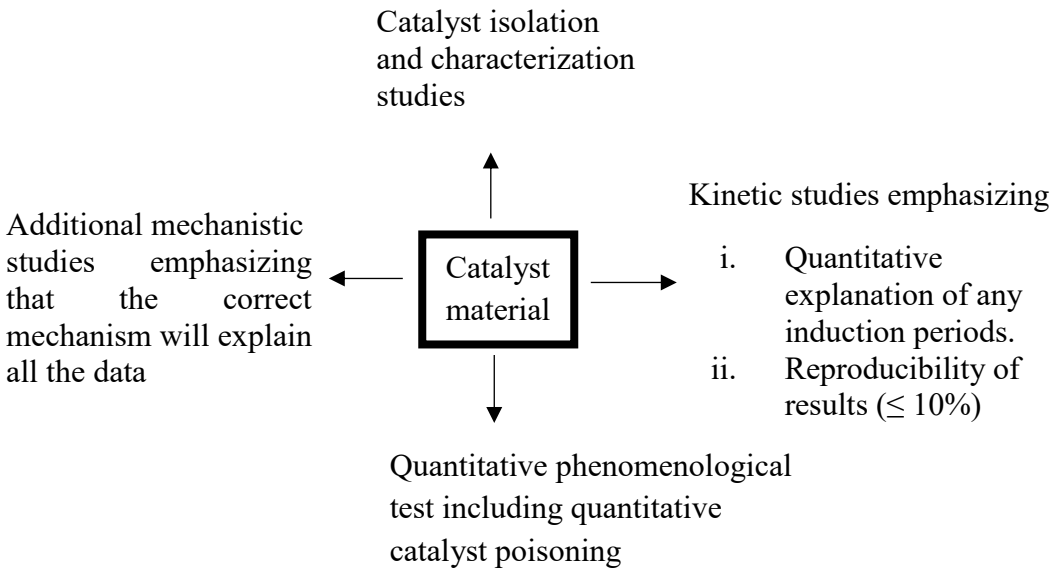

Figure 2.1: A general experimental approach for distinguishing homogeneous catalysts from heterogeneous catalysts

The hydrogenation of internal alkynes generally proceeds by three competitive reactions: i) full reduction to alkane, ii) partial hydrogenation to either *cis*- or *trans*-alkene, and iii) isomerization of *cis*- to *trans*-alkene (Scheme **2.1**).[97] For this reason, alkyne semi-reduction is challenging, but not impossible. For example, Lindlar's catalyst ($Pd/CaCO_3$, $Pb(OAc)_2$, quinoline) is efficient in partial hydrogenation of alkynes to give *Z*-alkenes.[98] This catalyst however, has a few drawbacks: i) facile *Z* to *E*-alkene isomerization, ii) use of toxic $Pb(OAc)_2$, and iii) over-reduction to the alkane,[99] hence current research into more efficient systems.

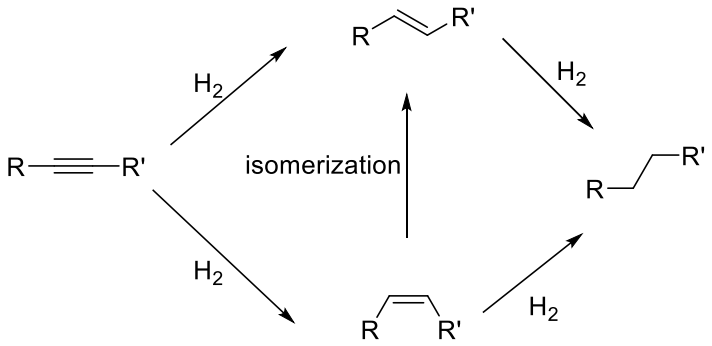

Scheme 2.1: Reaction scheme for the hydrogenation of alkynes

Recent developments in selective partial alkyne hydrogenation also includes the use of less toxic, earth-abundant first-row transition metal catalysts. For example, Garcia, *et al.*, reported the activity of [(dippe)Ni(μ-H)]$_2$ in partial hydrogenation of diphenylacetylene **38**, using NH_3BH_3 as the hydrogen source.[100] Selectivity was highly dependent on the solvent choice (Scheme **2.2**). The reaction in coordinating 1,4-dioxane favours the formation of *cis*-stilbene (83%), whereas the use of methanol promotes *cis*- to *trans*-stilbene isomerization, selectively producing *trans*-stilbene (86%). However, the reactions require prolonged reaction time (72 hours) for complete conversion.

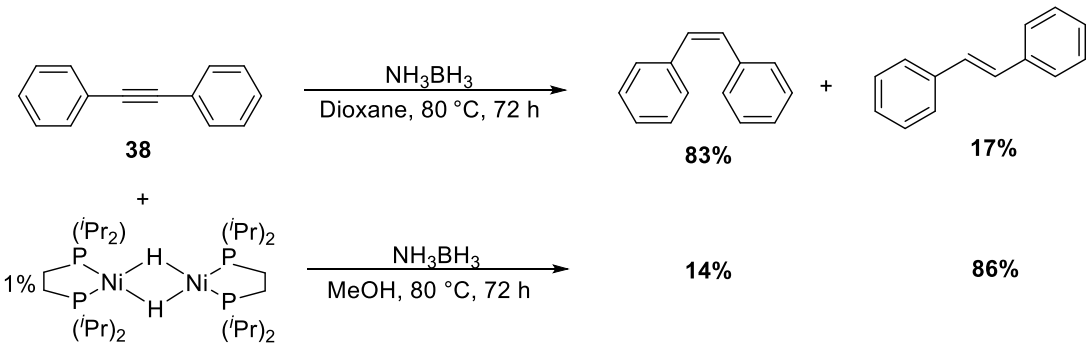

Scheme 2.2

Liu, *et al.*, reported the use of ligand-controlled cobalt catalysts to selectively reduce diphenylacetylene to either *cis* or *trans*-stilbene (Eq. **2.1**).[72] Interestingly, a small change in phosphine steric bulk from ^{i}Pr to ^{t}Bu significantly influences stereoselectivity. The less bulky system promotes *trans*-stilbene formation, as the catalyst facilitates the isomerization of *cis*-stilbene. For instance, complex **II** produces 8% *cis*-stilbene and 92% *trans*-stilbene, while pyridyl complex **III** results in the formation of 100% *trans*-stilbene. Highly hindered complex **I**, on the other hand, results in 94% *cis*-stilbene and 5% *trans*-stilbene.

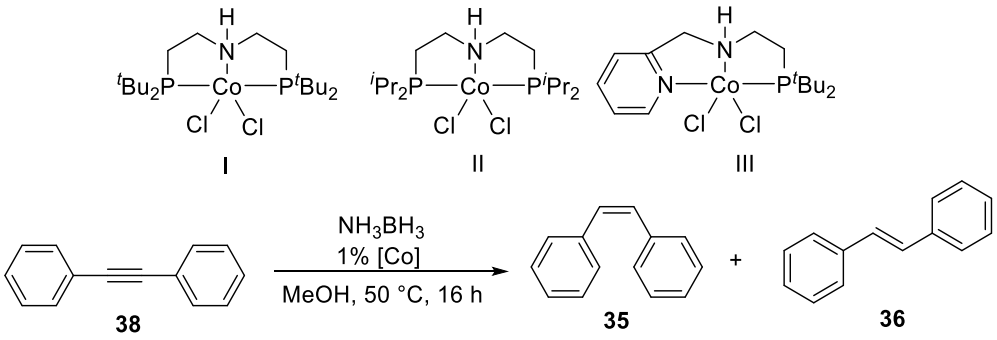

Equation 2.1

Non-toxic and extremely abundant ubiquitous iron has also been investigated for the development of alkyne and alkene hydrogenation catalysts.[73,87,101] Milstein and coworkers reported that an iron pincer complex selectively hydrogenates alkynes to the *E*-isomer *via cis*-to-*trans* isomerization under relatively mild conditions (Eq. **2.2**).[102] Higher activity and better selectivity were observed using a less coordinating solvent,

THF (99% trans-stilbene), as compared to methanol (12% cis-stilbene; 7% of trans-stilbene).

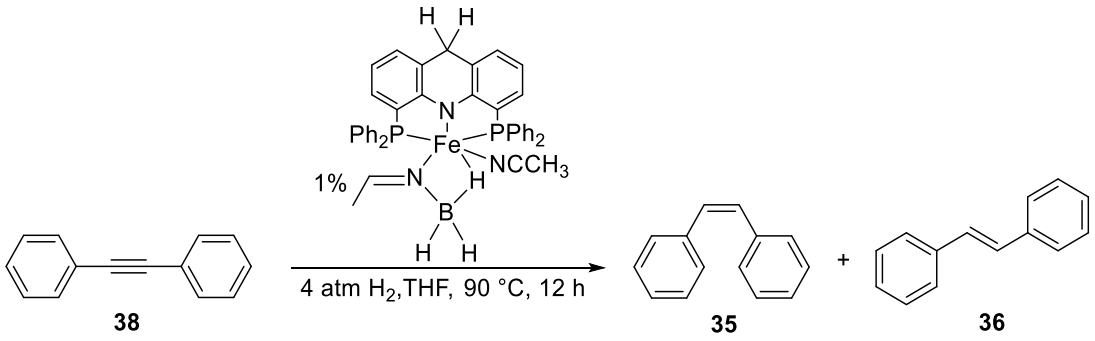

Equation 2.2

Our group has recently developed low-coordinate late first-row transition metal phosphoranimide clusters for applications to homogeneous and heterogeneous hydrodesulfurization and hydrodenitrogenation catalysis. Before HDS studies, alkene and alkyne hydrogenation activity is determined to establish the potential of the catalysts for more strenuous reactions. For this reason, extensive mechanistic studies on alkene and alkyne hydrogenation were not conducted. In this chapter, catalytic hydrogenations of allylbenzene **33**, diphenylacetylene **38**, *cis*-stilbene **35** and *trans*-stilbene **36** using the new catalysts, $[M(\eta^3\text{-}C_3H_5)(NPR_3)]_2$, M = Fe, Co or Ni **(24, 26, 31, 33)** are reported.

2.1 Results and discussion

2.1.1 Hydrogenolysis of nickel-allyl complex, [Ni(η^3-C_3H_5)($NPEt_3$)$_2$] 24

When η^3-allyl complexes of many transition metals are treated with hydrogen, the allyl group is hydrogenated and cleaved, affording propene (or propane) and the transition metal hydride.[103,104] The hydrogenolysis involves an η^1-allyl intermediate, which creates an empty coordination site for hydrogen activation.[105] Before studying catalytic hydrogenation, the stoichiometric hydrogenolysis and hydrogenation of allyl cluster **24** was investigated. As reported (Chapter 1), at 80 °C in the absence of hydrogen, cluster **24** undergoes rapid η^3-η^1-η^3 allyl conversion with concomitant η^1-allyl homolytic cleavage and dimerization to 1,5-hexadiene. In the presence of hydrogen, we anticipate the formation of propane and some form of active nickel hydride. Hydrogenolysis of the bridging triethylphosphoranimide to triethylphosphoranimine is also possible.

Thus, allyl dimer **24** in C_6D_6 under one atm H_2 was heated in sealed NMR tubes at 60 °C and 80 °C for one hour. After cooling to room temperature, ^{1}H and ^{31}P NMR spectroscopy were performed. ^{31}P NMR spectroscopy generated only starting material resonances, whereas the ^{1}H NMR spectrum revealed neither propane nor upfield Ni-H resonances.

Hydrogenolysis was also performed in a medium-walled glass reactor with efficient magnetic stirring which improves hydrogen dissolution kinetics and/or mass transfer. During heating, the solution changes from golden-yellow to dark brown. The gaseous phase was collected by vacuum transfer into a jointed NMR tube containing degassed C_6D_6. Analysis by ^1H NMR spectroscopy revealed only propane resonances, as determined by comparison with a literature spectrum.

To identify nickel hydride(s) and/or triethylphosphoranimine in the reaction mixture, the crude product was analyzed using ^1H and ^{31}P NMR spectroscopies. The spectra revealed only starting material. Under these reaction conditions, the Ni-N bond is thus more stable and less susceptible to hydrogenolysis than is the Ni-allyl bond. The absence of a nickel hydride resonance suggests that the hydride intermediate is unstable to isolation. Further studies are, however, essential to detect and/or isolate nickel hydride(s) intermediates.

2.1.1 Catalytic hydrogenation using [Ni(η^3-C_3H_5)(NPEt$_3$)]$_2$ 24

2.2.2.1 Alkene hydrogenation

Since cluster **24** is activated under reasonable conditions, we proceeded to investigate its activity in terminal and internal alkene hydrogenation (Scheme **2.3**). Allylbenzene **34** hydrogenation proceeded slowly to 80% propylbenzene without

detectable alkene isomerization to β-methylstyrene. For *cis*-stilbene **35,** the reaction afforded 12% *trans*-stilbene **36** and 22% bibenzyl **37.** *Trans*-stilbene was converted at an even notably slower rate, giving 7% bibenzyl as the sole organic product. These results suggest that precatalyst **24** is not efficient in alkene hydrogenation, attributed to the slow activation of **24** to generate the active species. Higher temperatures and pressures are likely to improve hydrogenation rate, but may also decompose the catalyst.

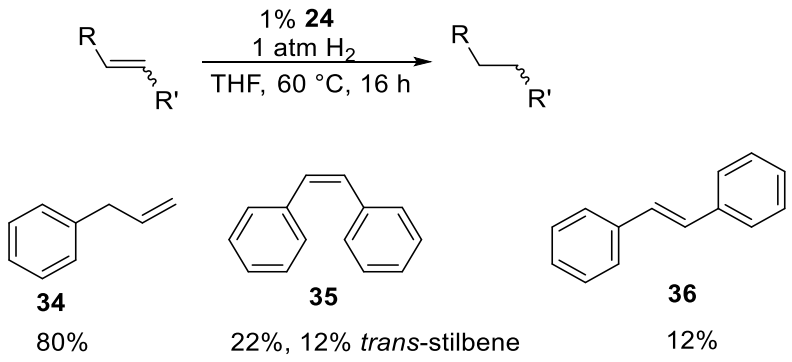

Scheme 2.3

The kinetic preference for hydrogenation of *cis*-stilbene on the other hand suggests that the coordination and insertion of *cis*-stilbene occurs faster than that of *trans*-stilbene (Scheme **2.4**). This is expected, as *cis*-stilbene is less thermodynamically stable and less sterically hindered. These results also establish that for *cis*-stilbene, part of the isomerization product is also hydrogenated to bibenzyl.

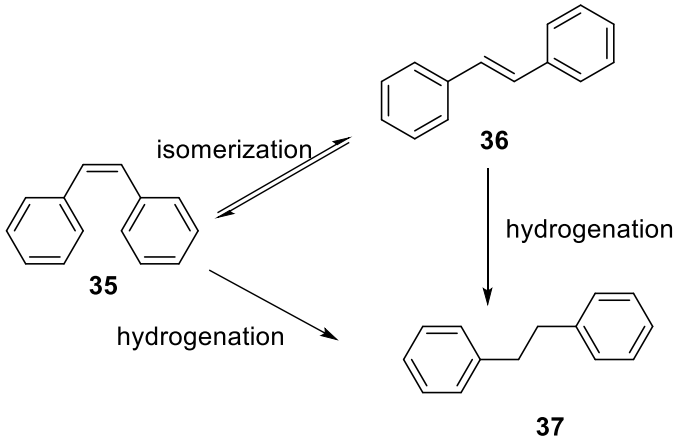

Scheme 2.4: Reaction scheme for the hydrogenation of **35**

2.2.2.2 Diphenylacetylene hydrogenation

Next, diphenylacetylene **38** hydrogenation was performed under various conditions (Table **2.1**) since temperature and solvent choice can influence the stability of the active species, the intermediate(s), and product solubility.[106] As expected, the hydrogenation rates and product selectivity were highly dependent on solvent choice and temperature. No conversion was observed at room temperature whereas at 60 °C, conversion to a mixture of stilbenes and bibenzyl was observed, suggesting competitive alkene reduction and isomerization reactions. On the other hand, notably lower conversions were observed at 80 °C, indicating catalyst decomposition into inactive material. At 60 °C, *trans*-stilbene was selectively formed in toluene (Entry 2), whereas in THF conversion primarily proceeded to both *cis*-stilbene and *trans*-stilbene (Entry 3).

Table 2.1: Summary of the hydrogenation of **38** with 1 mol% **24**.[a]

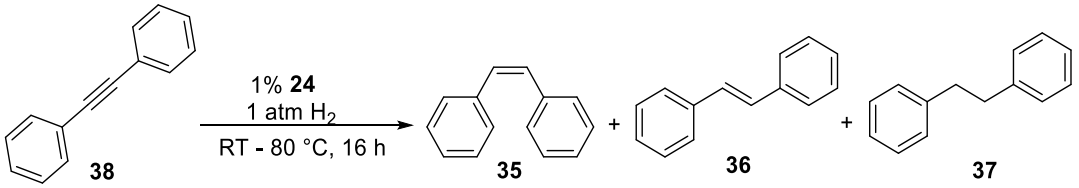

Entry	Solvent	Temperature (°C)	Total conversion	Conversion (%)[b]		
				35	**36**	**37**
1	THF	RT	0	0	0	0
2	Toluene	60	100	11	71	18
3	THF	60	100	31	56	13
4[c]	THF	60	87	78	1	8
5[d]	THF	60	85	85	6	9
6	Toluene	80	26	16	10	0
7	THF	80	27	17	10	0

a. Reactions were conducted in sealable medium walled glass pressure reactors charged with 1 atm H_2. The reactors were immersed in an aluminium dry block adapter plate equipped with a thermostat stirred vigorously for 16 hours at the set temperature. After 16 hrs, the reactions were opened to air and quenched with water and the organic phase extracted 3 times using the corresponding solvent.

b. Results obtained by quantitative GC using dodecane as internal standard. Remaining material is diphenylacetylene. c. Reaction performed at 34 atm H_2 d. 5 mol% precatalyst loading was used

Surprisingly, high hydrogen pressure (34 atm) and high catalyst loading (5 mol%) in THF and 60 °C separately favoured conversion to *cis*-stilbene (Entry 4-5). These results suggest that THF inhibits catalyst activity since lower *cis*- to *trans*-stilbene isomerization and hydrogenation to bibenzyl is observed in THF. At the same time, these results establish that diphenylacetylene coordination and reduction occurs faster than stilbene reduction, otherwise greater conversion to bibenzyl would be observed. Furthermore, these results also suggest that hydrogenation proceeds *via* partial

hydrogenation to the stilbenes with subsequent hydrogenation to the saturated product, however, time studies are necessary to establish the reaction pathway.

Based on these results a generalized reaction mechanism is proposed (Figure **2.2**) assuming the precatalyst remains dimeric under these reaction conditions. It is also likely that the catalyst decomposes to heterogeneous material (*vide infra*) as suggested by the results obtained at 80 °C (Entries 6-7), therefore, the mechanism is highly tentative as mechanistic studies have not been performed.

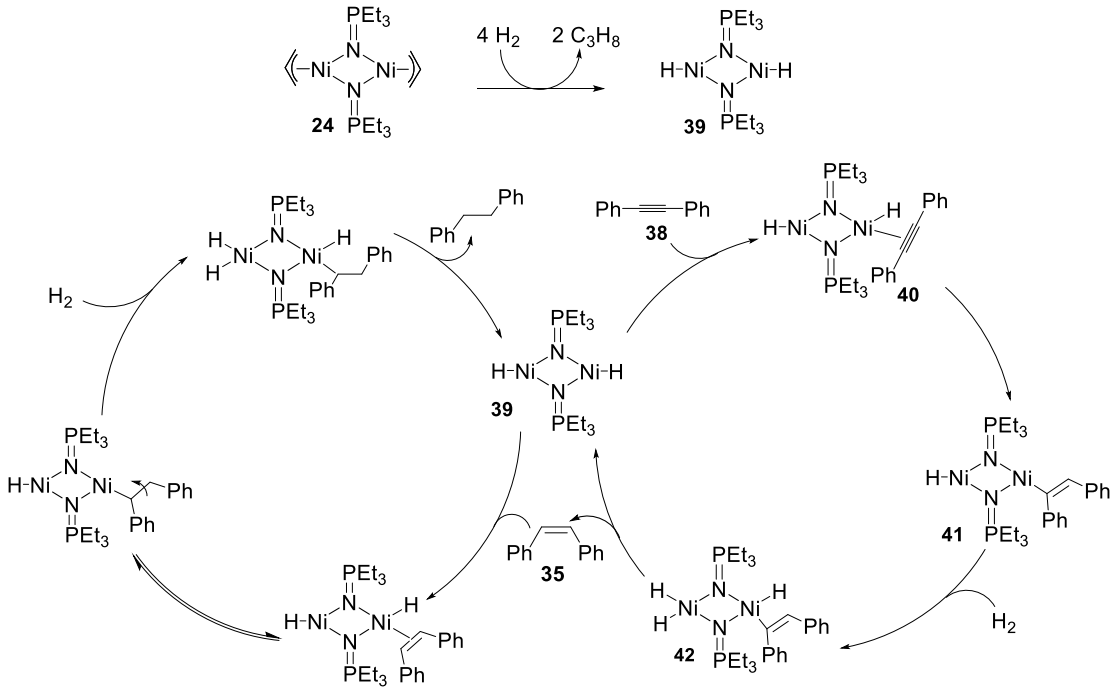

Figure 2.2: Generalized allyl nickel catalyzed alkyne hydrogenation mechanism

First, precatalyst **24** is transformed into the active catalyst **39** *via* allyl ligand hydrogenolysis which proceeds at a slow rate and hence is rate limiting. In the second step, the alkyne coordinates to nickel followed by hydride migratory insertion from nickel to the alkyne to form a *cis*-vinyl intermediate **41** (step *iii*). Bimetallic hydrogen activation occurs resulting in a trihydridonickel cluster **42.** Subsequent bimetallic reductive elimination releases *cis*-stilbene and generates the active catalyst.[107,108] *Cis*-stilbene recoordinates to the active catalyst followed by hydride migration from nickel to the stilbene resulting in a nickel-alkyl intermediate. Since our results suggest that M-alkyl hydrogenolysis is slow whereas *cis*- to *trans*-stilbene isomerization is fast, the alkyl-nickel and the η^2-alkene nickel complexes are in equilibrium. An equilibrium between the two complexes facilitates rotation about the C-C σ-bond, and subsequent reverse β-hydride elimination and metal-vinyl hydrogenolysis affords *trans*-stilbene. Bimetallic hydrogen activation of the alkyl-nickel complex followed by bimetallic reductive elimination generates bibenzyl and the active catalyst.

2.2.2.3 Catalyst homogeneity studies

Under reducing conditions, precatalysts can exist as transition-metal complexes or they can decompose to form either nanoparticles or metal films,[109] and since the results obtained at 80 °C suggest catalyst decomposition, several studies were performed to investigate the homogeneity of the catalyst.

i) Reproducibility of diphenylacetylene hydrogenation

Reproducible reaction kinetics are usually an indication of a homogeneous system,[109] hence diphenylacetylene hydrogenation (60 °C, one atm H_2, THF) was performed using different precatalyst **24** batches prepared the same way. The reactions afforded irreproducible conversion rates of 20 – 100% (Figure **2.4**).

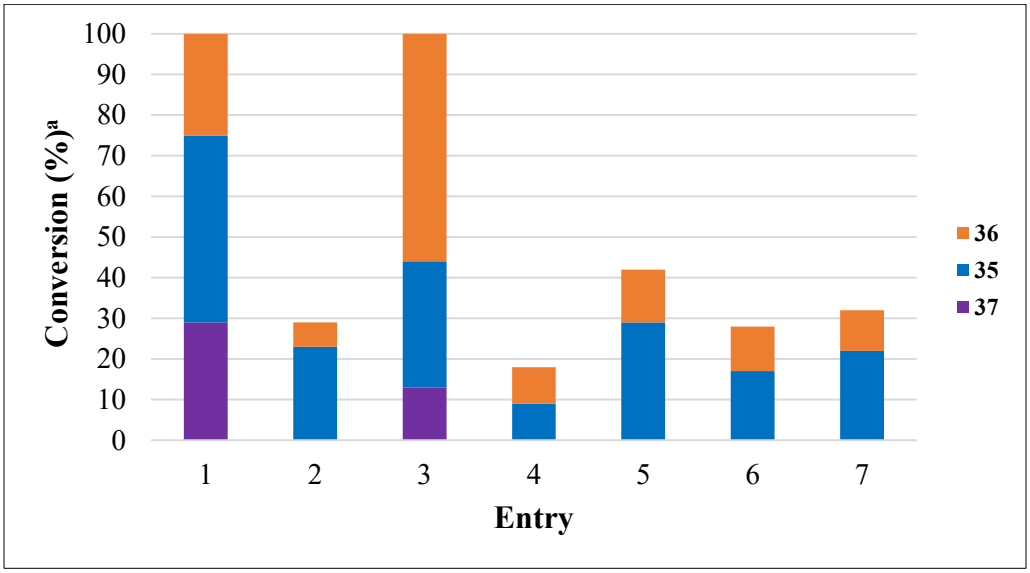

a. Reactions were conducted in sealable medium walled glass pressure reactors charged with 1 atm H_2 and THF. The reactors were immersed in an aluminium dry block adapter plate equipped with a thermostat. The reactions were stirred vigorously for 16 hours at 60 °C. Results were obtained by GC with dodecane as the standard. Remaining material is diphenylacetylene.

Figure 2.3: Reproducibility hydrogenation studies of **38** with 1 mol% **24.** Blue: *cis*-stilbene, orange: *trans*-stilbene, purple: bibenzyl.

There is also no trend in product selectivity. **Entry 3** shows selective formation of *trans*-stilbene but in **Entry 4**, equal conversion to *cis*- and *trans*-stilbene is observed. In all other entries, *cis*-stilbene is favoured. Meanwhile, significant conversion to

bibenzyl is only observed in **Entries 1** and **3**. These results reveal multiple catalyst sites and reaction pathways, suggesting at least partial decomposition to a heterogeneous system.[109,110,111,49]

ii) Catalyst heterogeneity: mercury test

To test catalyst heterogeneity, excess elemental mercury was added to reaction solutions. Excess mercury significantly inhibits the catalyst' activity, both at 60 °C and 80 °C (Figure **2.3**). Thus, we conclude that the active catalyst(s) is mainly heterogeneous at these temperatures.

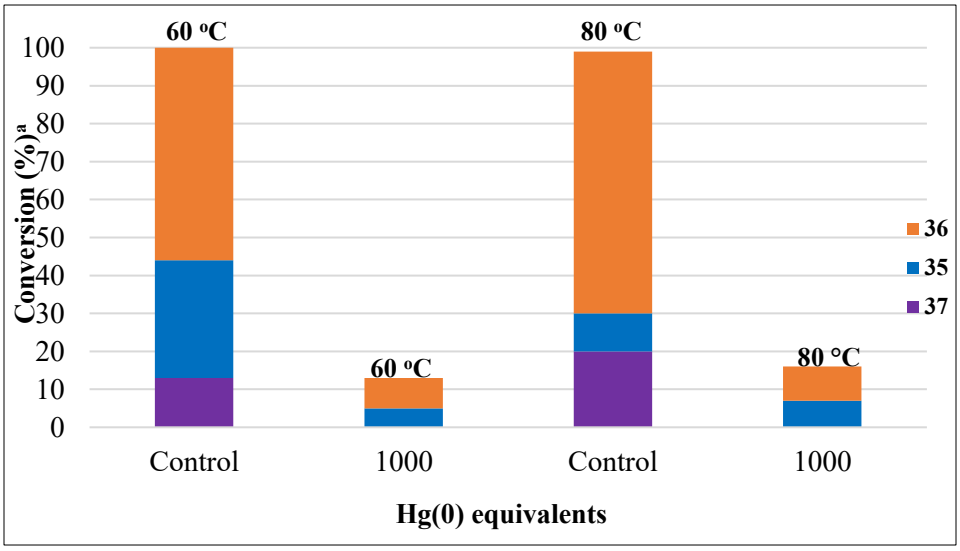

a. Sealable medium walled glass reactors were charged with THF, **24**, **38**, Hg and 1 atm H_2. The reactors were immersed in an aluminium dry block adapter plate equipped with a thermostat and heated at either 60 or 80 °C under vigorous stirring for 16 hours respectively. Calibrated GC results, remaining material is diphenylacetylene. The above reactions were performed side by side using the same precatalyst batch.

Figure 2.4: Hydrogenation of **38** using 1 mol% of **24** in the presence of Hg(0). Blue: *cis*-stilbene, orange: *trans*-stilbene, purple: bibenzyl.

iii) Identification of an induction period

The heterogeneity of the catalyst was further studied by investigating the intervention of an induction period. Long induction periods can be the result of precatalyst activation by reduction to colloidal or bulk metal(0) and can sometimes be reduced by pretreating the precatalyst under hydrogen.[112,113] For example, Blum, *et al*., observed an induction period in olefin hydrogenation using a Rh(III) precatalyst.[114] Pretreating the precatalyst under hydrogen eliminated this induction period with concomitant black precipitate formation indicative of Rh(0). Similarly, Whitesides reported that hydrogenation rates using (1,5-cyclooctadiene)dimethylplatinum(II) correlated directly with the reduction of Pt(II).[110]

When cluster **24** was heated in the presence of hydrogen, the solution intensified from golden-brown to dark brown, which can be indicative of soluble nanocluster formation.[115] Diphenylacetylene hydrogenation using this material afforded 62% conversion in just 4 hours whereas 32% was obtained in 16 h when **24** was not preactivated (Figure **2.5**). Thus, preactivating **24** significantly reduces the induction period. However, hydrogenation studies using isolated Ni(0) nanoclusters are necessary to establish the actual catalyst.[109]

In separate control reactions, **24** was heated in the absence of either H_2 or the substrate. No colour change was observed. Diphenylacetylene hydrogenation was also

investigated using this material. After 16 h, 55% overall conversion was observed, higher than the 32% conversion obtained without preactivation. This suggests precatalyst decomposition to active material. Precatalyst decomposition to M(0) with the evolution of 1,5-hexadiene under thermal conditions is known in other η^3-allyl complexes, including $[Pd(\eta^3\text{-}C_3H_5)(PPh_3)_2]BF_2$,[116] $[Pd(\eta^3\text{-}C_3H_5)(acac)]$,[117] and $[Fe(\eta^3\text{-}C_3H_5)(CO)_3]$.[117]

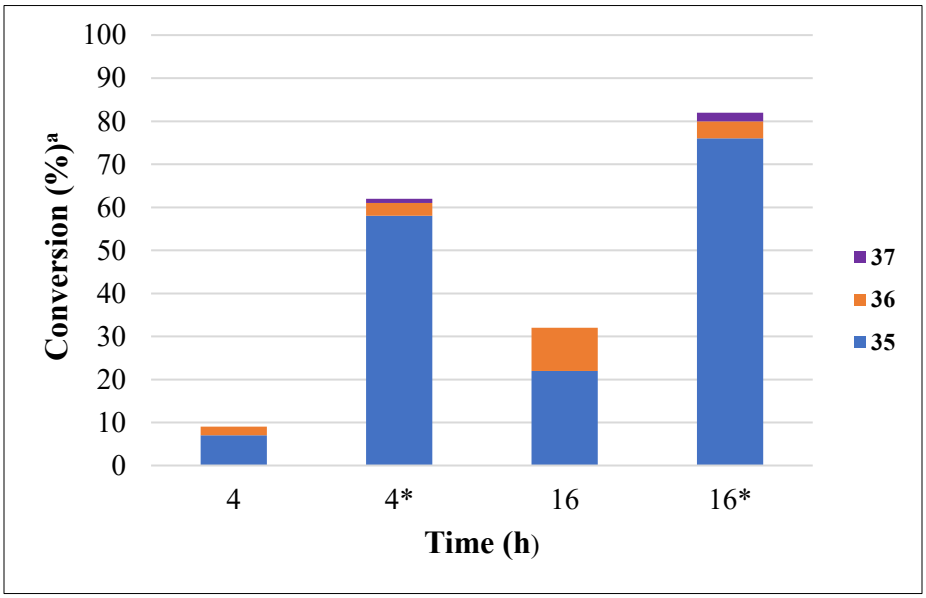

a. Sealable medium walled glass reactors were charged with THF, **24**, **38** and 1 atm H_2. The reactors were immersed in an aluminium dry block adapter plate equipped with a thermostat and heated at 60 °C under vigorous stirring for 4 or 16 hours respectively. Results obtained by GC.

* Cluster **24** was pretreated with 1 atm H_2 and THF in sealable medium walled glass reactors and heated for an hour at 60 °C in an aluminium dry block plate. The reactors were cooled to RT and charged with **38** in the glovebox and further heated for 4 or 16 hours respectively. Calibrated quantitative GC results using dodecane as internal standard.

Figure 2.5: Hydrogenation of diphenylacetylene with or without preactivating **24.** Blue: *cis*-stilbene, orange: *trans*-stilbene, purple: bibenzyl.

Further tests are, however, necessary to determine conclusively the phase of the true catalyst. We initially plan to pursue catalyst isolation and analysis by transmission electron microscopy (TEM). TEM will determine the particle size of the active phase, including the presence or absence of coordinated phosphoranimide.

2.1.2 Catalytic hydrogenation using [Ni(η^3-C_3H_5)($NPPh_3$)]$_2$ 26

As a control, the hydrogenation activity of the relatively electron deficient and more stable triphenylphosphoranimide dimer **26** was investigated. Dimer **26** was less efficient in *cis*- and *trans*-stilbene hydrogenation (Scheme **2.5**). The slow reaction rates indicate even slower precatalyst **26** activation attributed to the stability of **26** (Chapter 1). A stable system suggests slow η^3-η^1 allyl conversions, suppressing hydrogen activation leading to increased induction periods and reduced catalyst activity.

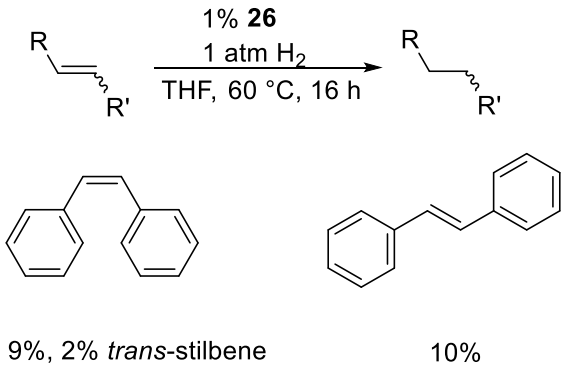

Scheme 2.5

Under the same conditions, diphenylacetylene hydrogenation proceeded at a similar rate to 8% bibenzyl with traces of *cis*-stilbene (Eq. **2.5**). Slightly higher conversions, primarily to *cis*-stilbene were observed at 80 °C (Eq. **2.5**). However, at 80 °C, the catalyst is mainly heterogeneous which is attributed to a more dynamic allyl system, promoting decomposition (Chapter 1).

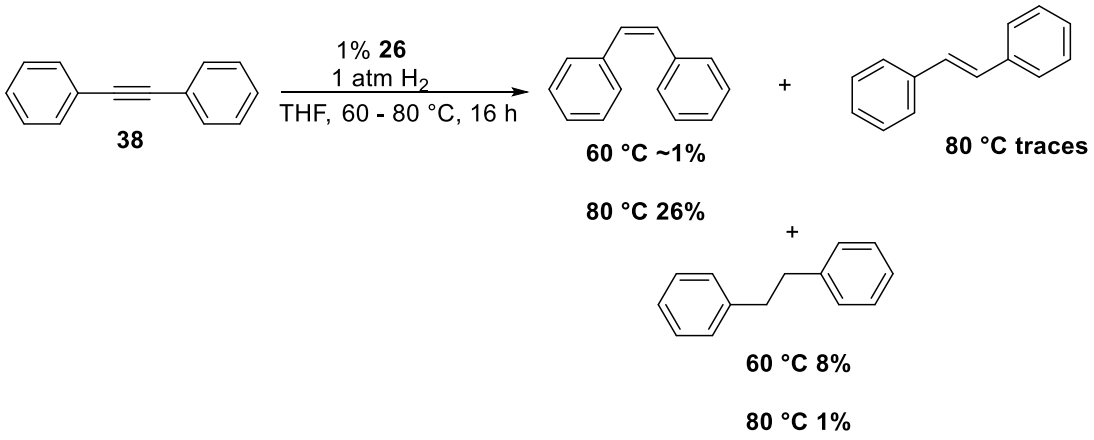

Equation 2.5

2.1.3 Comparing cobalt and nickel: Catalytic hydrogenation using [Co(η^3-C_3H_5)(NP^tBu_3)]$_2$ 31

Next, we investigated the activity of cobalt precatalyst **31** in diphenylacetylene hydrogenation. Unlike nickel cluster **24,** conversion was favoured in THF when compared to toluene (Table **2.3**, entry 1 *vs* 2). This suggests that THF stabilizes the activation process or the active catalyst itself. The activity of cobalt cluster **31** at room temperature also conclusively shows that it is a better hydrogenation catalyst when

compared to the nickel clusters **24** and **26**. The more electron donating ligand probably promotes a much more dynamic allyl system, even at room temperature, improving precatalyst activation. However, a dynamic system also suggests reduced catalyst stability indicated by the lower conversions at higher temperatures (Entry 2 *vs* 3). The lower conversions suggest catalyst decomposition to inactive material. Heterogeneity studies using this precatalyst are necessary, but limited by material availability. Such catalyst decompositions are also apparent in some allyl systems. For example, the high activity of Co(η^3-allyl)(P(OiPr$_3$))$_3$ in benzene hydrogenation is accompanied by a short lifetime when compared to less active Co(η^3-allyl)(P(OMe$_3$))$_3$.[118]

Table 2.2: Summary of the hydrogenation studies of **38** using 1 mol% **30**[a]

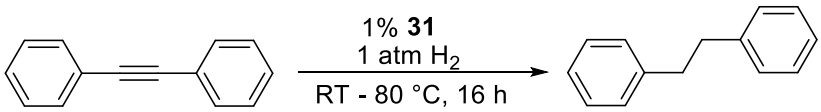

38 **37**

Entry	Solvent	Temperature (°C)	Conversion (%)[b]
			37
1	Toluene	RT	0
2	THF	RT	22
3	THF	50	9
4	THF	80	12

a. Reactions were conducted in sealable medium walled glass pressure reactors charged with **30**, 1 atm H_2 and THF. The reactors were immersed in an aluminium dry block adapter plate equipped with a thermostat set at 50/80 °C. The reactions were stirred vigorously for 16 hours.
b. Results obtained by GC with dodecane as the standard. Remaining material is **38.**

2.1.4 Catalytic hydrogenation using $[Fe(\eta^3\text{-}C_3H_5)(NP^tBu_3)]_2$ 33

Iron cluster **33** also catalyzes diphenylacetylene and *trans*-stilbene hydrogenation at room temperature (Eq. **2.6**), although at a slower rate when compared to cobalt cluster **31.** However, as with **31**, higher temperatures suppress catalyst activity. No diphenylacetylene hydrogenation was observed at 60 °C, establishing that **33** also decomposes rapidly into an inactive species. Interestingly, diphenylacetylene and *trans*-stilbene hydrogenation proceeded at the same rate when **33** was used. This suggests diphenylacetylene reduction proceeds *via* partial hydrogenation to *trans*-stilbene which is further reduced to bibenzyl.

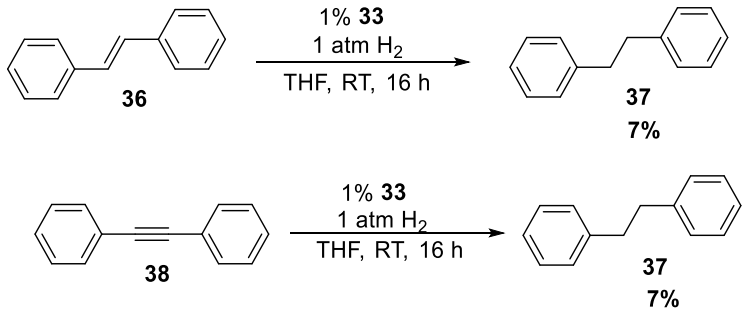

Equation 2.6

2.1.5 Proposed precatalyst activation mechanisms

The nature of the active catalyst(s) in these reactions remains poorly understood. However, some mechanistic points for precatalyst activation can be deduced from the results obtained and are summarized in Figure **2.6**. It is possible for one or more of these

mechanisms to be present in one reaction, explaining different reaction pathways and rates.

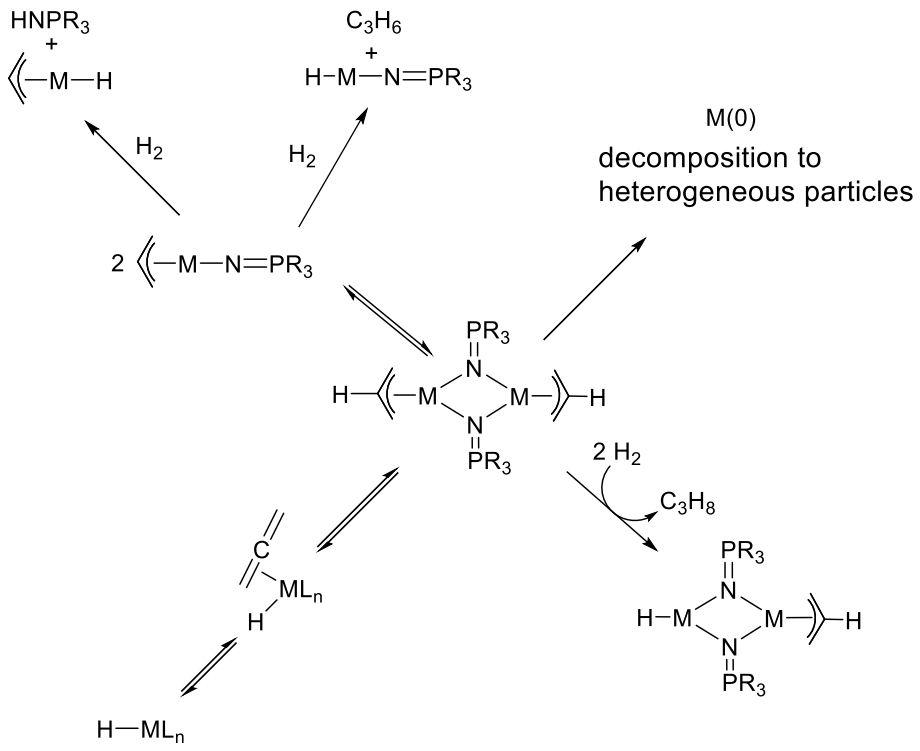

Figure 2.6: Proposed trialkylphosphoranimide allyl precatalyst activation methods

Proposal 1*: η^3-η^1 allyl isomerization followed by hydrogenolysis*.[118] As discussed, η^3-η^1 allyl isomerization is necessary for active metal hydride formation. This proceeds with the formation of propane which is observed with nickel cluster **24**. Slower isomerization rates result in long induction periods and low catalyst activity which explains the superior activity of cluster **24** *versus* more stable **26**. Furthermore, this accounts for the

activity of electron rich tri-*tert*-butylphosphoranimide clusters **31** and **33** at room temperature.

Proposal 2: *Dimer fragmentation to a monomer followed by allyl and/or trialkylphosphoranimide hydrogenolysis.* The allyl clusters could also fragment into monomers with subsequent allyl cleavage and propane generation.[50] Trialkylphosphoranimide hydrogenolysis to trialkylphosphoranimine is also possible. This would in turn also promote catalyst deactivation as discussed in Chapter 1, which might also explain the low hydrogenation rates observed with all the allyl precatalysts. Concentration dependence studies are essential in determining whether the active catalyst is unimolecular or not.

Proposal 3*: Catalyst decomposition to colloidal metal(0).* If allyl and trialkylphosphoranimide hydrogenolysis occur simultaneously, precatalyst decomposition to colloidal metal(0) is possible. This would explain the suppressed activity of nickel clusters **24** and **26** in the presence of mercury as well as the lower activity of cobalt cluster **31** and iron cluster **33** at elevated temperatures.

Proposal 4: *Allyl-metal hydride transfer.* Last but not least, when heated, η^3-allyl complexes can undergo allyl to metal hydrogen transfer, resulting in an η^2-allene

intermediate.[119] The allene intermediate can also be hydrogenated to propane and/or propene.

2.2 Conclusion

In conclusion, the nature of trialkylphosphoranimide ligands significantly affect alkene and alkyne hydrogenation reactions. Less bulky and electron rich triethylphosphoranimide appears to favour hydrogenation. Furthermore, temperature and solvent choice also have an adverse effect on reactivity, however, this is dependent on the precatalyst.

Triethylphosphoranimide nickel cluster **24** demonstrated the most alkene and alkyne hydrogenation activity. However, at elevated temperatures, **24** decomposes into a heterogeneous species as indicated by the mercury test and suppression of induction periods. Triphenylphosphoranimide nickel complex **26** on the other hand only decomposes at 80 °C. These results further establish the stability of **26** compared to **24** and for this reason, **26** is less active in alkene and alkyne hydrogenation, suggesting slow activation to the active catalyst.

On the other hand, cobalt cluster **31** and iron cluster **33** activation is facile and appears to occur at ambient temperatures, as either precatalyst facilitate

diphenylacetylene hydrogenation at room temperature. However, the reactions proceed at a slow rate. In addition, higher temperatures also suppress activity, attributed to catalyst decomposition and/or poisoning.

Characterization studies such as TEM are essential to determine the nature and nuclearity of the true catalyst in these reactions. In addition, concentration dependent studies should also be performed to determine whether the active catalyst(s) is dimeric or not. Lastly, time studies must be performed to track reaction progress providing an insight into diphenylacetylene reaction pathways.

Chapter 3. Dimeric Allyl-capped Triethylphosphoranimide Nickel(II) Cluster for Catalytic Hydrodesulfurization

3.1 Introduction

3.1.1 Hydrodesulfurization with heterogeneous catalysts

As discussed in Chapter 1, conventional HDS catalysts face several challenges, such as a lack of well-defined active sites, poorly understood reaction mechanisms, and low deep HDS activity. Furthermore, these catalysts require harsh reaction conditions for high activity.[120] Hence the development of various methods for improving conventional catalyst activity.[4] These methods include significant improvements in catalyst impregnation methods and catalyst support modification. As these methods have been extensively reviewed,[121,122] this section only provides a general overview.

3.1.1.1 Improvements in catalyst impregnation methods

Conventionally, HDS industrial catalysts are prepared by co-impregnating alumina with aqueous solutions of Co(Ni) and Mo salts, followed by drying, calcination and sulfidation.[123] Extensive characterization studies (EXAFS, Mössbauer emission spectroscopy, X-ray diffraction, and electron microscopy) suggest that Co(Ni)MoS is the catalytically active phase (Figure **3.1**).[124] This phase consists of layered MoS_2 crystallites decorated with Co(Ni) on their edges and corners. The co-impregnation

technique not only forms the active phase but also the inactive Co_9S_8 and Ni_3S_2 clusters.[125,126] The latter are formed because cobalt and nickel are sulfided faster than molybdenum. As a result, different impregnation methods for maximizing active phase formation have been reported.[4,127,128,129,130,131,132]

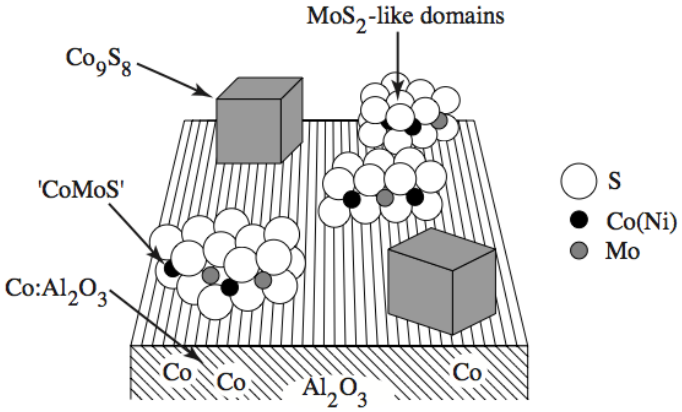

Figure 3.1: Cartoon representation of the surface of the conventional industrial catalysts.[133]

One of the most investigated methods is the addition of chelating agents (e.g. ethylenediaminetetraacetic acid (EDTA), nitrilotriacetic acid (NTA) and citric acid) to the impregnation solutions.[134,135] The chelating agents form stable cobalt(nickel)-chelate complexes, delaying Co and Ni sulfidation.[136,137] In the absence of a chelating agent, cobalt sulfidation (S_8) begins at 50 °C and is complete by 150 °C, whereas molybdenum sulfidation is complete only at 175 °C.[4] When a chelating agent is present, cobalt

sulfidation is delayed to 150 °C and is complete at 225 °C. In this way, cobalt and molybdenum sulfidation occur simultaneously, promoting active phase formation.

3.1.1.2 Effects of support

Metal-support interactions also influence active phase morphology, dispersion, and activity.[138,4] Strong metal-support interactions supress metal precursor sulfidation, reducing catalyst activity. Al_2O_3 is predominantly used as a support because of its high surface area, basic and acidic sites, high packing density, thermal stability, and recoverability.[139] However, Al_2O_3 strongly interacts with some metal precursors, hence recent research into alternative supports (e.g. ZrO_2, carbon, TiO_2, and SiO_2).[138, 140,141,142]

Supporting CoMoS on TiO_2 significantly improves sulfidation.[143] As a result, CoMoS supported on TiO_2 shows high HDS activity compared to when supported on Al_2O_3. TiO_2, however, has a lower specific surface area and is less stable at high temperatures, restricting its application in industry.[144] To overcome this, binary support systems have also been developed to exploit each supports' properties, dramatically improving activity.[145,4] Conventional catalysts supported on TiO_2-Al_2O_3 are more efficient in deep HDS compared to when supported on Al_2O_3.[146,147,148]

3.1.2 Hydrodesulfurization with homogeneous catalysts

Transition metal complexes have also been developed to model the conventional heterogeneous catalysts, providing insight into putative HDS mechanisms.[149,150,42] These complexes are usually low coordinate, to facilitate substrate coordination,[151,152] and often include multiple metal centres to model the metal-metal cooperativity assumed in heterogeneous catalysts.[153,154] Metal hydride complexes have also been reported, since a M-H intermediate is thought to be involved during all heterogeneous catalytic HDS processes.[155,156,157]

HDS of a typical organosulfur compound is proposed to proceed according the mechanism outlined in Figure **3.2**. First, the transition metal precatalyst complex is transformed into an active catalyst, usually by ligand dissociation and/or cluster fragmentation (step *i*). In the second step, the substrate coordinates to the unsaturated metal centre, followed by metal insertion into one of the C-S bonds. The new M-C bond then undergoes hydrogenolysis and a metal hydride species formed (step *iii*). If the M-S bond undergoes hydrogenolysis at this point, the partially desulfurized product is released. In the fourth step, the second C-S bond is activated, followed by another M-C bond hydrogenolysis (step *v*), affording a fully desulfurized hydrocarbon and a stable metal sulfide species. The last step, active catalyst regeneration and release of sulphur as H_2S, is rate limiting and reversible. The metal sulfide species reacts with hydrogen at

high pressure, with concomitant H_2S production. The latter is scavenged irreversibly from the gas phase.

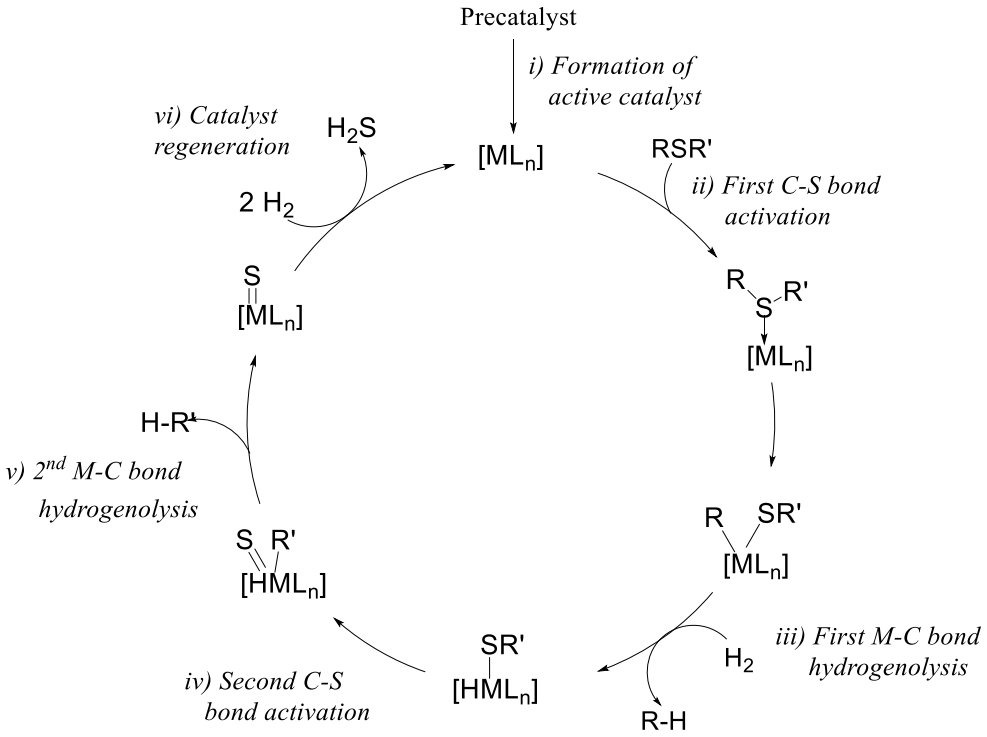

Figure 3.2: Generalized reaction mechanism for homogeneous catalytic hydrodesulfurization of an organosulfur compound RSR'.

Most homogeneous complexes however, form hydrogen-stable M-S bonds upon C-S activation. As a result, these systems are only capable of stoichiometric HDS or hydrogenative C-S bond cleavage.[158,159,160,150] For example, W. D. Jones, *et al*., reported a low valent cobalt complex that achieves stoichiometric thiophene C-S bond cleavage,

under very mild reaction conditions (Eq. **3.1**).[161] After C-S bond cleavage, the ring-opened thiophene remnants bridge two cobalt atoms, resulting in an isolable dimer.

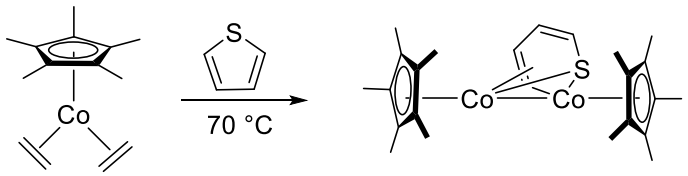

Equation 3.1

Dimetallic iridium hydride, $[Cp^*IrHCl]_2$, is more reactive, facilitating thiophene ring-opening and hydrogenation under mild conditions.[156] C-S bond cleavage of sterically hindered 2,5-dimethylthiophene on the other hand is only achieved after 3 days at 120 °C (Eq. **3.2**).[162]

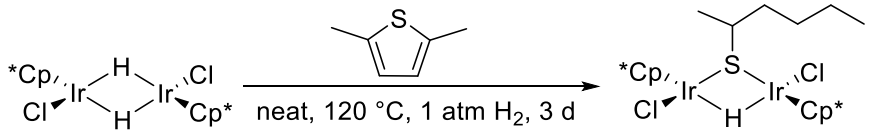

Equation 3.2

Although not catalytic, A.A Toutov, *et al*., recently reported a mild transition-metal free method for hydrodesulfurizing refractory organosulfur compounds (Eq**. 3.3**).[163] In a separate publication, the authors proposed that KO^{t}Bu stabilizes crucial intermediates through cation π-complexes.[164]

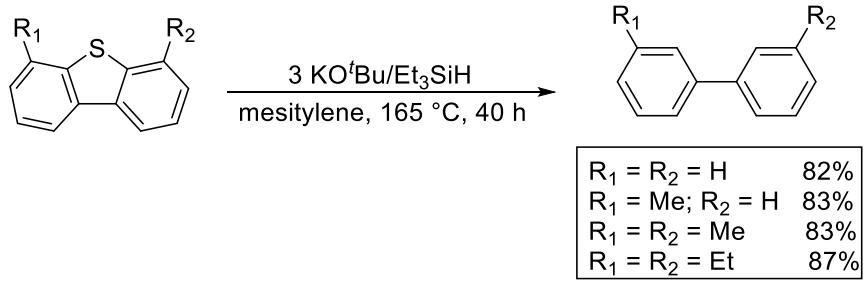

Equation 3.3

Our group has prepared and characterized a range of coordinatively unsaturated trialkylphosphoranimide clusters, some of which catalyze *base-promoted* HDS under mild reaction conditions. In this chapter, preliminary results of DBT hydrodesulfurization using catalytic [Ni(η^3-allyl)(NPEt$_3$)]$_2$ **24**, a stoichiometric amount of strong base, and relatively low hydrogen pressure (1–34 atm) and temperature (110-150 °C) are reported.

3.2 Results and discussion

3.2.1 The role of stoichiometric basic scavengers in HDS

For DBT hydrodesulfurization studies, we selected several bases based on their pKa values and, as a control, both sodium and potassium salts were evaluated (Table **3.1**).[165] Two equivalents of base are necessary to scavenge the acidic hydrogen from thiol intermediates and H_2S *in situ*, driving the equilibrium towards active catalyst

regeneration (Scheme **3.1**). However, many strong bases mediate stoichiometric HDS in the absence of a catalyst albeit slowly and under harsh conditions.[166,167,168] Thus, base screenings were performed in the absence of nickel precatalyst **24** to determine the extent of background HDS activity (Table **3.2**).

Table 3.1: pKa values of various bases

Entry	**[a]Base**	**pKa value[47]**
1	KTMP	37
2	NaTMP	36
3	KO^{t}Bu	29
4	NaO^{t}Bu	29

[a]pKa values in DMSO

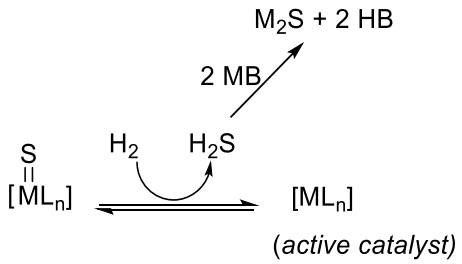

Scheme 3.1

From entries 1-4, it is clear that potassium 2,2,6,6-tetramethylpiperidide (KTMP) alone mediates DBT hydrodesulfurization under our reaction conditions. At lower

hydrogen pressure and temperature in toluene, the reaction proceeds primarily to 2-thiobiphenyl (Entries 1-2) whereas at 150 °C and 34 atm, DBT conversion to biphenyl increases (Entry 5). Interestingly, lower conversions were obtained in THF under the same conditions (Entries 1 and 4), strongly suggesting KTMP aggregation and/or

Table 3.2: Basic scavenger HDS control reactions[a]

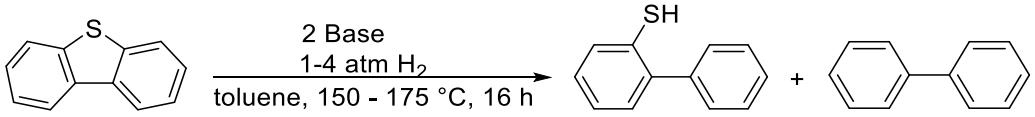

43 **44** **45**

Entry	Base	Temperature (°C)	H_2 pressure (atm)	Conversion (%)[c]	
				44	**45**
[d]1	KTMP	150	1	3	1
2	KTMP	150	1	68	8
3	KTMP	150	34	49	48
[d]4	KTMP	150	34	40	4
[b]5	KTMP	175	34	42	36
6	NaTMP	150	34	0	0
7	KO^{t}Bu	150	34	0	0
[b]8	KO^{t}Bu	175	34	0	0
9	NaO^{t}Bu	150	34	0	8

a. 1 atm H_2 reactions were conducted in sealable medium walled glass reactors charged with toluene, DBT, base and 1 atm H_2. The reactors were immersed in an aluminium dry block adapter plate equipped with a thermostat and heated at 110 or 150 °C under vigorous stirring for 16 hours. 34 atm H_2 reactions were conducted in a similar manner using stainless steel autoclaves and a thermostat-regulated oil bath. 1.3 and 1.5 equivalents of KTMP and NaTMP were used respectively. H_2 pressure is the pressure at RT, pressure was higher after heating b. Conversion in 4 hours in cyclooctane d. Reactions in THF

c. Calibrated quantitative GC conversions using dodecane as internal standard, remaining material is DBT.

solvent coordination.[169] Importantly, no background activity is observed using NaTMP (Entry 5), indicating that pKa may be less important than the alkali metal influence on base performance (*vide infra*). Less basic KO^{t}Bu, however, is also unreactive toward DBT under the same reaction conditions (Entries 7-8), suggesting that pKa remains important. The use of NaO^{t}Bu afforded 8% conversion to biphenyl, attributed to the presence of metal traces in the unpurified reagent. In the absence of a base, the precatalyst only achieves stoichiometric conversion to biphenyl. Based on these results, it can be concluded that KTMP behaves as an HDS "promoter" as it facilitates C-S bond cleavage and M-S bond hydrogenolysis in the absence of a catalyst.

Similar stoichiometric "promoter effects" have been observed with other catalysts and potassium-based bases. For example, J. Camacho-Bunquin in this group observed greater than three-fold higher catalyst activity when KH was used as a scavenger as opposed to NaH.[170] H. Brown and A. Vorapattanapong also obtained higher DBT conversions using potassium bases as compared to the sodium and lithium analogues (Table **3.3**).[22,171]

Table 3.3: Catalytic HDS of DBT using various bases

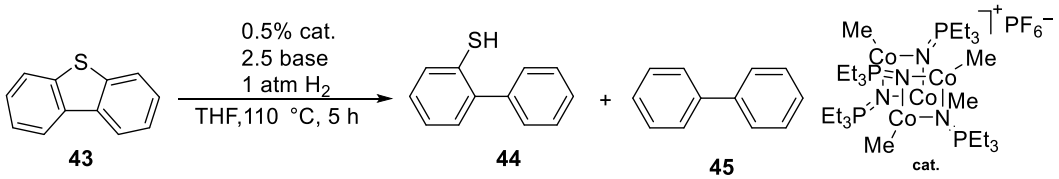

Entry	Base	% Conversion	Conversion (%)[a]	
			44	**45**
1	LiTMP	5	1	4
2	KTMP	23	11	12
3	NaH	2	0	2
4	KH	61	26[b]	35
5	NaO^{t}Bu	0	0	0
6	KO^{t}Bu	<1	0	<1

[a]Conversion according to uncalibrated GC peaks. [b]Total conversion in 2 hours

Aside from scavenger protons, the deeper role of the bases in HDS is unclear. However, deuterium isotopic labelling studies using D_2, KH and DBT in the absence of a catalyst result in deuterium incorporation at the *ortho* (2-) and *meta* (3-) positions of isolated 2-thiobiphenyl (Scheme **3.2**).[171] We propose that KH reversibly abstracts the C-4 proton in DBT, promoting deuterium exchange at that position. Deprotonation could also lead to C-S bond cleavage, giving a benzyne intermediate[172,173] (Scheme **3.2**), another reaction that could be reversible and lead to deuterium incorporation. Furthermore, alkali metals can achieve stoichiometric HDS in the presence of

hydrogen,[174,175] suggesting that KH could also reduce DBT *via* single electron transfer, promoting C-S bond cleavage.[176] Similar electron transfer processes in the presence of KO^{t}Bu have been reported.[177,164]

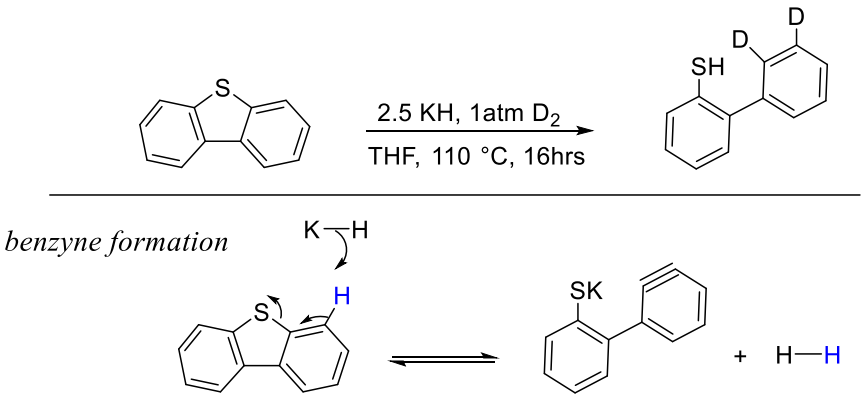

Scheme 3.2

The origin of the potassium cation promotional effect in catalysis remains unclear, although it is possible that K^+ offers a better orbital match for the sulfur lone pair compared to the other alkali metals. In addition, reports on alkali metal coordination to transition metal sulfides *via* a dative bond[178,179] suggest that the potassium cation may *uniquely* coordinate to the metal sulfide intermediates, accelerating sulfur extrusion and active catalyst regeneration (Figure **3.3**). Thus, in our group, attempts to synthesize metal sulfide complexes as possible catalytic intermediates are currently underway. These clusters could provide insight into the sulfur extrusion mechanism.

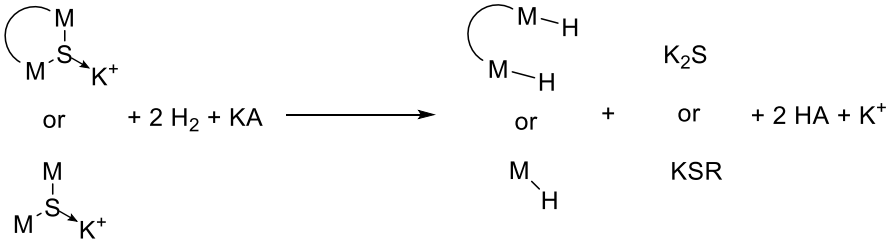

Figure 3.3: Proposed "potassium effect" mechanism

3.2.2 HDS of DBT using [Ni(η^3-allyl)(NPEt$_3$)]$_2$ 24 with MTMP (M= Na or K)

Following the stoichiometric base screenings, the HDS activity of nickel dimer **24** in the presence of KTMP was investigated under one atm hydrogen (Table **3.3**).

Table 3.4: Summary of DBT hydrodesulfurization with KTMP and **24**[a]

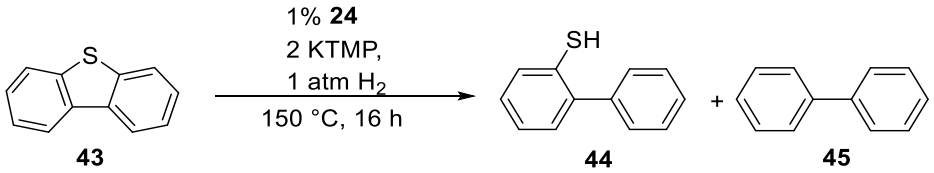

[a]Entry	Solvent	Total conversion	Conversion (%)[b]	
			44	**45**
1	THF	23	16	7
2	Toluene	88	37	51
3	Cyclooctane	73	51	22

a. Reactions were performed in sealable medium walled glass reactors charged with **24**, KTMP, solvent, stir bar and one atm H_2. The reactions were heated in aluminium dry block plates equipped with a thermostat at heated at 150 °C for 16 hours under vigorous stirring b. Calibrated quantitative GC results, dodecane as the internal standard, remaining Material is DBT.

In all cases, DBT conversion beyond the background activity was observed. DBT conversion proceeds faster in toluene and cyclooctane than THF. These results strongly suggest that THF inhibits the catalyst by competitive coordination or promotes catalyst decomposition and aggregation.

At a higher hydrogen pressure (34 atm), conversion to biphenyl increases regardless of solvent, although the reaction in THF proceeds much more slowly (Table

Table 3.5: Summary of the HDS reactions with KTMP and **24**, 34 atm H_2[a]

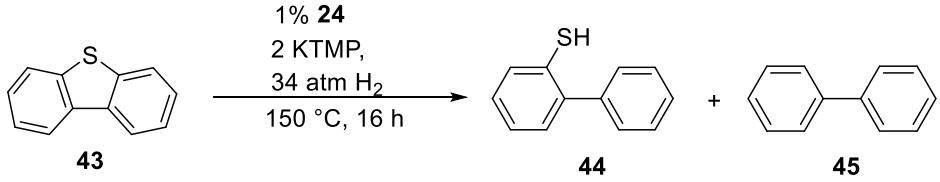

43 **44** **45**

Entry	Solvent	Total conversion	Conversion (%)[b]	
			44	**45**
1	THF	49	22	27
2	Toluene	96	1	95
3[c]	Toluene	67	3	64
4	Cyclooctane	97	1	96

a. Stainless steel autoclaves were charged with DBT, KTMP, catalyst, stir bar and solvent in the glovebox followed by 34 atm H_2 outside the box at RT. The reactors were immersed in thermostat-regulated oil baths and were left to stir vigorously for 16 hours.
b. Calibrated quantitative GC results using dodecane as an internal standard remaining material is DBT c. Reaction performed with NaTMP instead of KTMP

3.5). In addition, overall DBT conversion in THF under these conditions was similar to that obtained at one atm hydrogen (Entry 1). These results also strongly indicate catalyst inhibition in THF and also suggest saturation kinetics for hydrogen dependence or, possibly, that higher pressures suppress catalyst activity in THF. In the presence of NaTMP, only 67% total conversion was observed, further establishing the "K^+ promoter effect" (Entry 3).

3.2.3 HDS of DBT using [Ni(η^3-allyl)(NPEt$_3$)]$_2$ 24 with MO^{t}Bu (M=Na or K)

Catalytic DBT conversion using 2 equivalents of less basic promoter KO^{t}Bu, on the other hand, *requires* higher hydrogen pressure, and even then, the reaction only proceeds primarily to 2-thiobiphenyl (Table **3.6**). The reaction rates were also highly dependent on solvent choice; only stoichiometric conversion was observed in THF (Entry 1), while 78% and 76% conversions were obtained in toluene and cyclooctane, further supporting catalyst inhibition in THF. The "K^+ effect" is also prominent, as only 14% conversion is observed when using NaO^{t}Bu (Entry 3). To investigate the extent of this effect, the reaction was performed using a catalytic amount of KO^{t}Bu in the presence of stoichiometric NaO^{t}Bu (Entry 4). However, no significant improvement in

activity was observed, indicating potassium is consumed irreversibly, leaving only the low-activity sodium base to promote activity.

Table 3.6: Summary of the HDS reactions with KO^{t}Bu as the base

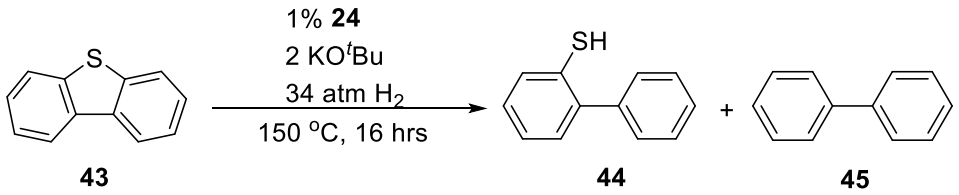

Entry	Solvent	Total conversion	Conversion (%)[a]	
			44	45
1	THF	s	0	s
2	Toluene	78	71	7
[b]3	Toluene	14	0	14
[c]4	Toluene	15	1	15
5	Cyclooctane	76	63	13

a. Stainless steel autoclaves were charged with DBT, KO^{t}Bu, **24**, stir bar and solvent in the glovebox followed by 34 atm H_2 on the hydrogen line. The reactors were immersed in thermostat-regulated oil baths set at 150 °C and were left to stir vigorously for 16 hours. H_2 pressure was the pressure at room temperature, pressure was higher after heating. Calibrated quantitative GC results using dodecane as an internal standard, remaining material is DBT b. Reaction performed in the presence of NaO^{t}Bu instead of KO^{t}Bu.

c. Reaction performed with 5% KO^{t}Bu and 2 equiv. NaO^{t}Bu.

These results demonstrate that cluster **24** is not an efficient precatalyst for DBT hydrodesulfurization using alkoxide bases. This is attributed to catalyst decomposition under the reaction conditions, as confirmed by mercury tests (Chapter 2).

3.2.4 An alumina-supported catalyst for DBT hydrodesulfurization

Transition metal complexes can be supported on Al_2O_3 *via* a M-O covalent bond (grafting) to give site-isolated and immobilized complexes, limiting catalyst decomposition pathways.[180,181,182] Orain Brown in this group observed that supporting $[Ni(NP^tBu_3)_2]_2$ on high surface area γ-alumina dramatically improves catalyst performance, possibly by maintaining catalyst stability and dispersion.[48] Thus, cluster **24** was supported on γ-alumina *in situ*, which we propose proceeds *via* allyl ligand protonolysis (Scheme **3.3**). However, characterization of supported-**24** using TEM and other surface methods is essential, as further coordination *via* the doubly-bridging nitrogen to a Lewis acidic site on Al_2O_3 is also more than likely. Detailed surface characterization is beyond the scope of this thesis, but the effect of catalyst immobilization on DBT hydrodesulfurization was investigated by grafting the same amount of precatalyst onto a range of alumina loadings.

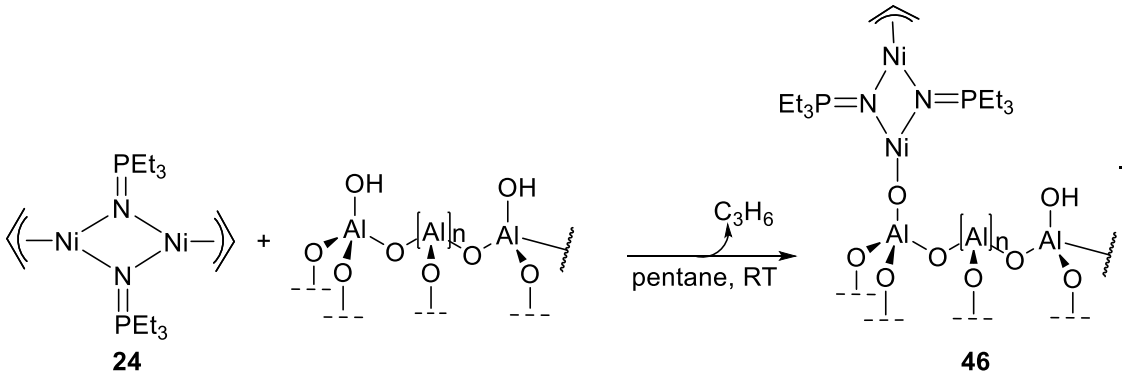

Scheme 3.3

DBT hydrodesulfurization was then investigated using supported catalyst **46** and KO^{t}Bu (Figure **3.3**). Under all reaction conditions, conversion to biphenyl was higher than that obtained by using unsupported **24**. At the same time, the conversion rates were highly dependent on the level of precatalyst dispersion (assuming the same quantity of catalyst at all loadings). DBT conversion to biphenyl dramatically increases at 1 wt% catalyst (from 15% to 80%), whereas above 1 wt% loading, conversion decreased (Figure **3.4**). This indicates that high catalyst loadings result in Al_2O_3 oversaturation, which presumably results in catalyst agglomeration and lower activity.[183,184]

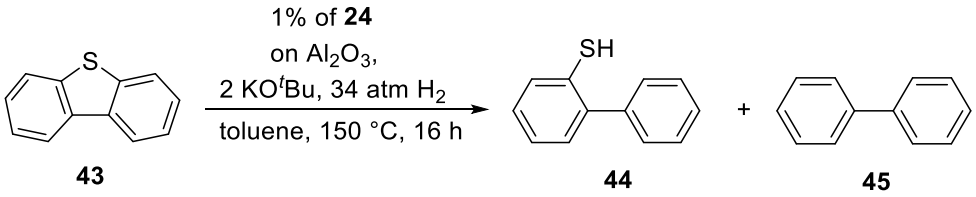

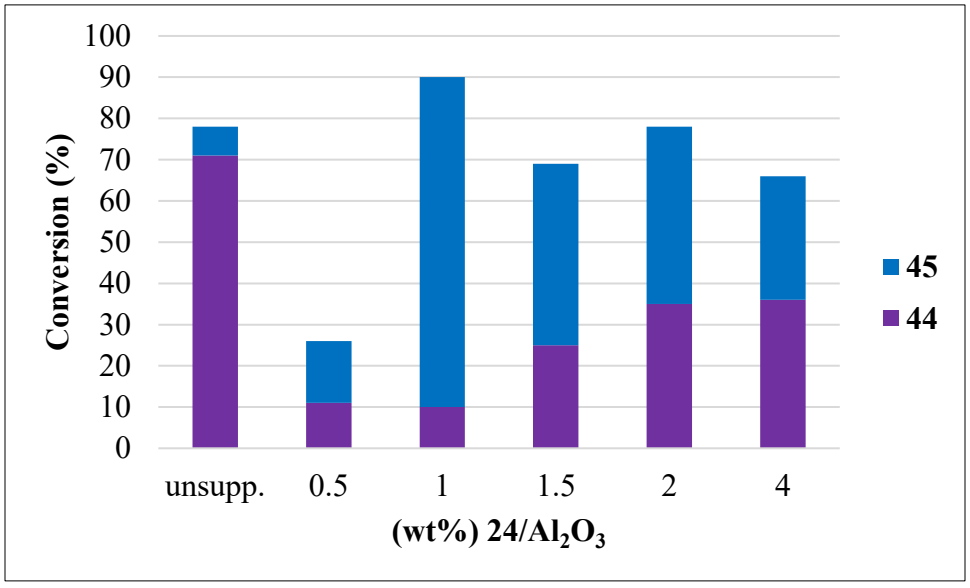

Figure 3.4: The effect of ally dimer **24** dispersion on HDS activity. Purple = 2-thiolbiphenyl, blue = biphenyl.

3.3 Conclusion

In this chapter, the effect of promoter basicity and alkali metal on nickel-catalyzed HDS activity was established. KTMP, the strongest base investigated, mediates HDS in the absence of catalyst, whereas no activity is observed with the equally strong base NaTMP. This difference in activity is generically attributed to a "potassium promoter effect" that efficiently desulfurizes the spent metal sulfide intermediate. Although this "potassium promoter effect" is not well understood, these results suggest that incorporating K^+ into our catalytic clusters could eliminate the use of stoichiometric bases in catalytic HDS.

We also established that optimal HDS activity using allyl dimer **24** occurs when the precatalyst is supported on γ-Al_2O_3 at low catalyst loading, in the presence of a weaker base, KO^{t}Bu. These results strongly affirm the effect of increased catalyst dispersion and stability on activity, and since catalyst activity is also influenced by the support, HDS studies using **24** supported on other substrates may be revealing. Further studies on catalyst recoverability are also necessary.

Chapter 4: Experimental procedures

4.1 General procedures (*adapted from previous Stryker group members*)

4.1.1 General experimental procedures

All manipulations were performed using standard Schlenk techniques on a vacuum/N_2 double manifold or using a Labmaster sp MBraun glovebox under a N_2 atmosphere. Glovebox experiments were performed when the O_2 level was <5 ppm as measured by a Pb-based fuel cell Teledyne O_2 sensor. Solvents were either distilled from Na/benzophenone (THF) or K/benzophenone (hexane, pentane, ether, dioxane) under nitrogen when dark blue or purple, or collected from Pure Process Technology free-standing solvent purification system (SPS) (Toluene, hexanes, pentanes, benzene and diethyl ether). Glovebox solvents were tested with a dilute Na/benzophenone solution in THF to ensure they were dry and degassed. Liquid reagents were either distilled under N_2 (or Ar) and stored in glass vessels (medium walled glass tubes with 14/20 sidearms that seal with a Teflon high vacuum valve) or passed through Activity I neutral alumina into a storage vessel and subsequently freeze-pump-thaw degassed three times. Hygroscopic solids were dried overnight in a vacuum oven to remove water before bringing them into the glovebox while hot. Non-hygroscopic solids were brought into the glovebox in vials covered with Kimwipes. Volatile solids were pumped into the glovebox inside of sealed nitrogen-filled Schlenk flasks. All glassware was flame-dried before use or dried for at least 3 h in a 150 °C oven before use. Low temperature

crystallizations were done at -35 °C in the glovebox freezer. Samples for air sensitive solid samples for IR were prepared as cast films on 25 mm by 4 mm KBr salt plates separated by nitrile rubber o-rings. For elemental analysis of air sensitive compounds, the samples were prepared in the glovebox using two preweighed tin boats. Approximately 1.6 mg of the sample was placed in one boat, folded into a cube and then inserted into the second boat, which was also folded into a cube. The cube was then sealed in a one-dram vial and immediately submitted for analysis. Duplicate samples were run whenever possible. NMR spectroscopy was performed in standard NMR tubes sealed with either plastic caps or in resealable J. Young-NMR tubes. For controlled heating of reaction mixtures, Ika stir plates with digital temperature control were used along with heavy mineral oil (<110 °C) or silicone oil (>110 °C) baths. Reactions performed in medium walled glass reactors were heated in an aluminium dry block multiwell heating adapter plate. For reactions requiring sustained low temperature, an immersion cooler (Neslab Cryotrol cc-100) equipped with a temperature controller was used. A high vacuum line, equipped with a three-stage diffusion pump, was used to dry materials for elemental analysis (<10-5 Torr).

4.1.2 Instrumentation (*adapted from previous Stryker group members*)

X-ray crystallography was performed using either a Bruker DB diffractometer or a Bruker PLATFORM diffractometer, both equipped with a SMART APEX II CCD area detectors. Diffraction data collection and crystal structures determinations were done by Dr. Robert McDonald or Dr. Michael Ferguson of the University of Alberta Department

of Chemistry X-ray Crystallography Laboratory. CHNS elemental analyses were performed on a Carlo Erba EA1108 Elemental Analyzer. Gas chromatography-mass spectrometry was performed using a Hewlett Packard GCD series G1800A GC-MS. The mass detectors used were either HP 5870 or 5971 MSD. The column used was an Agilent DB-5 MS 25m x 0.25 mm x 0.25-micron film thickness. The MS library was the NIST/EPA/NIH 2011 Mass Spectral Library and Software package was NIST11. Quantitative analyses of catalysis reaction products were performed using gas chromatography with flame ionization detection (GC-FID) on an Agilent 6890N gas chromatograph equipped with a HP-5 (5% phenyl)-methylpolysiloxane capillary column (Agilent). IR spectroscopic analyses were performed using a Nicolet Magna 750 FT-IR Spectrometer, or a Nicolet 8700 FT-IR Spectrometer operating by OMNIC Spectra Software. All elemental analyses, GC-MS and FT-IR data were obtained by staff at the University of Alberta Department of Chemistry Analytical and Instrumentation Laboratory. ^{1}H and ^{31}P NMR spectra were obtained using either an Agilent/Varian Inova 300 MHz spectrometer or an Agilent/Varian Inova 400 MHz spectrometer at 27 °C unless otherwise mentioned. Chemical shifts for ^{1}H NMR spectra are reported in ppm and referenced against the residual proton signals of the NMR solvent. ^{31}P NMR chemical shifts are reported in ppm, referenced to 85% phosphoric acid which is assigned a value of 0 ppm.

4.1.3 Chemical materials *(adapted from previous Stryker group members)*

All commercial reagents were purchased from Strem or Sigma-Aldrich companies and were used as received. Where necessary, reagent purifications were accomplished using standard methods. Potassium hydride required rigorous purification to remove traces of potassium metal and was thus heated overnight at reflux in THF with 20 mol% naphthalene, then washed three times with anhydrous THF, three times with dried hexanes and dried under vacuum before use.[172] Materials prepared by literature methods or modifications of such methods are noted in the appropriate experimental sections. Brockman activity I neutral alumina was heated in air at approximately 150 °C for at least 24 h.

4.2 Synthesis procedures

4.2.1 Synthesis of Et_3PBr_2 *(adapted from Stryker group members)*

$$PEt_3 + Br_2 \xrightarrow{\text{hexanes, RT, 16 h}} PEt_3Br_2$$

Bromine (1.64 g, 0.0102 moles) was slowly added to a solution of PEt_3 (1.21 g, 0.0102 moles) in 40 mL hexanes at room temperature under stirring. The mixture was then stirred for 16 h after which the solvent was removed under vacuum. Residual PEt_3 was extracted with 3 × 15 mL portions of hexane, affording a white solid, Et_3PBr_2 (2.69 g, 94.8 %). ^{31}P NMR (202 MHz, CD_2Cl_2) δ 103.423 (s), 87.616 (s). Two phosphorous peaks are observed because of inner and outer sphere coordination of bromine.

4.2.2 Synthesis of $KNPEt_3$

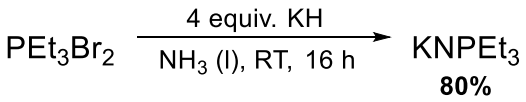

On the Schlenk line, 300 mL of NH_3 was condensed into a three-neck flask kept at -78 °C. KH weighed and transferred in a drybox (8.24 g, 0.206 mol) was slowly added to the NH_3 using a solid addition funnel. The solution changed to blue upon addition of KH indicating solvated electrons. PEt_3Br_2 **(**16.54 g, 0.0595 mol) was then added in 5 g portions after which the reaction was allowed to warm to room temperature overnight as the ammonia evaporated. The flask was then transferred into the drybox and the residual solid extracted with 3 × 20 mL hexanes and filtered through a Celite plugged frit. Hexane was evaporated under reduced pressure, yielding a beige powder in 80% yield, $KNPEt_3$ (8.185 g, 0.0478 mol). No further purification was required. Elemental analysis: C: 42.17 (42.08), H: 8.51 (8.83), N: 7.7854, 7.82 (8.18).

4.2.3 Synthesis of KNP^tBu_3 16

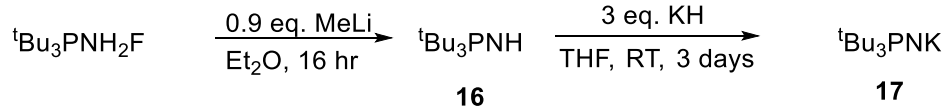

In the drybox, $^tBu_3PNH_2F_2$[46] (10 g, 0.0422 mol) and 100 mL diethyl ether were added to a Schlenk flask containing a magnetic stir bar. The Schlenk flask was then equipped with an addition funnel charged with methyl lithium (26 mL, 1.52 M in Et_2O, 0.0401

mol), removed from the drybox, and connected to the Schlenk line under nitrogen. The methyl lithium solution was added dropwise into the flask over 2 h. The reaction was left to stir overnight after which diethyl ether was removed under vacuum and the resulting solids washed with pentane. The pentane was removed under reduced pressure and the resulting product further extracted into benzene over 3 d. After benzene evaporation and drying under high vacuum, 7. 25 g $^{t}Bu_3PNH$ (77%) was obtained, the product was confirmed using ^{31}P NMR (162 MHz, C_6D_6): δ 56.116 (s).

In the drybox, $^{t}Bu_3PNH$ (3 g, 0.014 mol) was dissolved in THF in a 100 mL Schlenk flask. Purified KH (1.66 g, 0.042 mol) was slowly added under constant stirring resulting in a white suspension which became grey after stirring for 3 d. The resulting suspension was vacuum filtered on a Celite-plugged frit and the supernatant placed under reduced pressure. The solid product was washed with hexane to remove residual $^{t}Bu_3PNH$, and after solvent evaporation, placed on the high vacuum line. After drying, $KNP^{t}Bu_3$ was obtained (2.55 g, 0.0098 mol, 70%). Elemental analysis C: 49.18 (56.43), H: 9.43 (10.66), N: 5.31 (5.48). ^{31}P NMR (162 MHz, C_6D_6) δ 16.73 (s).

4.2.4 Synthesis of[Ni(η^3-allyl)(NPEt$_3$)]$_2$ 24

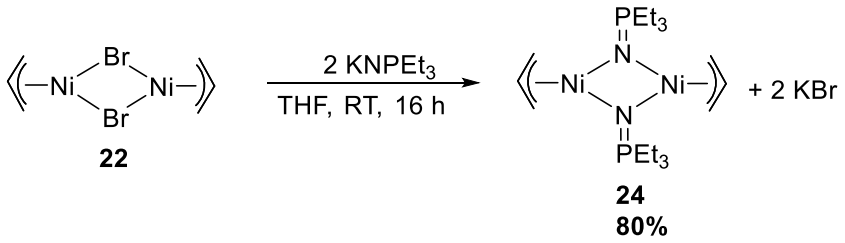

In the drybox, [Ni(η^3-allyl)Br]$_2$[53] **23** (300 mg, 0.83 mmol) and KNPEt$_3$ (277 mg, 1.62 mmol) were separately dissolved in 5 mL THF in 5-dram vials. KNPEt$_3$ was then added drop-wise to **23**, resulting in a brown suspension. The reaction mixture was left to stir overnight, after which the suspension was filtered through a Celite-plugged pipette, resulting in a dark-brown solution. The volatiles were removed under vacuum and the resulting solid triturated into pentane and left in the freezer overnight to precipitate traces of KBr. The following day, the solution was filtered through a Celite-plugged pipette and the pentane evaporated under vacuum, leaving an orange-brown oil (300 mg, 0.64 mmol, 80%) which was further dried to a solid under high vacuum. Elemental analysis: C: 46.51 (46.61) H: 8.47 (8.69) N: 5.58 (6.04). ^{1}H NMR (400 MHZ, C_6D_6) δ 5.293 (tt, *J* = 8.6, 6.8 Hz, 1H), 5.229 (tt, *J* = 8.6, 6.8, 1H), 2.190 (d, *J* = 6.8 Hz, 2H), 2.153 (d, *J* = 6.8 Hz, 2H), 1.479 (d, *J* = 8.6 Hz, 2H), 1.450 (d, *J* = 8.6 Hz, 2H), 1.376 (m, 6H), 1.339 (m, 6H), 1.158 (td, *J* = 8, 7.5 Hz, 9H), 1.127 (td, *J* = 8, 7.5Hz, 9H). ^{31}P NMR (162 MHz, C_6D_6) δ 34.62 (s), 34.16 (s). ^{13}C-NMR: δ 99.221, 99.000, 43.741, 43.561, 22.810, 22.797, 22.211, 22.198.

4.2.5 Synthesis of [Ni(η^3-allyl)(NPEt$_3$)]$_2$•AlH$_3$ 25

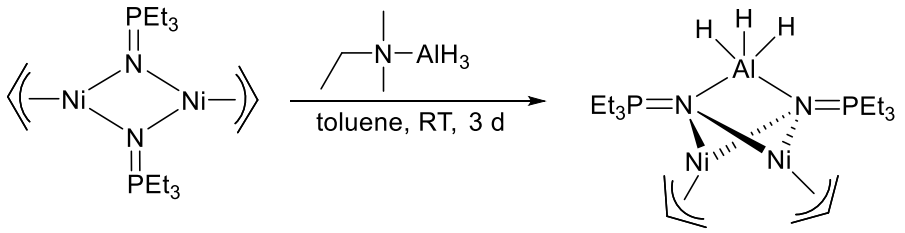

24 **25**
50%

In the drybox, 0.5 M alane•dimethylethylamine complex in toluene (1 mL, 0.53 mmol) was added dropwise a solution of [Ni(η^3-allyl)(NPEt$_3$)]$_2$ **24** (246 mg, 0.53 mmol) in 10 mL toluene under constant stirring. An immediate colour change from golden-brown to dark-brown was observed. After 3 d, the resulting suspension was filtered through Celite and the volatiles evaporated under reduced pressure, resulting in a dark-brown solid. The solid was extracted into pentane, followed by filtration and evaporation under vacuum, leaving dark-brown crystals (130 mg, 0.265 mmol), pure by elemental analysis. The crystals did not diffract, however. Elemental analysis, calc. for $C_{18}H_{43}AlN_2Ni_2P_2$; C: 43.85 (43.78), H: 8.3 (8.78), N: 5.55 (5.67). IR: ν/cm^{-1} pentane cast film = 980 m, 1171 s, 1411 m, 1457 s, 1493 w, 2000 w, 2090 w, 2879-2954 s.

4.2.6 Synthesis of [Ni(η^3-allyl)(NPPh$_3$)]$_2$ 26

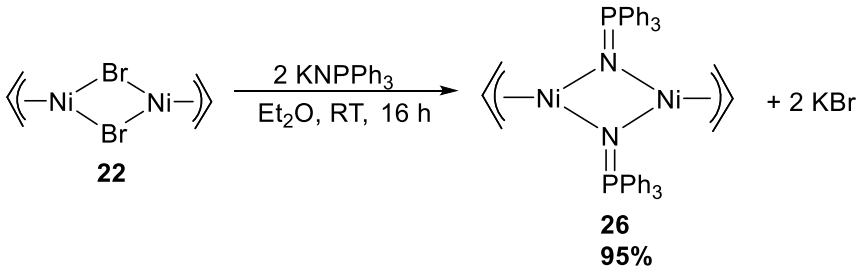

22 **26**
95%

In the dry-box, [Ni(η^3-allyl)Br]$_2$ **22** (57 mg, 0.16 mmol) and KNPPh$_3$[46] (100 mg, 0.32 mmol) were separately dissolved in 5 mL Et$_2$O. Upon slow addition of KNPPh$_3$**,** a rapid colour change from red to orange was observed. The reaction mixture was left to stir overnight, after which it was filtered through Celite, resulting an orange solution. The volatiles were evaporated under vacuum leaving orange microcrystals. of [Ni(η^3-allyl)(NPPh$_3$)]$_2$ **26** (95% yield, 114 mg, 0.15 mmol) after drying under high vacuum. Single crystals of **26** were obtained at -35 °C from a saturated solution in hexane layered on THF. Elemental analysis: C: 66.32 (67.07) H: 5.50 (5.36) N: 3.53 (3.72). ^{1}H NMR (400 MHZ, C$_6$D$_6$) δ 5.106 (tt, *J* = 12.4, 6.8, 1H), 4.844 (tt, *J* = 12.4, 6.8, 1H), 1.770 (d, *J* = 6.8 Hz, 2H), 1.728 (d, *J* = 6.8 Hz, 2H), 1.625 (d, *J* = 12.4 Hz, 2H), 1.174 (d, *J* = 12.4 Hz, 2H). ^{31}P NMR (162 MHz, C$_6$D$_6$) δ 24.797 (s), 24.023 (s).

4.2.7 Synthesis of [Ni(η^3-allyl)(NP^{t}Bu$_3$)]$_2$ 27

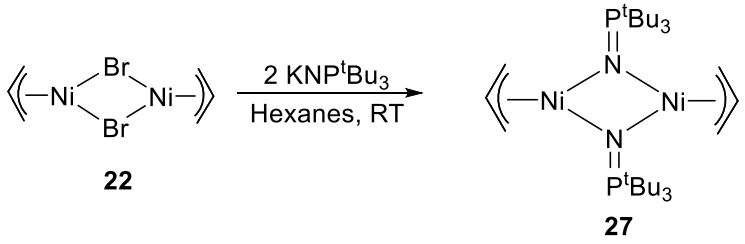

22 **27**

[Ni(η^3-allyl)Br]$_2$ **22** (106 mg, 0.590 mmol) and KNP^{t}Bu$_3$ (150 mg, 0.590 mmol) were each dissolved in 5 mL hexane in the drybox after which KNP^{t}Bu$_3$ was slowly added to **22**. The reaction immediately became turbid without any colour change. After 3 days of stirring, a colour change from red to bottle green was observed affording a green solution after filtration. The solvent was then evaporated under reduced pressure resulting in a green solid which was extracted in pentane, filtered and the volatiles removed. The product was further dried under high vacuum resulting in [Ni(η^3-allyl)(NP^{t}Bu$_3$)]$_2$ (60%, 223 mg, 0.353 mmol), pure by elemental analysis. Elemental analysis calculated for $C_{30}H_{64}N_2Ni_2P_2$; C: 57.2 (57.0) H: 10.8 (10.2) N: 5.0 (4.4). IR: ν/cm^{-1} hexane cast film = 932 w, 1195 w, 1384 w, 1472 w, 1482 w, 2902-3000 m.

4.2.8 Synthesis of [Co(η^3-allyl)Cl]$_2$ 29

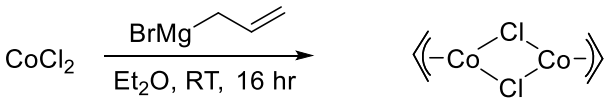

29
40%

In the drybox, anhydrous $CoCl_2$ (1.3 g, 10 mmol) and 150 mL of diethyl ether were added into a Schlenk flask equipped with a large round magnetic stir bar. The flask was then removed from the drybox and connected to the Schlenk line under nitrogen. Allyl magnesium bromide (1 M in Et_2O, 10 mL, 10 mmol) was slowly added by syringe over one hour with constant stirring. Upon addition, the reaction mixture became brown and turbid. The reaction was stirred overnight and the suspension filtered by cannula, resulting in a green solution. The solvent was evaporated under reduced pressure and an impure pale green powder was isolated (0.54 g, 2 mmol, 40%) after drying under high vacuum. CHNS elemental analysis calculated for: $C_6H_{10}Co_2Cl_2$; C: 22.71 (26.40) H: 4.32 (4.43). This material was used without further purification or characterization.

4.2.9 Synthesis of $[Co(\eta^3\text{-allyl})(NP^tBu_3)]_2$ 31

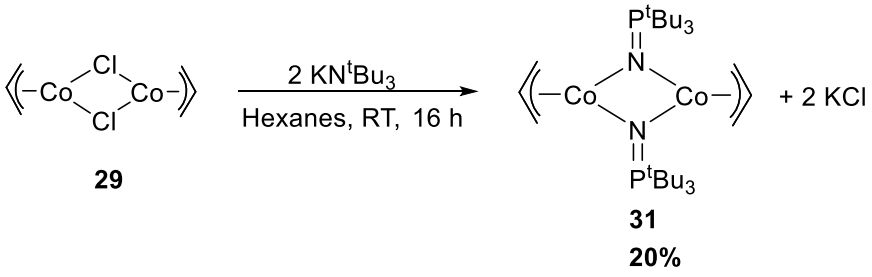

29 **31** **20%**

In the drybox, $[Co(\eta^3\text{-allyl})Cl]_2$ **29** (54 mg, 0.40 mmol) and 100 mg (0.20 mmol) of KNP^tBu_3 were separately dissolved in 10 mL hexanes. The dropwise addition of KNP^tBu_3 to **29** resulted in a yellow solution. The reaction was left to stir overnight and after filtration, a pale-yellow solution was obtained. Evaporation under reduced pressure

gave an orange-brown powder, which after drying under high vacuum resulted in $[Co(\eta^3\text{-allyl})(NP^tBu_3)]_2$ (20%, 50 mg, 0.08 mmol), as confirmed by elemental analysis. Empirical formula $C_{30}H_{64}N_2Co_2P_2$; C: 56.54 (56.77) H: 10.67 (10.48) N: 4.81 (4.41).

4.2.10 Synthesis of $[Fe(\eta^3\text{-allyl})Cl]_2$ 32

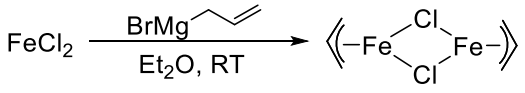

32

In the drybox, a 500 mL Schlenk flask was charged with anhydrous $FeCl_2$ (1.28 g, 10 mmol), a magnetic stir bar and 150 mL diethyl ether. The flask was removed from the drybox and connected to the Schlenk line under nitrogen. Allyl magnesium bromide (1 M in Et_2O, 10 mL, 10 mmol) was slowly added to the $FeCl_2$ suspension using a syringe over a period of one hour with constant stirring. The solution became green the addition of allyl magnesium bromide. The reaction was left to stir overnight and then filtered by cannula, resulting in a green solution. The volatiles were removed under reduced pressure, affording an impure pale green powder (66 mg, 2.5 mmol, 50%). CHNS elemental analysis $C_6H_{10}Fe_2Cl_2$; C: 28.50 (27.02%), H: 4.53 (4.73%). This material was used without further purification.

4.2.11 Synthesis of [Fe(η^3-allyl)(NP^{t}Bu$_3$)]$_2$ 33

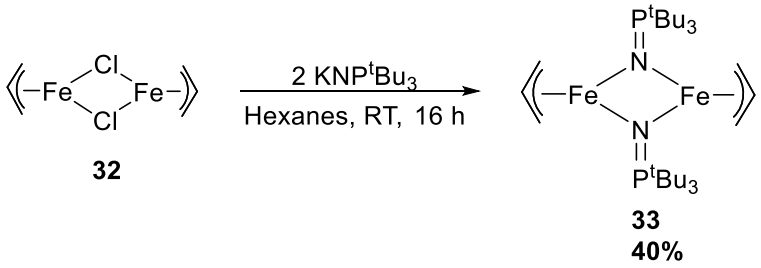

32 **33**
40%

In the dry-box, [Fe(η^3-allyl)Cl]$_2$ **32** (60 mg, 0.45 mmol) was dissolved in 5 mL hexanes. 100 mg (0.45 mmol) of KNP^{t}Bu$_3$ was suspended separately in diethyl ether (10 mL) and slowly added to **32**. The reaction mixture changed from green to golden-brown and was left to stir for 2 d. The resulting reaction mixture was filtered through Celite and the solvent evaporated under vacuum affording impure **33** (112 mg, 0.18 mmol, 40% assuming pure) as a golden-brown powder. Elemental analysis $C_{30}H_{64}N_2Fe_2P_2$; C: 50.58 (57.33), H: 9.34 (10.58), N: 4.18 (4.46). The complex could not be further purified without decomposition.

4.3 Catalytic hydrogenation procedures

4.3.1 Hydrogenolysis of [Ni(η^3-allyl)(NPEt$_3$)]$_2$ 24. Variable temperature ^{1}H and ^{31}P NMR spectroscopy

In the drybox, 15 mg of [Ni(η^3-allyl)(NPEt$_3$)]$_2$ **24** was dissolved in 0.7 mL C_6D_6 and added into a J. Young NMR pressure tube. This was removed from the box and connected to the hydrogen line, freeze-pump-thaw degassed three times, and then

charged with one atm H_2. ^1H and ^{31}P NMR spectra were obtained at room temperature and after heating the sample for one hour at 60 °C or 80 °C. The spectra revealed only resonances of the starting material.

4.3.2 Hydrogenolysis of [Ni(η^3-allyl)(NPEt$_3$)]$_2$ 24

In the drybox, complex **24** (40 mg, 0.086 mmol) was dissolved in 5 mL C_6D_6 and added into a resealable medium-walled glass reactor equipped with a magnetic stir bar. The glass reactor was then freeze-pump-thaw degassed once on the hydrogen line and charged with one atm H_2. The reactor was then heated at 60 °C in an aluminium dry-block heater for one hour under stirring. A colour change from golden-brown to dark-brown was observed. The reaction mixture was allowed to cool to room temperature and the volatiles removed by vacuum transfer directly into a J-NMR tube containing dry and degassed C_6D_6. ^1H NMR spectroscopy revealed only propane resonances. ^1H NMR (400 MHZ, C_6D_6) δ 0.86 (t, 6H), 1.26 (s, 2H). The glass reactor was transferred into the drybox and the resulting solid dissolved in C_6D_6 and analyzed by ^1H and ^{31}P NMR spectroscopy. The spectra revealed resonances identical to those of unreacted starting material.

4.3.3 General procedure for catalytic alkene and alkyne hydrogenation

In the drybox, a medium-walled glass reactor fitted with a Teflon high vacuum valve was charged with substrate, precatalyst, 6 mL solvent, and a magnetic stir bar. The reactor was then connected to a hydrogen manifold line and degassed by one freeze-pump-thaw cycle and charged with one atm H_2. The reaction mixture was then heated at 60 or 80 °C in an aluminium heating block for 4 or 16 h. The reactor was then allowed to cool to room temperature, degassed, and quenched with water. The organics were extracted three times using diethyl ether, and the combined ethereal extracts dried over magnesium sulfate and passed through a Florisil-plugged pipette into a 25 mL volumetric flask. The organic layer was diluted to the mark with diethyl ether and 20 μL of the standard, *n*-dodecane, added to the flask. A portion of the solution was added to a gas chromatography (GC) vial and analyzed.

4.3.4 Calibration of GC detection for *cis*-stilbene, *trans*-stilbene, bibenzyl and diphenylacetylene (*adapted from previous group members*)

To quantify all four compounds involved in diphenylacetylene hydrogenation, GC analysis was carried out using *n*-dodecane as an internal standard. A new temperature program was created to improve separation and detection by GC. In this method, the oven was first held at 100 °C for 2 min. The temperature was then increased at 4 °C/min until it reached 156 °C, after which a rate of 20 °C/min was applied until the temperature reached 300 °C. For each compound, 10 samples of various dodecane/analyte ratios

were separated and detected by GC. The ratio of signal integration and ratio of concentration for each compound was determined from the resulting linear correlation. All the indexes for this linear correlation were obtained, which eventually facilitated the quantitative characterization of all four compounds by GC. The calibration data for the four compounds are presented below.

Table 4.1: *Cis*-stilbene **35** calibration

m(*cis*-stilbene) (mg)	V(dodecane) (μL)	Total solvent (mL)	[M](*cis*-stilbene)/ [M](dodecane)	Area(*cis*-stilbene)/ Area(dodecane)
6	20	10	0.363448202	0.425090137
8.4	20	10	0.508827483	0.59611824
15.4	20	10	0.932850386	1.173724024
18.8	20	10	1.138804367	1.371522755
26.5	20	10	1.60522956	1.960682141
32.2	20	10	1.950505352	2.323473695
36.8	20	10	2.229148974	2.605162593
52.2	20	10	3.16199936	3.80815463
65.8	20	10	3.985815285	4.724426126
89.8	20	10	5.439608094	6.61730652

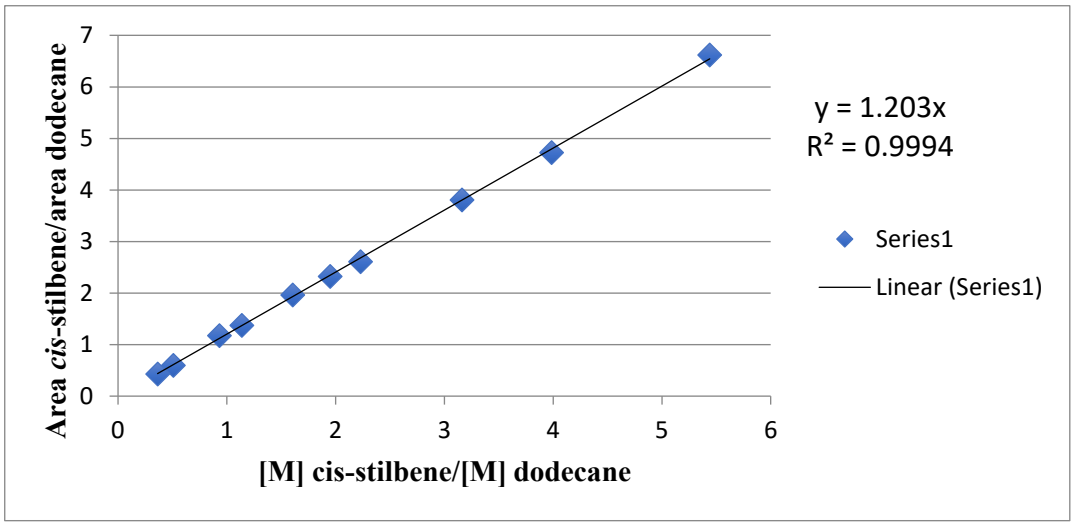

Table 4.2: *Trans*-stilbene **36** calibration

m(*trans*-stilbene) (mg)	V(dodecane) (μL)	Total solvent (mL)	[M](*trans*-stilbene)/ [M](dodecane)	Area(*trans*-stilbene)/ Area(dodecane)
5.7	20	10	0.345275792	0.446801123
10.26	20	10	0.621496426	0.785044894
15.89	20	10	0.962531989	1.220643098
20.11	20	10	1.218157225	1.561147394
31.09	20	10	1.883267435	2.346496218
43.34	20	10	2.625307514	3.200445247
50.04	20	10	3.031158007	3.650730165
59.99	20	10	3.633876276	4.48275673
82.61	20	10	5.004075998	5.710508657
103.41	20	10	6.264029766	7.700191404

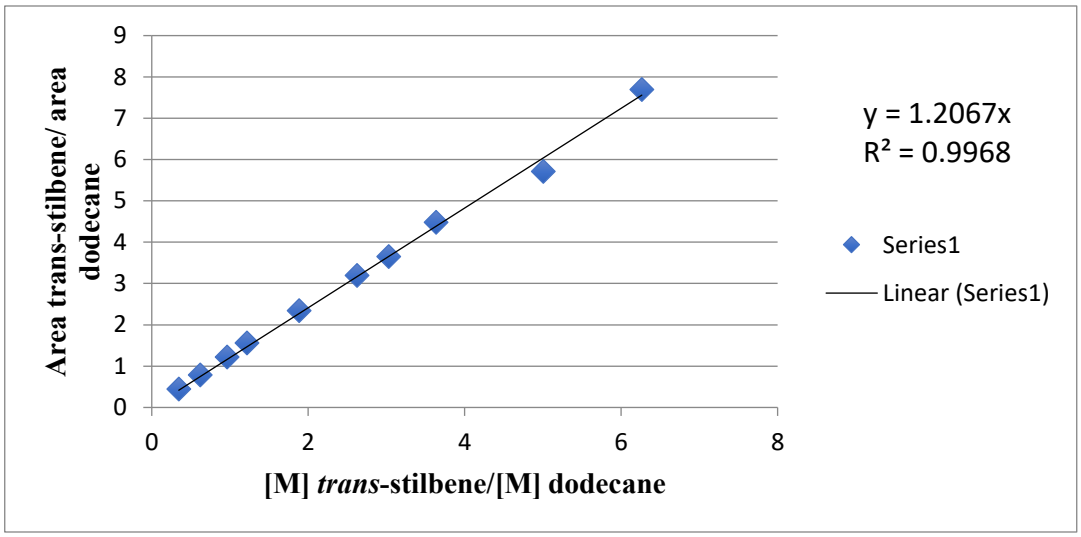

Table 4.3: Biphenyl **37** calibration

m(bibenzyl) (mg)	V(dodecane) (μL)	Total solvent (mL)	[M](bibenzyl)/ [M](dodecane)	Area(bibenzyl)/ Area(dodecane)
5.86	20	10	0.351053088	0.496311592
11.17	20	10	0.669157508	0.920307249
16.7	20	10	1.000441395	1.335193704
20.94	20	10	1.254445678	1.64956812
35.47	20	10	2.124889598	2.698088088
43.76	20	10	2.621515896	3.322828859
46.82	20	10	2.804830307	3.588208305
64.21	20	10	3.846607305	4.987665409
77.88	20	10	4.665531489	5.813845735
98.29	20	10	5.888226632	7.702462797

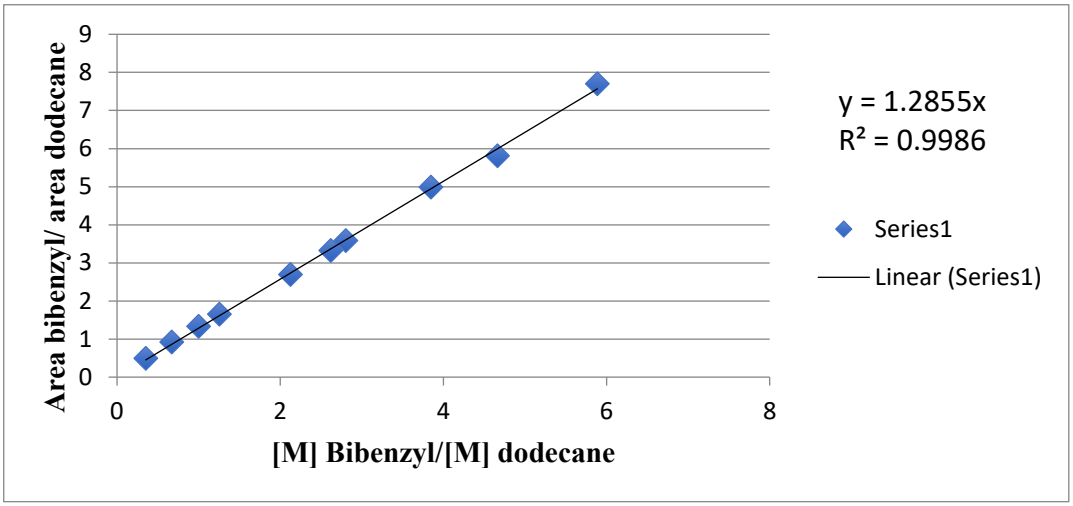

Table 4.4: Diphenylacetylene **38** calibration

m(PhCCPh) (mg)	V(dodecane) (μL)	Total solvent (mL)	[M](PhCCPh)/ [M](dodecane)	Area(PhCCPh)/ Area(dodecane)
5.7	20	10	0.349169443	0.446152511
9.03	20	10	0.553157907	0.711625359
11.75	20	10	0.719779115	0.894118761
17.26	20	10	1.057309577	1.418145766
22.09	20	10	1.353184737	1.808594299
31.54	20	10	1.932070918	2.526466128
43.14	20	10	2.642661364	3.297378599
50.38	20	10	3.086167815	3.840739665
64.98	20	10	3.980531651	5.04924082
103.8	20	10	6.358559332	7.751969193

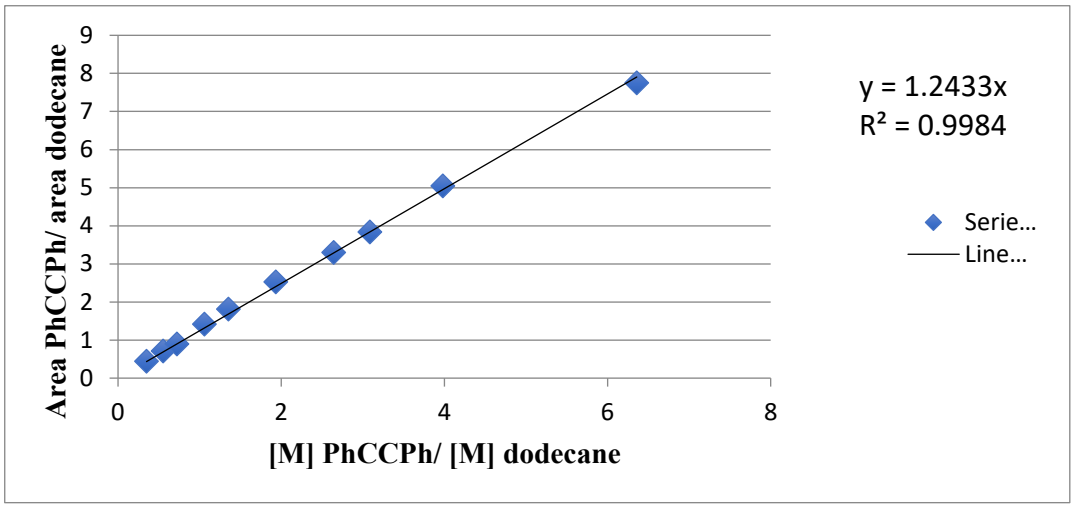

4.3.5 Hydrogenation of allylbenzene 34 using [Ni(η^3-allyl)(NPEt$_3$)]$_2$ 24

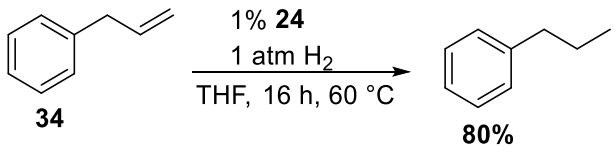

The general procedure was applied for the hydrogenation of allylbenzene (75.9 mg, 0.64 mmol) using 1 mol% [Ni(η^3-allyl)(NPEt$_3$)]$_2$ **24** (3 mg, 0.0064 mmol). GC-MS and ^{1}H NMR spectroscopy were used to characterize the product, 1-phenylpropane. Remaining material was unreacted allyl benzene.

4.3.6 Hydrogenation of *cis*-stilbene 35 using [Ni(η^3-allyl)(NPEt$_3$)]$_2$ 24

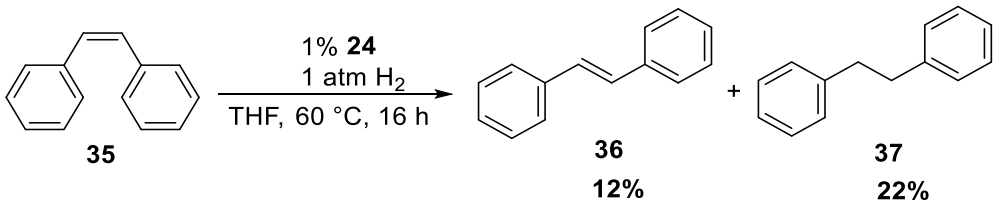

The general procedure was applied for *cis*-stilbene hydrogenation (115.8 mg, 0.64 mmol) using 1 mol% [Ni(η^3-allyl)(NPEt$_3$)]$_2$ **24** (3 mg, 0.0064 mmol).

4.3.7 Hydrogenation of *trans*-stilbene 36 using [Ni(η^3-allyl)(NPEt$_3$)]$_2$ 24

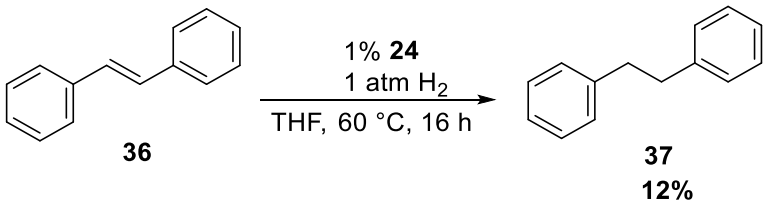

Trans-stilbene (115.8 mg, 0.64 mmol) hydrogenation using [Ni(η^3-allyl)(NPEt$_3$)]$_2$ **24** (3 mg, 0.0064 mmol) was performed according to the general procedure.

4.3.8 Hydrogenation of diphenylacetylene 38 using [Ni(η^3-allyl)(NPEt$_3$)]$_2$ 24

Diphenylacetylene (114.5mg, 0.64mmol) hydrogenation using **[**Ni(η^3-allyl)(NPEt$_3$)]$_2$ **24** (3 mg, 0.0064 mmol) was performed according to the general procedure.

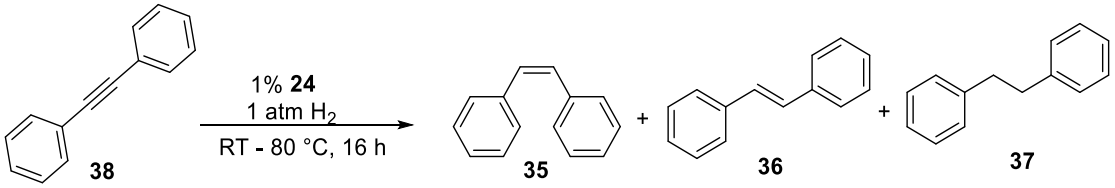

Entry	Solvent	Temperature (°C)	Total conversion	Conversion (%)		
				35	36	37
1	THF	RT	0	0	0	0
2	Toluene	60	100	11	71	18
3	THF	60	100	31	56	13
4[a]	THF	60	87	78	1	8
5[b]	THF	60	85	85	6	9
6	Toluene	80	26	16	10	0
7	THF	80	27	17	10	0

a. Reaction performed at 34 atm H_2 b. 5 mol% precatalyst loading was used

4.3.9 Mercury test for heterogeneity. Hydrogenation of diphenylacetylene using [Ni(η^3-allyl)(NPEt$_3$)]$_2$ 24

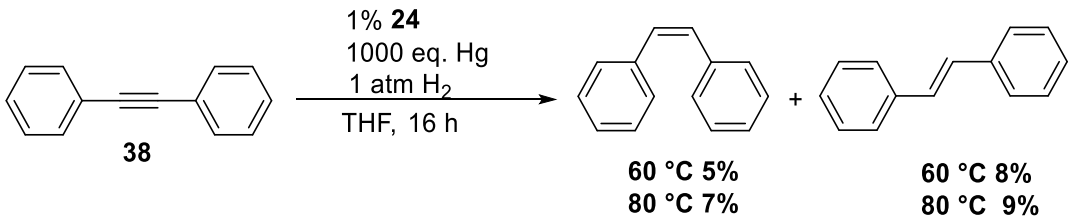

The general procedure was followed, but in the presence of excess Hg (1.3 g, 6.5 mmol, 1000 equiv), diphenylacetylene (114.5 mg, 0.64 mmol) and 1% [Ni(η^3-allyl)(NPEt$_3$)]$_2$

24 (3 mg, 0.0064 mmol). After cooling and venting, the solution was decanted from the mercury puddle and the general analysis procedure applied.

4.3.10 Hydrogenation of diphenylacetylene using "preactivated" [Ni(η^3-allyl)(NPEt$_3$)]$_2$ 24

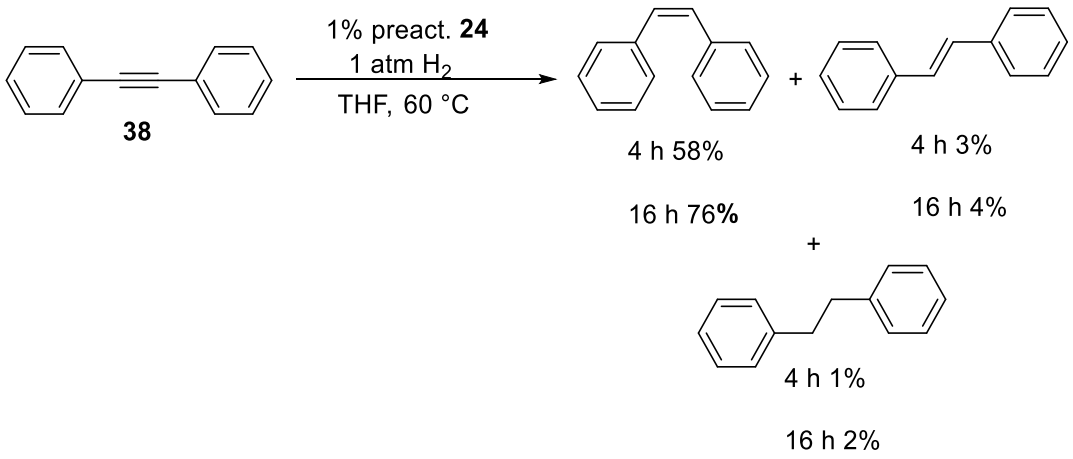

In the drybox, a medium-walled glass reactor was charged with [Ni(η^3-allyl)(NPEt$_3$)]$_2$ **24** (3 mg, 0.0064 mmol), 5 mL THF, and a magnetic stir bar. The vessel was removed form the drybox, transferred to the hydrogen line, degassed by one freeze-pump-thaw cycle and charged with one atm H_2. The reactor was heated at 60 °C for one hour in an aluminium dry-block heating adapter. A colour change from golden-brown to dark brown was observed. After one hour, the reaction mixture was allowed to cool to room temperature and transferred into the drybox, where it was charged with diphenylacetylene (114.5 mg, 0.64 mmol) and one mL THF. The reactor was transferred

out of the box and heated at 60 °C for 4 or 16 hours. The reaction mixture was quenched and analyzed according to the general procedure.

4.3.11 Hydrogenation of diphenylacetylene using "preheated" [Ni(η^3-allyl)(NPEt$_3$)]$_2$ **24**

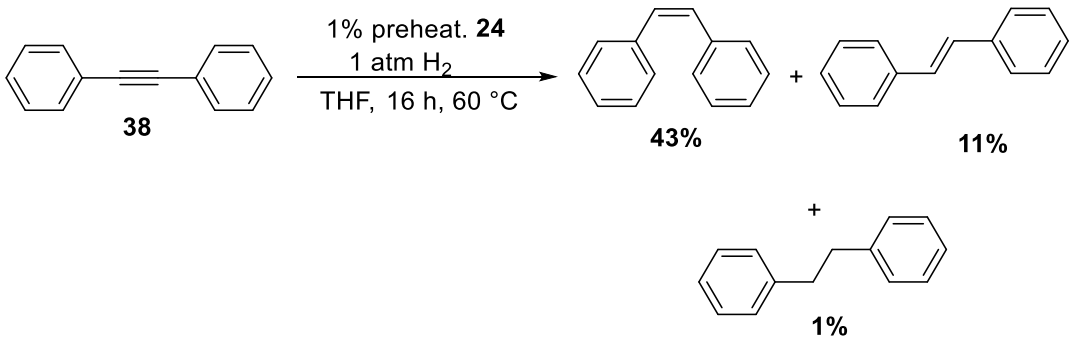

A medium-walled glass reactor was treated with [Ni(η^3-allyl)(NPEt$_3$)]$_2$ **24** (3 mg, 0.0064 mmol) and 5 mL THF in the drybox. The glass reactor was heated for one hour at 60 °C in an aluminium dry-block heating adapter, during which no colour change occurred. The reaction mixture was allowed to cool to room temperature and transferred into the drybox and charged with diphenylacetylene (114.5 mg, 0.64 mmol) and one mL THF. The reactor removed from the box and connected to the hydrogen line, degassed by one freeze-pump-thaw cycle, and charged with one atm H_2. The reaction was quenched and analyzed according to the general procedure.

4.3.12 Hydrogenation of *cis*-stilbene 35 using [Ni(η^3-allyl)(NPPh$_3$)]$_2$ 26

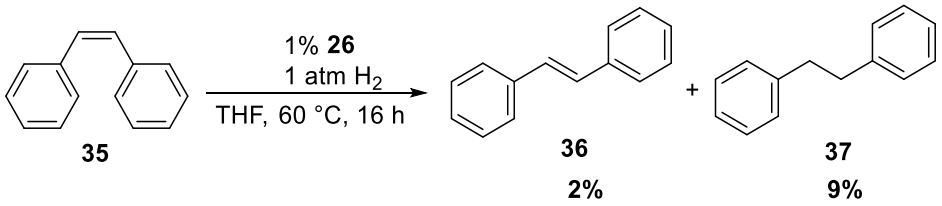

The general procedure was applied for the hydrogenation of *cis*-stilbene (71.2 mg, 0.40 mmol) with [Ni(η^3-allyl)(NPPh$_3$)]$_2$ **25** (3 mg, 0.0040 mmol).

4.3.13 Hydrogenation of *trans*-stilbene 37 using [Ni(η^3-allyl)(NPPh$_3$)]$_2$ 26

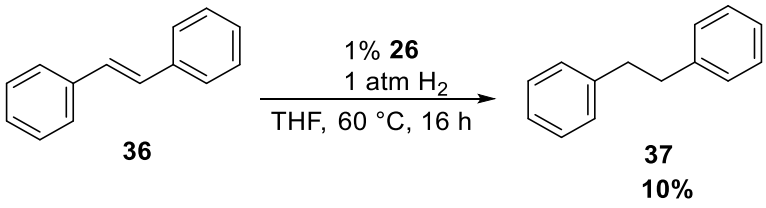

Trans-stilbene (71.2 mg, 0.40 mmol) hydrogenation using [Ni(η^3-allyl)(NPPh$_3$)]$_2$ **26** (3 mg, 0.0040 mmol) was performed according to the general procedure.

4.3.14 Hydrogenation of diphenylacetylene 38 using [Ni(η^3-allyl)(NPPh$_3$)]$_2$ 26

Diphenylacetylene (70.4 mg, 0.39 mmol) in the presence of [Ni(η^3-allyl)(NPPh$_3$)]$_2$ **26** (3 mg, 0.0039 mmol) was investigated according to the general procedure.

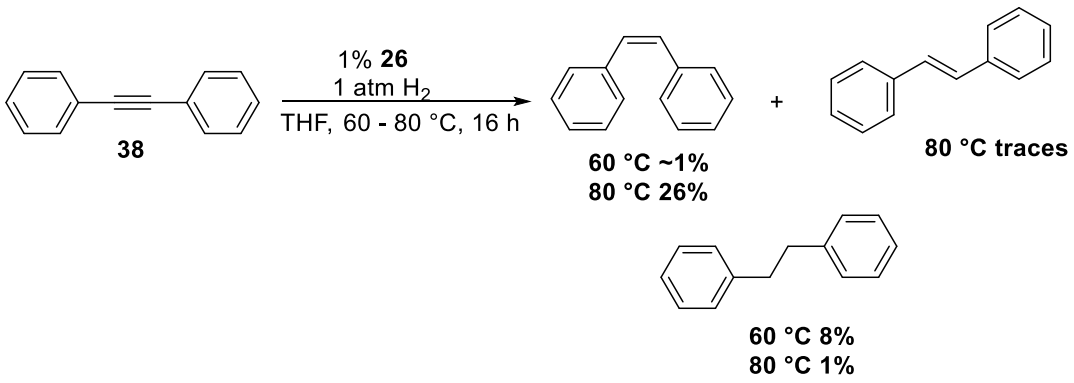

4.3.15 Mercury heterogeneity test for the hydrogenation of diphenylacetylene using [Ni(η^3-allyl)(NPPh$_3$)]$_2$ 26

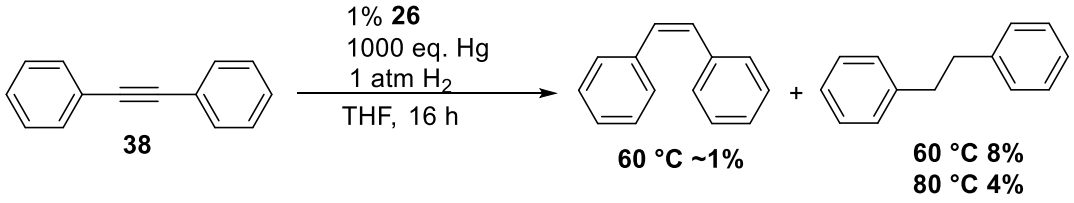

A medium-walled glass reactor was charged with diphenylacetylene (70.4 mg, 0.39 mmol), [Ni(η^3-allyl)(NPPh$_3$)]$_2$ (3 mg, 0.0039 mmol), magnetic stir bar, 6 mL THF, and excess Hg (1.3 g, 6.5 mmol), following the general procedure. After cooling and venting, the solution was decanted from the mercury, quenched, and analyzed according to the general procedure applied.

4.3.16 Hydrogenation of diphenylacetylene 38 using [Co(η^3-allyl)(NP^{t}Bu$_3$)]$_2$ 31

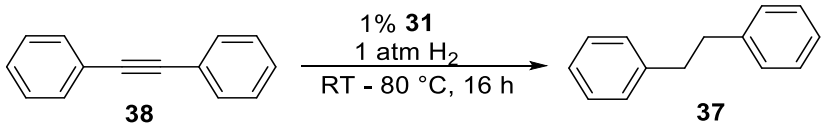

The hydrogenation of diphenylacetylene (128 mg, 0.72 mmol) using [Co(η^3-allyl)(NP^{t}Bu$_3$)]$_2$ **31** (2.3 mg, 0.0072 mmol) was performed according to the general procedure.

Entry	Solvent	Temperature (°C)	Conversion (%)[b]
			37
1	Toluene	RT	0
2	THF	RT	20
3	THF	50	9
4	THF	80	12

4.3.17 Hydrogenation of *trans*-stilbene 36 using [Fe(η^3-allyl)(NP^{t}Bu$_3$)]$_2$ 33

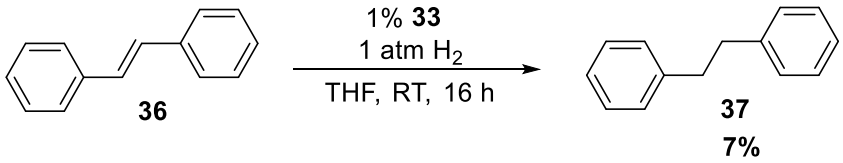

Trans-stilbene (142 mg, 0.79 mmol) hydrogenation in the presence of **[**Fe(η^3-allyl)(NP^{t}Bu$_3$)]$_2$ **33** (2.5 mg, 0.008 mmol) was investigated according to the general procedure.

4.3.18 Hydrogenation of diphenylacetylene 38 using [Fe(η^3-allyl)(NP^{t}Bu$_3$)]$_2$ 33

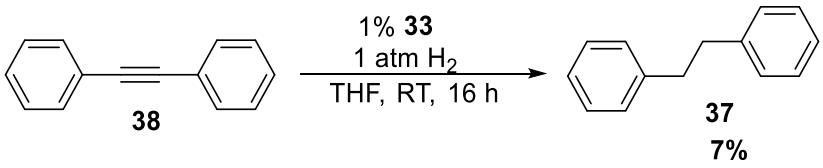

Diphenylacetylene (145 mg, 0.79 mmol) hydrogenation in the presence of [Fe(η^3-allyl)(NP^{t}Bu$_3$)]$_2$ **33** (2.5 mg, 0.008 mmol) was performed according to the general procedure.

4.4 Hydrodesulfurization reactions

HDS reactions were conducted at hydrogen pressures ranging from 1-34 atm and 110-175 °C. Reactions at one atm were performed in medium-walled glass reactors sealed with a Teflon high vacuum valve. The reactor was heated in a preheated aluminum dry block heating adapter. Reactions at higher hydrogen pressure (10-34 atm) were performed in steel screw-cap autoclaves (Parr) fitted with cylindrical glass liners. The

steel reactor was heated by immersion in a preheated oil bath. Conversions were obtained from calibrated quantitative GC; *n*-dodecane was used as the standard.

4.4.1 The general procedure for dibenzothiophene HDS studies

Inside a nitrogen drybox, the reactor was charged with DBT, 1 mol% of precatalyst **24**, base (2 equiv. unless stated otherwise), 6 mL solvent, and a magnetic stir bar and sealed in the drybox. The reactor was removed from the drybox, connected to a hydrogen manifold, and charged with hydrogen. For the medium-walled glass reactors, the solution was degassed by one freeze-pump-thaw cycle before hydrogen charging to the indicated pressure. The reactor was sealed and maintained under static pressure, while heating at the indicated temperature and stirring at 1200 rpm for 16 h. The following day, the reactor was cooled to room temperature, vented, opened, and the reaction quenched with 10% HCl. The organic layer was extracted three times using toluene and the combined organic phases dried with magnesium sulfate and filtered through Florisil. The organic layer was then added to a 25 mL volumetric flask and diluted to the mark using toluene. Precisely 20 μL of *n*-dodecane was added to this solution and a portion added into a GC vial. Each sample run for 12 min. Conversions were determined by GC-FID analysis using dodecane as an internal standard. Detector calibration curves for DBT, 2-biphenylthiol and biphenyl were created. Each calibration curve was constructed using solutions of varying concentrations of each analyte along with dodecane. The

concentration of DBT, 2-thiolbiphenyl and biphenyl in the reaction mixtures were calculated using the calibration curves below.

4.4.2 Calibration of GC for biphenyl, biphenylthiol and dibenzothiophene (*adapted from previous group members*)

Table 4.5: Dibenzothiophene **43** calibration

m(DBT) (mg)	V(dodecane) (μL)	Total solvent (mL)	[M](DBT)/ [M](dodecane)	Area(DBT)/ Area(dodecane)
0.07425	5	50	17.58112771	16.11516854
0.1425	10	100	16.87077911	22.54077253
0.135	10	100	15.98284337	17.04778157
0.1275	10	100	15.09490763	15.06369427
0.12	10	100	14.20697188	16.1
0.1125	10	100	13.31903614	13.875
0.105	10	100	12.4311004	13.0952381
0.09	10	100	10.65522891	13.52459016
0.075	10	100	8.879357427	9.365853659
0.06	10	100	7.103485942	9.385650224
0.045	10	100	5.327614456	6.655737705
0.03	10	100	3.551742971	3.338557994
0.015	10	100	1.775871485	1.869257951
0.0015	10	100	0.177587149	0.211320755

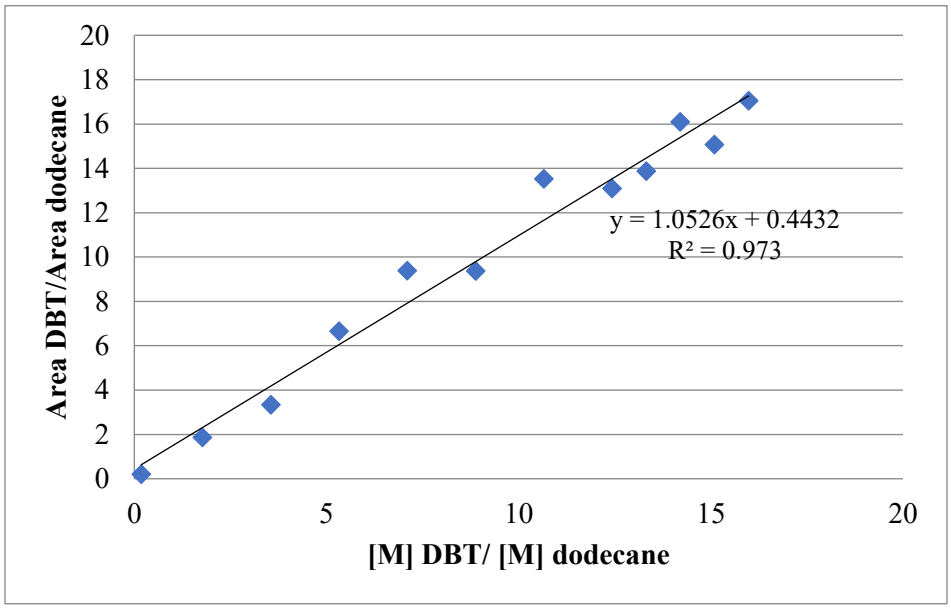

Table 4.6: Biphenylthiol **44** calibration

m(RSH) (mg)	V(dodecane) (μL)	Total solvent (mL)	[M](RSH)/ [M](dodecane)	Area(RSH)/ Area(dodecane)
2	10	50	0.234227791	0.228380503
13	10	50	1.522480642	1.333457778
11.5	10	25	1.346809799	1.170280183
22.5	10	25	2.63506265	2.533568905
54.2	10	25	6.34757314	5.840881105
45.4	10	10	5.316970859	5.259952429
48.1	10	5	5.633178377	5.454527851
90.1	10	5	10.55196199	11.29558588

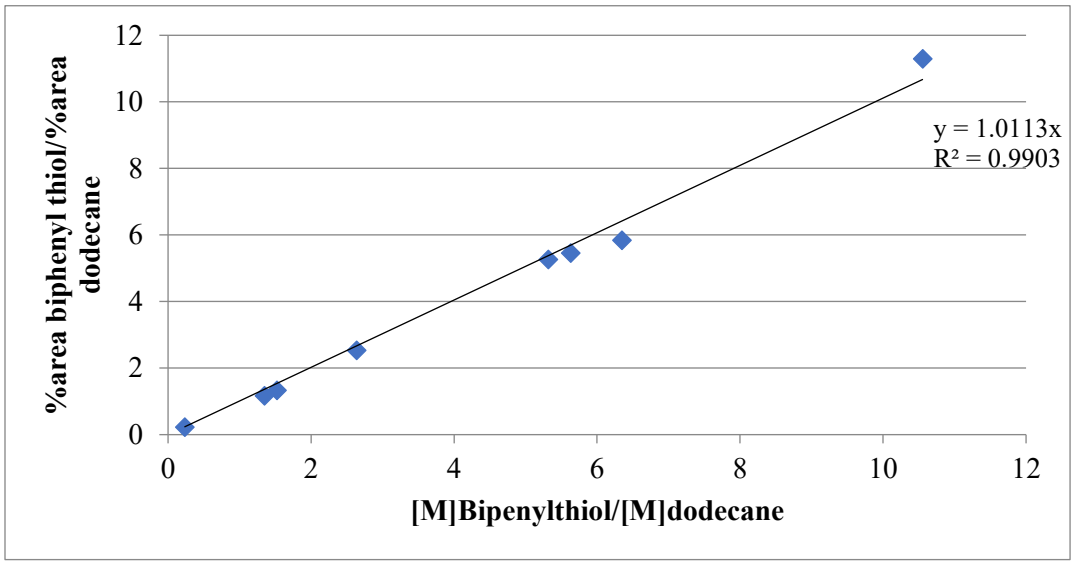
%area biphenyl thiol/%area dodecane
[M]Bipenylthiol/[M]dodecane
y = 1.0113x
R² = 0.9903
0
2
4
6
8
10
12

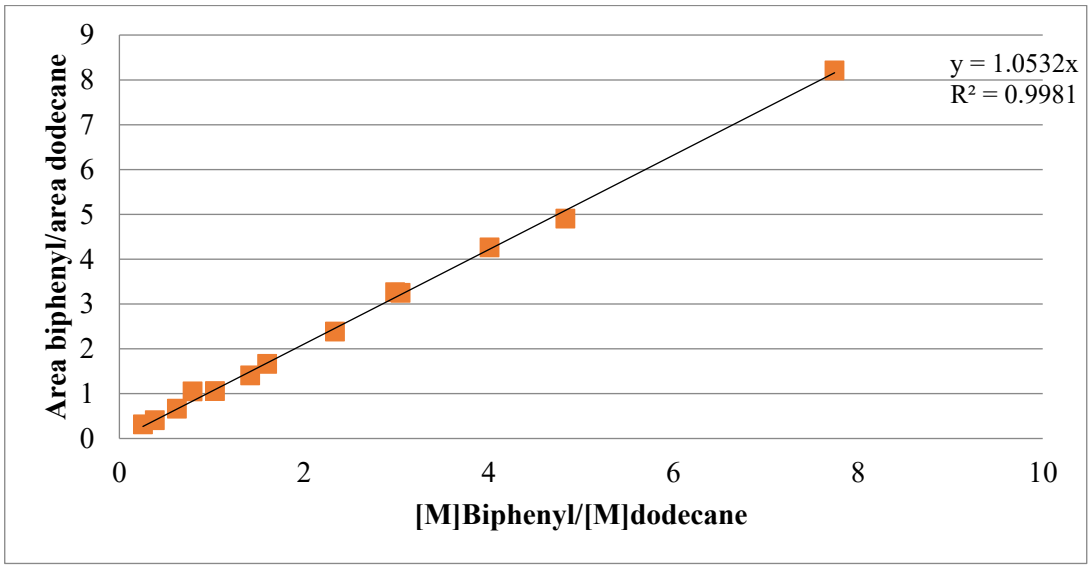
Area biphenyl/area dodecane
[M]Biphenyl/[M]dodecane
y = 1.0532x
R² = 0.9981
0
1
2
3
4
5
6
7
8
9
10

Table 4.7: Biphenyl **45** calibration

m(biphenyl) (mg)	V(dodecane) (μL)	Total solvent (mL)	[M](biphenyl)/ [M](dodecane)	Area(biphenyl)/ Area(dodecane)
2.7	10	5	0.38233827	0.406746757
4.4	10	5	0.623069773	0.664890783
7.3	10	5	1.033729397	1.059138456
11.3	10	5	1.600156463	1.661981579
16.5	10	5	2.33651165	2.383425302
21.1	10	5	2.987902777	3.261484701
28.3	10	5	4.007471497	4.260389269
34.1	10	5	4.828790743	4.905628064
1.8	10	50	0.25489218	0.316863757
5.6	10	50	0.792997893	1.052840104
10	10	25	1.416067667	1.408419836
21.5	10	25	3.044545483	3.247547042
54.7	10	25	7.745890136	8.212344542

4.4.3 Hydrodesulfurization control experiments using MO^{t}Bu (M= K, Na), MTMP (M= K, Na)

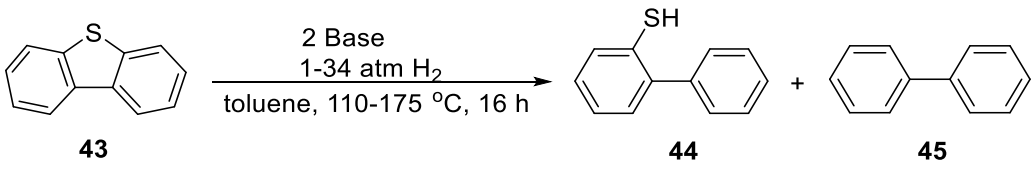

Base screening reactions were performed according to the general procedure (excluding the precatalyst) using dibenzothiophene (118.4 mg, 0.64 mmol), the designated base, and 6 mL toluene.

Entry	Base	Temperature (°C)	H_2 pressure (atm)	Conversion (%)	
				44	**45**
1	KTMP	110	1	8	1
2	KTMP	150	1	68	8
[a]3	KTMP	175	34	42	36
4	NaTMP	150	34	0	0
5	KO^{t}Bu	150	34	0	0
[a]6	KO^{t}Bu	175	34	0	0
7	NaO^{t}Bu	150	34	0	8

a. Conversion in 4 hours in cyclooctane.

4.4.4 Hydrodesulfurization of dibenzothiophene using catalyst 24 and stoichiometric MO^{t}Bu

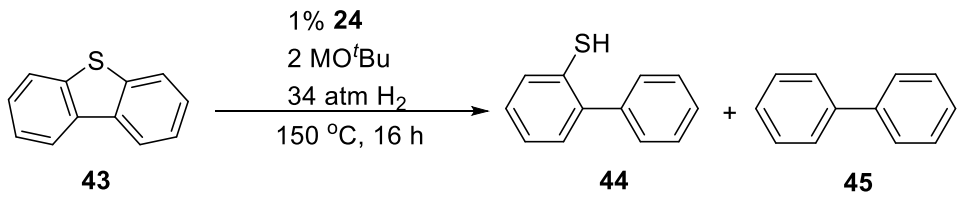

43 **44** **45**

Dibenzothiophene (118.4 mg, 0.64 mmol) hydrodesulfurization was performed using [Ni(η^3-allyl)(NPEt$_3$)]$_2$ **24** (3 mg, 0.0064 mmol), MO^{t}Bu (M = K or Na; 1.28 mmol) in THF, and toluene or cyclooctane solvent, according to the general procedure.

Entry	**Solvent**	**Total conversion**	**Conversion (%)**	
			44	**45**
1	THF	S	0	s
2	Toluene	78	71	7
[a]3	Toluene	14	0	14
[b]4	Toluene	15	1	15
5	Cyclooctane	76	63	13

d. Reaction performed in the presence of NaO^{t}Bu instead of KO^{t}Bu.
e. Reaction performed with 5% KO^{t}Bu and 2 equiv. NaO^{t}Bu.

4.4.5 Hydrodesulfurization of dibenzothiophene using 24 and stoichiometric MTMP

The hydrodesulfurization of dibenzothiophene (118.4 mg, 0.64 mmol), using [Ni(η^3-allyl)(NPEt$_3$)]$_2$ **24** (3 mg, 0.0064 mmol) and MTMP (M= Na or K, 1.28 mmol, 2 equiv.) in THF or toluene or cyclooctane was performed according to the general procedure.

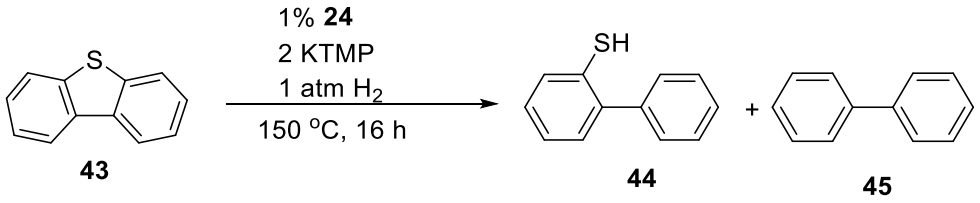

Entry	Solvent	Total conversion	Conversion (%)	
			44	**45**
1	THF	36	17	19
2	Toluene	88	37	51
3	Cyclooctane	73	51	22

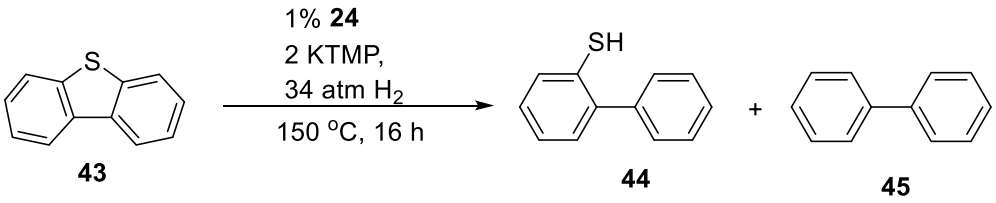

Entry	Solvent	Total conversion	Conversion (%)	
			44	**45**
1	THF	49	22	27
2	Toluene	96	1	95
3[a]	Toluene	67	3	64
4	Cyclooctane	97	1	96

a. Reaction performed with NaTMP instead of KTMP

4.4.6 Mercury heterogeneity test for the hydrodesulfurization of DBT using [Ni(η^3-allyl)(NPEt$_3$)]$_2$ 24

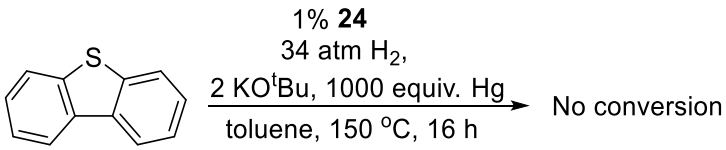

DBT (118.4 mg, 0.64 mmol) hydrodesulfurization was performed according to the general procedure in the presence of catalytic [Ni(η^3-allyl)(NPEt$_3$)]$_2$ **24** (3 mg, 0.0064 mmol), KO^{t}Bu (144 mg, 1.28 mmol), and excess Hg (1.3 g, 6.5 mmol, 1000 equiv). After cooling and venting, the solution was decanted from the mercury and analyzed according to the general procedure. No conversion was detected.

4.4.7 Alumina-supported [Ni(η^3-allyl)(NPEt$_3$)]$_2$

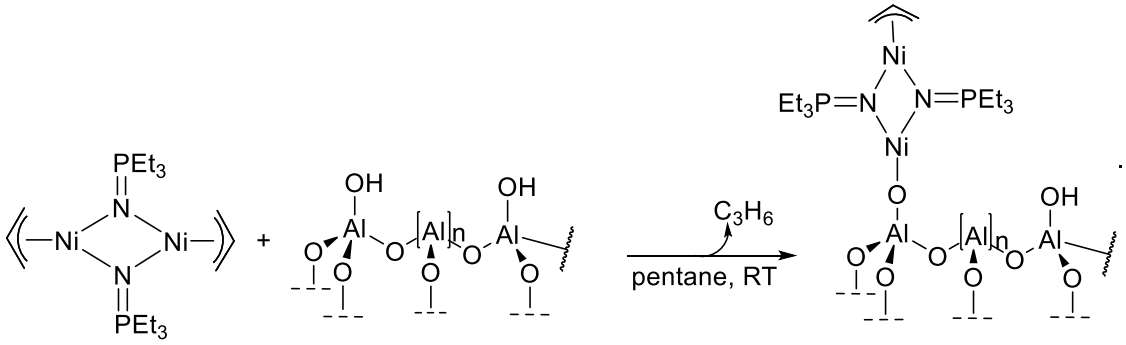

Dehydrated Al_2O_3 (quantity specified) was suspended in 2 mL pentane and a solution of **24** (3 mg, 0.006 mmol) in 2 mL pentane slowly added under vigorous stirring. The solution rapidly decolourized over 15 sec to 3 min, depending on the amount of alumina

used. The resulting slurry was filtered, providing beige solids. The supernatant was evaporated under reduced pressure, affording a thin white film around the vial. The thin film was dissolved in C_6D_6 and analyzed by ^{31}P NMR spectroscopy, which did not reveal any signals for liberated phosphoranimine.

Entry	**wt% (24/Al_2O_3)**	**Al_2O_3 (mg)**
1	4.0	70
2	2.0	144
3	1.5	200
4	1.0	288
5	0.5	576

4.4.8 Hydrodesulfurization of dibenzothiophene using 24 with KO^{t}Bu

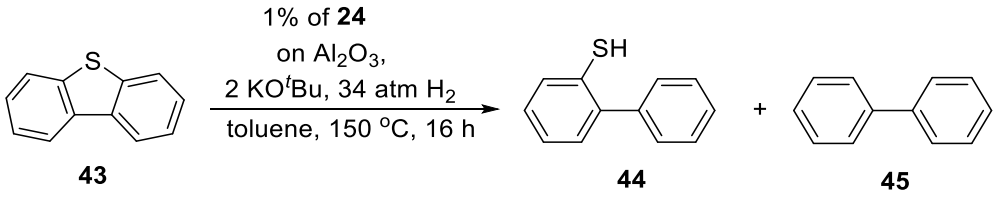

The general procedure was applied to the hydrodesulfurization of dibenzothiophene (118.4 mg, 0.64 mmol) in the presence of supported-**24** (0.006 mmol, assuming all precatalyst was loaded onto the alumina) and KO^{t}Bu (1.28 mmol).

Entry	**wt%(24/Al_2O_3)**	**Total conversion**	**Conversion (%)**	
			44	**45**
1	0.5	26	11	15
2	1	90	10	80
3	1.5	69	25	44
4	2	78	35	43
5	4	66	36	30

Bibliography

(1) Bachmann, R. T.; Johnson, A. C.; Edyvean, R. G. J. *Int. Biodeterior. Biodegradation* **2014**, *86*, 225–237.

(2) Schuman, S. C.; Shalit, H. *Catal. Rev.* **1971**, *4*, 245–318.

(3) Argyle, M. D.; Bartholomew, C. H. *Catalysts* **2015**, *5*, 145–269.

(4) Stanislaus, A.; Marafi, A.; Rana, M. S. *Catal. Today* **2010**, *153*, 1–68.

(5) Corro, G. *React. Kinet. Catal. Lett.* **2002**, *75*, 89–106.

(6) Environment and Climate Change Canada - Air - Sulphur in Gasoline Regulations https://www.ec.gc.ca/energie-energy/default.asp?lang=En&n=BEA13229-1 (accessed Mar 29, 2017).

(7) Rodríguez-Reinoso, F.; Santana, P.; Palazon, E. R.; Diez, M.-A.; Marsh, H. *Carbon N. Y.* **1998**, *36*, 105–116.

(8) Sawarkar, A. N.; Pandit, A. B.; Samant, S. D.; Joshi, J. B. *Can. J. Chem. Eng.* **2007**, *85*, 1–24.

(9) Derakhshesh, M.; Eaton, P.; Newman, B.; Hoff, A.; Mitlin, D.; Gray, M. R. *Energy & Fuels* **2013**, *27*, 1856–1864.

(10) Sánchez-Delgado, R. A. *J. Mol. Catal.* **1994**, *86*, 287–307.

(11) Schuit, G. C. A.; Gates, B. C. *AIChE J.* **1973**, *19*, 417–438.

(12) Cornell, P. W. Hydrodesulfurization of petroleum hydrocarbons. US2614066 A, 1952.

(13) Torres-Nieto, J.; Brennessel, W. W.; Jones, W. D.; García, J. J. *J. Am. Chem. Soc* **2009**, *131*, 4120–4126.

(14) Song, C. *Catal. Today* **2003**, *86*, 211–263.

(15) Quartararo, J.; Mignard, S.; Kasztelan, S. *J. Catal.* **2000**, *192*, 307–315.

(16) Burns, A. W.; Layman, K. A.; Bale, D. H.; Bussell, M. E. *Appl. Catal. A Gen.* **2008**, *343*, 68–76.

(17) Cecilia, J. A.; Infantes-Molina, A.; Rodriguez-Castellon, E.; Jimenez-Lopez, A. *J. Phys. Chem. C* **2009**, *113*, 17032–17044.

(18) Staudinger, H.; Hauser, E. *Helv. Chim. Acta* **1919**, *2*, 635–646.

(19) Gröb, T.; Müller, C.; Massa, W.; Miekisch, T.; Seybert, G.; Harms, K.; Dehnicke, K. *Zeitschrift für Anorg. und Allg. Chemie* **2001**, *627*, 2191.

(20) Courtenay, S.; Wei, P.; Stephan, D. W. *Can. J. Chem.* **2003**, *81*, 1471–1476.

(21) Sundermann, A.; Schoeller, W. W. *J. Am. Chem. Soc* **2000**, *122*, 4729–4734.

(22) Brown, H. J. S. Mixed-Valence First-Row Metal Clusters for Catalytic Hydrodesulfurization and Hydrodeoxygenation, 2013.

(23) Stephan, D. W. *Organometallics* **2005**, 2548–2560.

(24) Stephan, D. W.; Stewart, J. C.; Guérin, F.; Courtenay, S.; Kickham, J.; Hollink, E.; Beddie, C.; Hoskin, A.; Graham, T.; Wei, P.; Rupert, E.; Spence, H.; Xu, W.; Koch, L.; Gao, X.; Harrison, D. G. *Organometallics* **2003**, *22*, 1937–1947.

(25) Stephan, D. W. *Macromol. Symp.* **2001**, *173*, 105–115.

(26) Martin, R.; Buchwald, S. L. *Acc. Chem. Res.* **2008**, *41*, 1461–1473.

(27) Aranyos, A.; Old, D. W.; Kiyomori, A.; Wolfe, J. P.; Sadighi, J. P.; Buchwald, S. L. *J. Am. Chem. Soc.* **1999**, *121*, 4369–4378.

(28) Matsui, S.; Mitani, M.; Saito, J.; Tohi, Y.; Makio, H.; Matsukawa, N.; Takagi, Y.; Tsuru, K.; Nitabaru, M.; Nakano, T.; Tanaka, H.; Kashiwa, N.; Fujita, T. *J. Am. Chem. Soc.* **2001**, *123*, 6847–6856.

(29) Gibson, V. C.; Spitzmesser, S. K. *Chem. Rev.* **2003**, *103*, 283–315.

(30) Park, S.; Han, Y.; Kim, S. K.; Lee, J.; Kim, H. K.; Do, Y. *J. Organomet. Chem.* **2004**, *689*, 4263–4276.

(31) Baier, M. C.; Zuideveld, M. A.; Mecking, S. *Angew. Chemie Int. Ed.* **2014**, *53*, 9722–9744.

(32) Honeyman, C. H.; Lough, A. J.; Manners, I. *Inorg. Chem.* **1994**, *33*, 2988–2993.

(33) Roesky, H. W.; Hesse, D.; Rietzel, M.; Noltemeyer, M. *Z. Naturforsch* **1990**, 4–8.

(34) Nusshar, D.; Weller, F.; Dehnicke, K. *Z. anorg. allg. Chem* **1993**, *619*, 1121.

(35) Roesky, H. W.; Leichtweis, I.; Noltemeyer, M. *Inorg. Chem.* **1993**, *15*, 5102–5104.

(36) Stahl, M. M.; Faza, N.; Massa, W.; Dehnicke, K. *Z. anorg. allg. Chem* **1998**, *624*, 209–214.

(37) LePichon, L.; Stephan, D. W.; Gao, X.; Wang, Q. *Organometallics* **2002**, *21*,

1362–1366.

(38) Dehnicke, K.; Krieger, M.; Massa, W. *Coord. Chem. Rev.* **1999**, *182*, 19–65.

(39) Camacho-Bunquin, J.; Ferguson, M. J.; Stryker, J. M. *J. Am. Chem. Soc* **2013**, *135*, 5537–5540.

(40) de Beer, V. H. J.; Duchet, J. C.; Prins, R. *J. Catal.* **1981**, *72*, 369–372.

(41) Chianelli, R. R.; Berhault, G.; Torres, B. *Catal. Today* **2009**, *147*, 275–286.

(42) Toulhoat, H.; Raybaud, P.; Kasztelan, S.; Kresse, G.; Hafner, J. *Catal. Today* **1999**, *50*, 629–636.

(43) Mai, H.-J.; Meyer zu Kocker, R.; Wocaldo, S.; Massa, W.; Dehnicke, K. *Angew. Chemie Int. Ed. English* **1995**, *83*, 1235–1236.

(44) Trimethylsilyl azide MSDS - 818026 - MilliporeSigma http://www.emdmillipore.com/Web-CA-Site/en_CA/-/CAD/ProcessMSDS-Start?PlainSKU=MDA_CHEM-818026&ReferrerURL=https%3A%2F%2Fwww.google.ca%2F&Origin=PDP&bd=1 (accessed Jun 20, 2017).

(45) Zimmer, H.; Jayawant, M.; Gutsch, P. *J. Org. Chem.* **1970**, *35*, 2826–2828.

(46) Hamilton, R. J. *manuscript in prep.*

(47) Hebert, D.; Stryker, J. M. *Unpubl. Work*.

(48) Brown, O. *Unpublished work*.

(49) Widegren, J. A.; Bennett, M. A.; Finke, R. G. *J. Am. Chem. Soc.* **2003**, *125*, 10301–10310.

(50) Birkenstock, U.; Bonnenmann, B.; Bogdanović, B.; Walter, D.; Wilke, G. *Adv. Chem.* **1974**, 250–265.

(51) Lee, C. E.; Tiege, P. B.; Xing, Y.; Nagendran, J.; Bergens, S. H. *J. Am. Chem. Soc.* **1997**, *119*, 3543–3549.

(52) Oberhansli, W. E.; Dahl, L. F. *J. Organomet. Chem. 3*, 43–54.

(53) Wilke, G.; Bogdanović, B.; Hardt, P.; Heimbach, P.; Keim, W.; Kröner, M.; Oberkirch, W.; Tanaka, K.; Steinrücke, E.; Walter, D.; Zimmermann, H. *Angew. Chemie Int. Ed. English* **1966**, *5*, 151–164.

(54) Bönnemann, H.; Grard, C.; Kopp, W.; Pump, W.; Tanaka, K.; Wilke, G. *Angew. Chemie Int. Ed. English* **1973**, *12*, 964–975.

(55) Henc, B.; Jolly, P. W.; Salz, R.; Stobbe, S.; Wilke, G.; Benn, R.; Mynott, R.; Seevogel, K.; Goddard, R.; Kr??ger, C. *J. Organomet. Chem.* **1980**, *191*, 449–475.

(56) Fischer, E. O.; Burger, G. *Z. Naturforsch.* **1961**, *16 b*, 77–78.

(57) Zhao, T. Phosphoranimide-supported Nickel Clusters for Hydrotreatment, University of Alberta, 2016.

(58) Dehm, H. C.; Chien, J. C. W. *J. Am. Chem. Soc.* **1960**, *82*, 4429–4430.

(59) Brian Mann, B. E.; Pietropaolo, R.; Shaw, B. L.; Xxxiii, P.; Gill, D. F.; Mann, B. E.; Shaw, B. L.; Robinson, S. D.; Chem Soc, J.; Vrieze, K.; Volger, H. C.; N M Van Lceuwen, P. W.; Volger, E. C.; Chem Product Res, E.; Coates, G. E.; H Green, M. L.; Wade, K.; Dalton, O.-J. *J. Chem. Soc. Dalt. Trans.* **1973**, *3*, 2390–2393.

(60) Cotton, F. A.; Faller, J. W.; Mucso, A. *Inorg. Chem* **1967**, *6*, 179.

(61) Mcclellan, W. R.; Hoehn, H. H.; Cripps, H. N.; Muetterties, E. L.; Howk, B. W. **1961**.

(62) Brunkan, N. M.; Jones, W. D. *J. Organomet. Chem.* **2003**, *683*, 77–82.

(63) Herrmann, J.; Pregosin, P. S.; Salzmann, R. *Organometallics* **1995**, 3311–3318.

(64) Trost, B. M.; Van Vranken, D. L. *Chem. Rev.* **1996**, *96*, 395–422.

(65) Abrams, M. B.; Yoder, J. C.; Loeber, C.; Day, M. W.; Bercaw, J. E. *Organometallics* **1999**, *18*, 1389–1401.

(66) VRIEZE, K. In *Dynamic Nuclear Magnetic Resonance Spectroscopy*; 1975; pp 441–487.

(67) Rabaa, H.; Khaledi, H.; Olmstead, M. M.; Sundholm, D. *J. Phys. Chem. A* **2015**, *119*, 5189–5196.

(68) Frommel, T.; Peters, W.; Wunderlich, H.; Kuchen, W. *Angew. Chemie - Int. Ed.* **1992**, *31*, 612–613.

(69) Bridgeman, A. J. *Dalt. Trans.* **2008**, *2*, 1989–1992.

(70) Riese, U. Phosphanimato-komplexe electronereicher ubergangsmetalle, Philips-Universitat, Marbugg.

(71) Shobatake, K.; Nakamoto, K. *J. Am. Chem. Soc.* **1970**, *92*, 3339–3342.

(72) Fu, S.; Chen, N.-Y.; Liu, X.; Shao, Z.; Luo, S.-P.; Liu, Q. *J. Am. Chem. Soc.*

2016, *138*, 8588–8594.

(73) Phua, P.-H.; Lefort, L.; Boogers, J. A. F.; Tristany, M.; De Vries, J. G. *Chem. Commun.* **2009**, 3747–3749.

(74) Carenco, S.; Leyva-Pérez, A.; Concepción, P.; Boissière, C.; Mézailles, N.; Sanchez, C.; Corma, A. *Nano Today* **2012**, *7*, 21–28.

(75) Yu, W.; Porosoff, M. D.; Chen, J. G. *Chem. Rev.* **2012**, *112*, 5780–5817.

(76) Simakova, I. L.; Simakova, O. A.; Romanenko, A. V; Yu Murzin, D. *Ind. Eng. Chem. Res* **2008**, *47*, 7219–7225.

(77) Pandarus, V.; Gingras, G.; Ois Beíand, F.; Ciriminna, R.; Pagliaro, M. *Org. Process Res. Dev.* **2012**, *16*, 1307–1311.

(78) Belkacemi, K.; Boulmerka, A.; Arul, J.; Hamoudi, S. *Top. Catal.* **2006**, *37*, 113–120.

(79) Stanislaus, A.; Cooper, B. *Catal. Rev.* **1994**, *36*, 75–123.

(80) Navarro, R. M.; Pawelec, B.; Trejo, J. M.; Mariscal, R.; Fierro, J. L. G. *J. Catal.* **2000**, *189*, 184–194.

(81) Cooper, B. H.; Donnis, B. B. L. *Appl. Catal. A Gen.* **1996**, *137*, 203–223.

(82) Arbelaez, O.; Correa, L.; Parapat, R. Y.; Knemeyer, K.; Bustamante, F.; Villa, A. L.; Schwarze, M. *Chem. Eng. Technol.* **2015**, *38*, 2291–2298.

(83) Farnetti, E.; Di Monte, R.; Kašpar, J. *Inorg. BIO-INORGANIC Chem. – 2*.

(84) Shylesh, S.; Schünemann, V.; Thiel, W. R. *Angew. Chemie Int. Ed.* **2010**, *49*, 3428–3459.

(85) Cole-Hamilton, D. J. *Science (80-.).* **2003**, *299*.

(86) Blazina, D.; Duckett, S. B.; Dyson, P. J.; Lohman, J. A. B. *Chem. - A Eur. J.* **2003**, *9*, 1045–1061.

(87) Coperet, C.; van Santen, R.; Pérez-Ramírez, J.; Bridier, B.; Lopez Dalton Trans, N.; Janssen, M.; Müller, C.; Vogt, D.; Trans, D.; Noureddine Ajellal, C.; Carpentier, J.-F.; Guillaume, C.; Guillaume, S. M.; Helou, M.; Poirier, V.; Sarazin, Y.; Trifonov, A.; Rangheard, C.; de Julián Fernández, C.; Phua, P.-H.; Hoorn, J.; Lefort, L.; de Vries, J. G. *Dalt. Trans* **2010**, *39*, 8464–8471.

(88) Sonnenberg, J. F.; Coombs, N.; Dube, P. A.; Morris, R. H. *J. Am. Chem. Soc* **2012**, *134*, 5893–5899.

(89) Bedford, R. B.; Betham, M.; Bruce, D. W.; Davis, S. A.; Frost, R. M.; Hird, M. *Chem. Commun.* **2006**, 1398–1400.

(90) Dyson, P. J. *Dalt. Trans.* **2003**, 2964–2974.

(91) Lin, Y.; Finke, R. G. *Inorg. Chem* **1994**, *33*, 4891–4910.

(92) Xu, R.; Chakraborty, S.; Bellows, S. M.; Yuan, H.; Cundari, T. R.; Jones, W. D. *ACS Catal.* **2016**, *6*, 2127–2135.

(93) Sajiki, H.; Mori, S.; Ohkubo, T.; Ikawa, T.; Kume, A.; Maegawa, T.; Monguchi, Y. *Chem. - A Eur. J.* **2008**, *14*, 5109–5111.

(94) Carrasco, J.; Vile Delia Fernadez-Torre, G.; Peez, R.; Peez-Ramírez, J.; Veroica Ganduglia-Pirovano, M. *J. Phys. Chem.* **2014**, *118*, 5352–5360.

(95) Bridier, B.; Pé Rez-Ramírez, J. *J. Am. Chem. Soc* **2010**, *132*, 4321–4327.

(96) Richmond, E.; Moran, J. *J. Org. Chem.* **2015**, *80*, 6922–6929.

(97) Bramwell, P. L.; Gao, J.; de Waal, B.; de Jong, K. P.; Klein Gebbink, R. J. M.; de Jongh, P. E. *J. Catal.* **2016**, *344*, 129–135.

(98) Oger, C.; Balas, L.; Durand, T.; Galano, J.-M. *Chem. Rev.* **2013**, *113*, 1313–1350.

(99) Chinchilla, R.; Naera, C. *Chem. Rev.* **2014**, *114*, 1783–1826.

(100) Barrios-Francisco, R.; García, J. J. *Appl. Catal. A Gen.* **2010**, *385*, 108–113.

(101) Gieshoff, T. N.; Chakraborty, U.; Villa, M.; Jacobi von Wangelin, A. *Angew. Chemie Int. Ed.* **2017**, *129*, 3639–3643.

(102) Srimani, D.; Diskin-Posner, Y.; Ben-David, Y.; Milstein, D. *Angew. Chemie - Int. Ed.* **2013**, *52*, 14131–14134.

(103) Kirss, R. U. *Organomet. Chem.* **1995**, *498*, 171–176.

(104) Muetterties, E. L.; Tau, K. D.; Kirner, J. F.; Harris, T. V; Stark, J.; Thompson, M. R.; Day, V. W.; Nebraska, L. *Organometallics* **1982**, *1*, 1562–1567.

(105) Solin, N.; Lmá, K.; Szabó, J. *Organometallics* **2001**, *20*, 5464–5471.

(106) Dyson, P.; Jessop, P. *Catal. Sci. Technol.* **2016**, *6*, DOI: 10.1039/C5CY02197A.

(107) Schleyer, D.; Niessen, H. G.; Bargon, J. *New J. Chem.* **2001**, *25*, 423–426.

(108) Adams, R. D.; Captain, B. *Angew. Chemie Int. Ed.* **2008**, *47*, 252–257.

(109) Widegren, J. A.; Finke, R. G. *J. Mol. Catal. A Chem.* **2003**, *198*, 317–341.

(110) Whitesides, G. M.; Hackett, M.; Brainard, R. L.; Lavalleye, J. P. P. M.; Sowinski, A. F.; Izumi, A. N.; Moore, S. S.; Brown, D. W.; Staudt, E. M. *Organometallics* **1985**, *4*, 1819–1830.

(111) Anton, D. R.; Crabtree, R. H. *Organometallics* **1983**, *2*, 855–859.

(112) Roucoux, A.; Schulz, J.; Patin, H. *Chem. Rev.* **2002**, *102*, 3757–3778.

(113) Weddle, K. S.; Aiken, J. D.; Finke, R. G. *J. Am. Chem. Soc.* **1998**, *120*, 5653–5666.

(114) Blum, J.; Amer, I.; Vollhardt, K. P. C.; Schwarz, H.; Hoehne, G. *J. Org. Chem.* **1987**, *52*, 2804–2813.

(115) Alley, W. M.; Hamdemir, I. K.; Wang, Q.; Frenkel, A. I.; Li, L.; Yang, J. C.; Menard, L. D.; Nuzzo, R. G.; Özkar, S.; Johnson, K. A.; Finke, R. G. *Inorg. Chem.* **2010**, *49*, 8131–8147.

(116) Goel, A. 8. *Tetrahedron Lett. Form. DIARYL(ALLYL)PHOSPHINE* **1984**, *25*, 4599–4600.

(117) Pruchnik, F. P.; Duraj, S. A. In *Organometallic Chemistry of the Transition Elements*; Springer US: Boston, MA, 1990; pp 427–470.

(118) Rakowski, M. C.; Hirsekorn, F. J.; Stuhl, L. S.; Muetterties, E. L. *Inorg. Chem.* **1976**, *15*, 976–2379.

(119) Stephen H. K. Ng; Craig S. Adams; Trevor W. Hayton; Peter Legzdins, * and; Patrick, B. O. *J. Am. Chem. Soc* **2003**, *125*, 15210–15223.

(120) Ninh, T. K. T.; Massin, L.; Laurenti, D.; Vrinat, M. *Appl. Catal. A Gen.* **2011**, *407*, 29–39.

(121) Dhar, G. M.; Srinivas, B. .; Rana, M. .; Kumar, M.; Maity, S. . *Catal. Today* **2003**, *86*, 45–60.

(122) Shyamal K. Bej, *, †; Samir K. Maity, ‡ and; Turaga§, U. T. *Energy & Fuels* **2004**, *18*, 1227–1237.

(123) Topsoe, H.; Clausen, B. S.; Candia, R.; Wivel, C.; Morup, S. *J. Catal.* **1981**, *68*, 433–452.

(124) Topsøe, H.; Clausen, B. S. *Appl. Catal.* **1986**, *25*, 273–293.

(125) Laurenti, D.; Phung-Ngoc, B.; Roukoss, C.; Devers, E.; Marchand, K.; Massin, L.; Lemaitre, L.; Legens, C.; Quoineaud, A.-A.; Vrinat, M. *J. Catal.* **2013**, *297*, 165–175.

(126) Nikulshin, P. A.; Ishutenko, D. I.; Mozhaev, A. A.; Maslakov, K. I.; Pimerzin, A. A. *J. Catal.* **2014**, *312*, 152–169.

(127) Vakros, J.; Papadopoulou, C.; Voyiatzis, G. A.; Lycourghiotis, A.; Kordulis, C. *Catal. Today* **2007**, *127*, 85–91.

(128) Høj, M.; Linde, K.; Hansen, T. K.; Brorson, M.; Jensen, A. D.; Grunwaldt, J.-D. *Appl. Catal. A Gen.* **2011**, *397*, 201–208.

(129) Blanchard, P.; Frizi, N.; Mary, S.; Baranek, P.; Lancelot, C.; Lamonier, C.; Payen, E. *Comptes Rendus Chim.* **2016**, *19*, 1286–1302.

(130) Srivastava, V. C. *RSC Adv.* **2012**, *2*, 759–783.

(131) Okamoto, Y.; Ishihara, S.; Kawano, M.; Satoh, M.; Kubota, T. *J. Catal.* **2003**, *217*, 12–22.

(132) Farag, H.; Whitehurst, D. .; Sakanishi, K.; Mochida, I. *Catal. Today* **1999**, *50*, 9–17.

(133) Sanchez-Delgado, R. A. *Organometallic Modeling of the HDS and HDN Reactions*; 2002.

(134) Frizi, N.; Blanchard, P.; Payen, E.; Baranek, P.; Rebeilleau, M.; Dupuy, C.; Dath, J. P. *Catal. Today* **2008**, *130*, 272–282.

(135) Castillo-Villalón, P.; Ramirez, J.; Vargas-Luciano, J. A. *J. Catal.* **2014**, *320*, 127–136.

(136) Mazoyer, P.; Geantet, C.; Diehl, F.; Loridant, S.; Lacroix, M. *Catal. Today* **2008**, *130*, 75–79.

(137) Wu, H.; Duan, A.; Zhao, Z.; Qi, D.; Li, J.; Liu, B.; Jiang, G.; Liu, J.; Wei, Y.; Zhang, X. *Fuel* **2014**, *130*, 203–210.

(138) Jiang, S.; Zhou, Y.; Ding, S.; Wei, Q.; Zhou, W.; Shan, Y. *RSC Adv.* **2016**, *6*, 106680–106689.

(139) Trueba, M.; Trasatti, S. P. *Eur. J. Inorg. Chem.* **2005**, 3393–3403.

(140) Nikulshin, P. A.; Minaev, P. P.; Mozhaev, A. V.; Maslakov, K. I.; Kulikova, M. S.; Pimerzin, A. A. *Appl. Catal. B Environ.* **2015**, *176*, 374–384.

(141) Gutiérrez, O. Y.; Klimova, T. *J. Catal.* **2011**, *281*, 50–62.

(142) Cui, F.; Li, G.; Li, X.; Lu, M.; Li, M. *Catal. Sci. Technol.* **2015**, *5*, 549–555.

(143) Shen, B.; Li, H.; Zhang, W.; Zhao, Y.; Zhang, Z.; Wang, X.; Shen, S. *Catal.*

Today **2005**, *106*, 206–210.

(144) Olguin, E.; Vrinat, M.; Ceden˜o, L.; Ramirez, J.; Borque, M.; López-Agudo, A. *Appl. Catal. A Gen.* **1997**, *165*, 1–13.

(145) Nakano, K.; Ali, S. A.; Kim, H.-J.; Kim, T.; Alhooshani, K.; Park, J.-I.; Mochida, I. *Fuel Process. Technol.* **2013**, *116*, 44–51.

(146) Saih, Y.; Nagata, M.; Funamoto, T.; Masuyama, Y.; Segawa, K. *Appl. Catal. A Gen.* **2005**, *295*, 11–22.

(147) Guevara-Lara, A.; Bacaud, R.; Vrinat, M. *Appl. Catal. A Gen.* **2007**, *328*, 99–108.

(148) Escobar, J.; De Los Reyes, J. A.; Ulín, C. A.; Barrera, M. C. *Mater. Chem. Phys.* **2013**, *143*, 213–222.

(149) Curtis, M. D.; Druker, S. H. *J. Am. Chem. Soc* **1997**, *119*, 1027–1036.

(150) Shoshani, M. M.; Johnson, S. A. *Inorg. Chem.* **2015**, *54*, 11977–11985.

(151) Brown, C. A.; Brown, H. C. *J. Am. Chem. Soc.* **1963**, *85*, 1003–1005.

(152) and, D. A. V.; William D. Jones*, †. *Organometallics* **1998**, *17*, 3411–3413.

(153) Claudio Bianchini, *; M. Victoria Jiménez; Andrea Meli; Simonetta Moneti; Véronique Patinec, A.; Vizza, F. *Organometallics* **1997**, *16*, 5696–5705.

(154) Jorge Torres-Nieto; Alma Arévalo, A.; García*, J. J. *Organometallics* **2007**, *26*, 2228–2233.

(155) Neurock, M.; Van Santen, R. A. *J. Am. Chem. SOC* **1994**, *116*, 4427–4439.

(156) Vicic, D. A.; Jones*, W. D. *Organometallics* **1997**, *16*, 1912–1919.

(157) Kouki Matsubara, ‡; Rei Okamura, ‡; Masako Tanaka, † and; Hiroharu Suzuki*, ‡. *J. Am. Chem. Soc* **1998**, *120*, 1108–1109.

(158) Sattler, A.; Parkin, G. *J. Am. Chem. Soc* **2011**, *133*, 3748–3751.

(159) Lin, S.; Herbert, D. E.; Velian, A.; Day, M. W.; Agapie, T. *J. Am. Chem. Soc* **2013**, *135*, 15830–15840.

(160) Vicic, D. A.; Jones, W. D. *J. Am. Chem. Soc* **1999**, *121*, 7606–7617.

(161) Jones, W. D.; Chin, R. M. *J. Organomet. Chem.* **1994**, *472*, 311–316.

(162) Grochowski, M. R.; Brennessel, W. W.; Jones, W. D. *Organometallics* **2009**, *28*, 2661–2667.

(163) Toutov, A. A.; Salata, M.; Fedorov, A.; Yang, Y.; Liang, Y.; Cariou, R.; Betz, K. N.; Couzijn, E. P. A.; Shabaker, J. W.; Houk, K. N.; Grubbs, R. H. *Nat. Energy* **2017**, *17008*, 1–7.

(164) Banerjee, S.; Yang, Y.-F.; Jenkins, I. D.; Liang, Y.; Toutov, A. A.; Liu, W.-B.; Schuman, D. P.; Grubbs, R. H.; Stoltz, B. M.; Krenske, E. H.; Houk, K. N.; Zare, R. N. *J. Am. Chem. Soc.* **2017**, *139*, 6880–6887.

(165) Ripin, D. H.; Evans, D. A. evans_pKa_table http://evans.rc.fas.harvard.edu/pdf/evans_pKa_table.pdf (accessed May 24, 2017).

(166) Brown, H. J. S.; Stryker, J. M.; Hebert, D. Catalysts for hydrodesulfurization. US 9458395 B2, 2013.

(167) Brown, H. J. S.; Stryker, J. M.; Hebert, D. Mixed-valent transition metal-phosphoranimide catalysts. US 20140350275 A1, 2014.

(168) Camacho-Bunquin, J.; Stryker, J. M. Transition metal catalysts for hydrodesulfurization. US 20140174989 A1, 2014.

(169) Wiedemann, S. H.; Ramírez, A.; Collum, D. B. *J. Am. Chem. Soc* **2003**, *125*, 15893–15901.

(170) Camacho-Bunquin, J. Empowering the Base Metals: Rational Design of High-Activity Homogeneous Catalysts for Reduction of Organic Unsaturates and Mild-Condition Hydrotreatment, University of Alberta, 2013.

(171) Vorapattanapong, A. *unpublished work*.

(172) Yiping, Z.; Shijian, L.; Yun, X. *J. Mol. Catal.* **1993**, *84*, 211–221.

(173) Pellissier, H.; Santelli, M. *Tetrahedron* **2003**, *59*, 701–730.

(174) Bearden, R.; Fink, T. Alkali metal desulfurization process for petroleum oil stocks using low pressure hydrogen. US3787315 A, 1974.

(175) Al-Haj-Ibrahim, H.; Morsi, B. I. *Ind. Eng. Chem. Res.* **1992**, *31*, 1835–1840.

(176) Connelly, N. G.; Geiger, W. E. *Chem. Rev.* **1996**, *96*, 877–910.

(177) Barham, J. P.; Coulthard, G.; Emery, K. J.; Doni, E.; Cumine, F.; Nocera, G.; John, M. P.; Berlouis, L. E. A.; Mcguire, T.; Tuttle, T.; Murphy, J. A. *J. Am. Chem. Soc* **2016**, *138*, 7402–7410.

(178) Duhme, A.-K.; Strasdeit, H. *Eur. J. Inorg. Chem.* **1998**, *1998*, 657–662.

(179) Kan, Y.; Ken Chi-Hang Tso, ab; Lai-Fung Chan, S.; Guan, X.; Che, C.-M. *New J. Chem. New J. Chem* **2013**, *37*, 1811–1816.

(180) Shylesh, S.; Jia, M.; Thiel, W. R. *Eur. J. Inorg. Chem.* **2010**, *2010*, 4395–4410.

(181) Rimoldi, M.; Mezzetti, A. *Catal. Sci. Technol. Catal. Sci. Technol* **2014**, *4*, 2724–2740.

(182) Trovitch, R. J.; Guo, N.; Janicke, M. T.; Li, H.; Marshall, C. L.; Miller, J. T.; Sattelberger, A. P.; John, K. D.; Baker, R. T. *Inorg. Chem* **2010**, *49*, 2247–2258.

(183) Xie, W.; Huang, X.; Li, H. *Bioresour. Technol.* **2006**, *98*, 936–939.

(184) Haji, S.; Zhang, Y.; Kang, D.; Aindow, M.; Erkey, C. *Catal. Today* **2004**, *99*, 365–373.

Appendix

A1.1 $[Ni_2(allyl)_2(NPPh_3)_2]$

STRUCTURE REPORT

XCL Code: JMS1630 **Date:** 2 August 2016

Compound: $[Ni_2(allyl)_2(NPPh_3)_2]$

Formula: $C_{42}H_{40}N_2Ni_2P_2$

Supervisor: J. M. Stryker **Crystallographer:** M. J. Ferguson

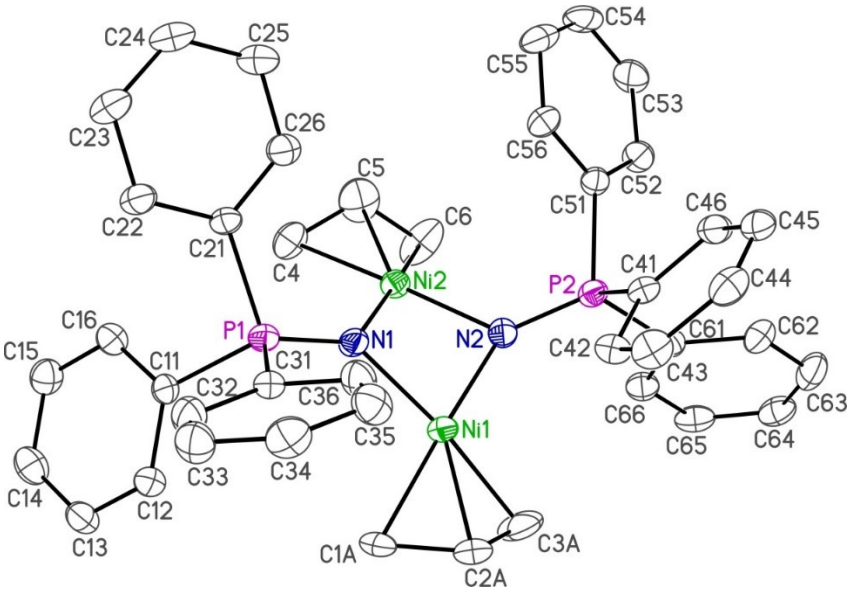

Figure Legends

Figure 1. Perspective view of the $[Ni_2(allyl)_2(NPPh_3)_2]$ molecule showing the atom labelling scheme. Non-hydrogen atoms are represented by Gaussian ellipsoids

at the 30% probability level. Only the major (80%) orientation of the disordered allyl group is shown. Hydrogen atoms are not shown.

Table 1. Crystallographic Experimental Details

A. Crystal Data	
formula	$C_{42}H_{40}N_2Ni_2P_2$
formula weight	752.12
crystal dimensions (mm)	0.11 x 0.08 x 0.04
crystal system	triclinic
space group	$P\bar{1}$ (No. 2)
unit cell parameters[a]	
a (Å)	10.1737 (10)
b (Å)	12.4313 (13)
c (Å)	16.5924 (17)
α (deg)	99.5200 (14)
β (deg)	101.6119 (13)
γ (deg)	111.9704 (13)
V (Å^3)	1838.1 (3)
Z	2
ρ_{calcd} (g cm^{-3})	1.359
μ (mm^{-1})	1.143
B. Data Collection and Refinement Conditions	
diffractometer	Bruker PLATFORM/APEX II CCD[b]
radiation (λ [Å])	graphite-monochromated Mo Kα (0.71073)
temperature (°C)	–80
scan type	ω scans (0.3°) (30 s exposures)

data collection 2θ limit (deg)	50.96
total data collected	12918 ($-12 \le h \le 12$, $-14 \le k \le 15$, $-20 \le l \le 20$)
independent reflections	6804 ($R_{int} = 0.0652$)
number of observed reflections (*NO*)	3934 [$F_o^2 \ge 2\sigma(F_o^2)$]
structure solution method	intrinsic phasing (*SHELXT-2014*[c])
refinement method	full-matrix least-squares on F^2 (*SHELXL–2014*[d])
absorption correction method	Gaussian integration (face-indexed)
range of transmission factors	1.0000–0.8167
data/restraints/parameters	6804 / 0 / 445
goodness-of-fit (*S*)[e] [all data]	0.954
final *R* indices[f]	
R_1 [$F_o^2 \ge 2\sigma(F_o^2)$]	0.0511
wR_2 [all data]	0.1261
largest difference peak and hole	0.554 and –0.441 e Å^{-3}

[a]Obtained from least-squares refinement of 2203 reflections with $4.46° < 2\theta < 41.04°$.

[b]Programs for diffractometer operation, data collection, data reduction and absorption correction were those supplied by Bruker.

[c]Sheldrick, G. M. *Acta Crystallogr.* **2015**, *A71*, 3–8. (*SHELXT-2014*)

[d]Sheldrick, G. M. *Acta Crystallogr.* **2015**, *C71*, 3–8. (*SHELXL-2014*)

[e]$S = [\Sigma w(F_o^2 - F_c^2)^2/(n-p)]^{1/2}$ (n = number of data; p = number of parameters varied; $w = [\sigma^2(F_o^2) + (0.0480P)^2]^{-1}$ where $P = [\mathrm{Max}(F_o^2, 0) + 2F_c^2]/3$).

[f]$R_1 = \Sigma||F_o| - |F_c||/\Sigma|F_o|$; $wR_2 = [\Sigma w(F_o^2 - F_c^2)^2/\Sigma w(F_o^4)]^{1/2}$.

A1.2 IR spectrum $[Ni_2(\eta^3\text{-allyl})_2(NPEt_3)_2]$

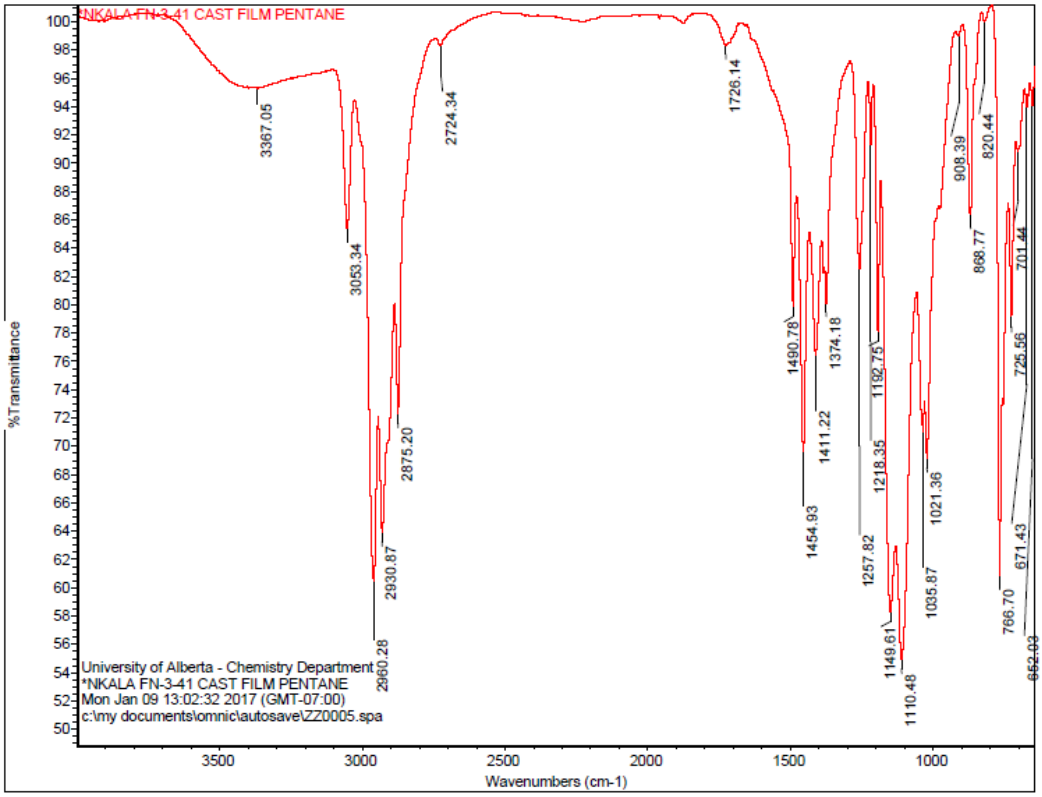

A1.3 IR spectrum $[Co_2(\eta^3\text{-allyl})_2(NP^tBu_3)_2]$

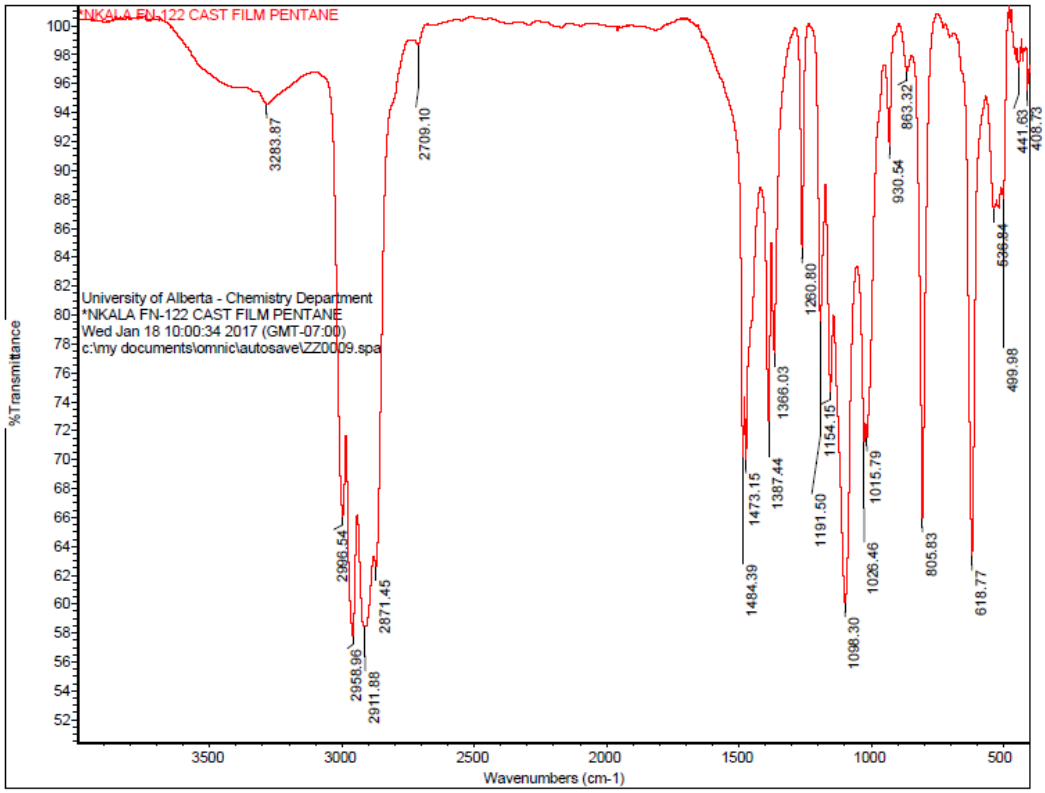

A1.3 IR spectrum $[Fe_2(\eta^3\text{-allyl})_2(NP^tBu_3)_2]$

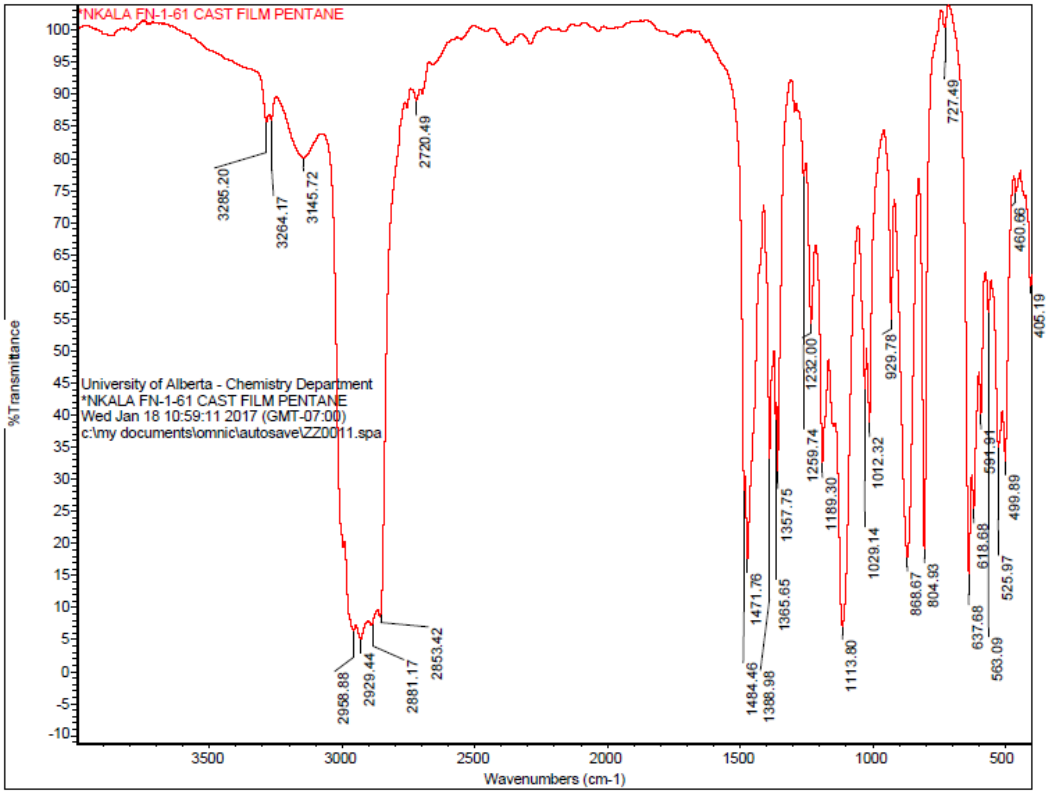

A1.4 IR spectrum $[Ni_2(\eta^3\text{-allyl})_2(NP^tBu_3)_2]$

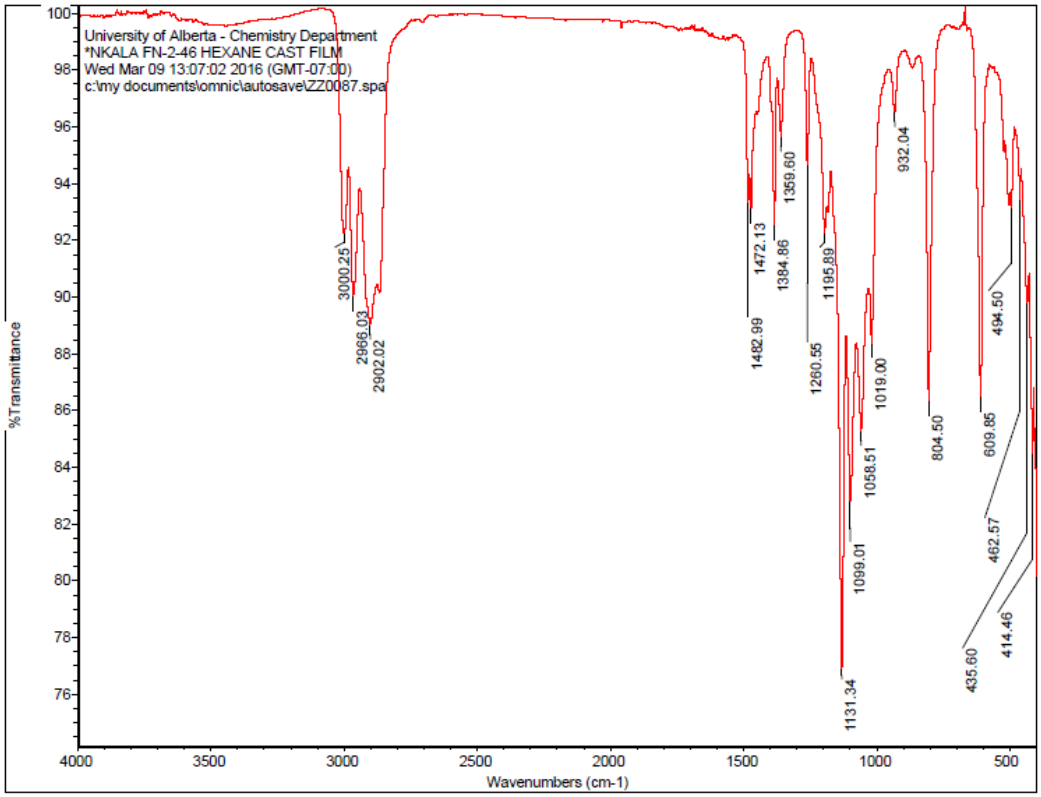

A1.4 IR spectrum [Ni(η^3-allyl)(NPEt$_3$)]$_2$•AlH$_3$